POLYMER/OIL RELATIVE PERMEABILITIES IN CARBONATE RESERVOIRS

A THESIS SUBMITTED TO
THE GRADUATE SCHOOL OF NATURAL AND APPLIED SCIENCES
OF
MIDDLE EAST TECHNICAL UNIVERSITY

BY

İLKER CANKARA

IN PARTIAL FULFILLMENT OF THE REQUIREMENTS
FOR
THE DEGREE OF MASTER OF SCIENCE
IN
PETROLEUM AND NATURAL GAS ENGINEERING

Approval of the Graduate School of Middle East Technical University

Prof. Dr. Canan Özgen
Director

I certify that this thesis satisfies all the requirements as a thesis for the degree of Master of Science.

Prof. Dr. Birol Demiral
Head of Department

This is to certify that we have read this thesis and that in our opinion it is fully adequate, in scope and quality, as a thesis for the degree of Master of Science.

Assoc. Prof. Dr. Serhat Akın
Supervisor

Examining Committee Members

Prof. Dr. Birol Demiral	(METU, PETE)	
Assoc. Prof. Dr. Serhat Akın	(METU, PETE)	
Prof. Dr. Fevzi Gümrah	(METU, PETE)	
Ast. Prof. Dr. Evren Özbayoğlu	(METU, PETE)	
Prof. Dr. Nurkan Karahanoğlu	(METU, GEOE)	

I hereby declare that all information in this document has been obtained and presented in accordance with academic rules and ethical conduct. I also declare that, as required by these rules and conduct, I have fully cited and referenced all material and results that are not original to this work.

İlker Cankara

ABSTRACT

POLYMER/OIL RELATIVE PERMEABILITIES IN CARBONATE RESERVIORS

Cankara, İlker
M.S., Department of Petroleum and Natural Gas Engineering
Supervisor: Assoc.Prof. Dr. Serhat Akın

Mayıs 2005, 173 pages

In the history of a reservoir, after the period of primary production, about 30 to 40%, of the original oil in place may be produced using a secondary recovery mechanism. Polymer injection, which is classified as a tertiary method, can be applied to the remaining oil in place.

In this thesis, oil/water relative permeabilities, effect of polymer injection on end point relative permeabilities and residual oil saturations in heterogeneous carbonate reservoirs were investigated. Numereous core flood experiments were conducted on different heteroegneous carbonate cores taken from Midyat Formation. Before starting the displacement experiments, porosity, permeability and capillary pressure experiments were performed. The heterogeneity of the cores are depicted from thin sections.

Besides the main aim stated above, effect of flow rate and fracture presence on end point relative permeability and on residual oil saturation and were investigated.

According to the results of the displacement tests, end point hexane relative permeability increased when polymer solution was used as the displacing phase.Besides, end point hexane relative permeability increased with polymer injection and fracture presence.

Keywords: Relative Permeability, Polymer Flooding, Heterogeneous Carbonate Reservoir.

ÖZ

KARBONATLI KAYAÇLARDA POLİMER/PETROL GÖRELİ GEÇİRGENLİĞİ

Cankara, İlker
Yüksek Lisans, Petrol ve Doğal Gaz Mühendisliği Bölümü
Tez Yöneticisi: Doç. Dr. Serhat Akın

Nisan 2005, 173 sayfa

Bir petrol rezervininin geçmişinde, birincil üretim döneminden sonra, kalan petrolün %30-%40 lık bölümü ikincil üretim teknikleriyle üretilebilir. Kalan petrolü çıkarmak için üçüncül üretim metodlarından biri olarak sınıflandırılan polimer enjeksiyonu kullanılabilir.

Bu tezde, heterojen karbonat rezervouarlarında polimer solüsyonu enjeksiyonunun su/petrol göreli geçirgenliklerine, petrol son nokta göreli geçirgenliğine ve indirgenemez petrol doymuşluğuna etkileri incelenmiştir. Midyat formasyonundan alınmış heterojen karbonat karot tapaları kullanılarak çok sayıda enjeksiyon deneyi yapılmıştır. Su basma deneylerine başlamadan önce, gözeneklilik, geçirgenlik ve kapiler basınç deneyleri yapılmıştır. Karotların heterojen yapısı, alınan ince kesit görüntüleriyle ortaya konmuştur.

Yukarıda belirtilen temel amaç yanında, enjeksiyon debisi ve çatlaklı ortamın son nokta hegzan göreli geçirgenliğe ve indirgenemez petrol doymuşluğuna olan etkileri araştırılmıştır.

Yapılan deneyler sonucunda, öteleyen faz olarak polimer solüsyonu kullanımının petrol son nokta hegzan petrol göreli geçirgenliğini artırdığı sonucuna varılmıştır. Ayrıca polimer solüsyonu kullanıldığında ve çatlak varlığında petrol son nokta petrol göreli geçirgenliği artmıştır.

Anahtar Kelimeler: Göreli Geçirgenlik, Polimer Enjeksiyonu, Heterojen Karbonat Rezervuarı.

ACKNOWLEDGEMENTS

The author wishes to express his gratitude to his thesis advisor Assoc. Prof. Dr. Serhat Akın for his patience and understanding; his guidance, advice, criticism and encouragement throughout the study.

Above all, the author is deeply grateful to his parents; Mete Cankara, Tülay Cankara and his grandfather Emin Cankara for providing by all means the conditions for him to study and especially his sister Çiğdem Cankara for her continuous effort in dealing with the editing.

The author also wishes his gratitude to his aunt Pervin Cankara for her unconditional support and care, patience and understanding, fostering and always being there to listen.

TABLE OF CONTENTS

LIST OF TABLES

LIST OF FIGURES

NOMENCLATURE

A: cross sectional area, cm^2

Q: flow rate, cc/sec

k_r: end point relative permeability to oil

μ: viscosity, centipoises

k_{abs}: absolute permeability, darcy.

ΔP: pressure loss, atm.

v: velocity

L= length, over which pressure loss is measured, cm

d: diameter of conductor, cm

ρ: fluid density, gr/cc

f: friction factor, dimensionless

r: radius

h_1: height 1 above standard datum

h_2: height 2 above standard datum

s: distance in direction of flow, cm

v_s: volume flux across a unit area

g: gravitational acceleration, cm/sq cm

k_t: total permeability

k_m: matrix permeability

k_f: fracture permeability

P_{cf}: capillary pressure of the fracture

λ: mobility

CHAPTER 1

LITERATURE SURVEY

1.1 Fracture Relative Permeability

Romm **[1]** was the first one to perform a laboratory study on fracture relative permeability. He lined glass plates with waxed paper and added waxed paper strips running through the plates as spacers. He concluded that fracture relative permeability is a linear function of saturation with end point values at 0 and 1, **Figure 1**. Romm's work, however, was designed to obtain a large degree of phase segregation. Since that time, very few attempts have been made to calculate relative permeability in fractures.

Merill **[2]** and Pieters and Graves **[3]** attempted to duplicate Romm's experiments without using waxed paper strips. Merill found that the wetting phase saturations were scattered around a value of 0,72 for nearly the entire range of flow rates and fractional flows. Deviations from this behavior only occurred when both the total flow rate and the fractional flow were high. This behavior was also seen when Merill performed experiments on epoxy sealed Barea sandstone blocks.

Pan and Wong **[4]** reported similar observations for steady state flow of fluids in a smooth fracture. Rangel-German et al. **[5]** observed the same behavior for unsteady-state experiments monitored using a computerized tomography scanner.

They also reported saturation measurements in the fracture. These were performed using a constant fracture aperture limitation.

Pruess and Tsang **[6]** developed a percolation model using a log normal aperture distribution. They assumed that grid block occupancy was dependent only on the capillary pressure of the block (accessibility was ignored). Pruess and Tsang's numerical simulation of a fracture showed (contrary to Romm's findings) that there was considerable interference between phases. For short range correlations, very little multiphase flow occurred.

Persoff et al. **[7]** performed experiments on natural rock fractures and on transparent epoxy replicas of natural fractures. Air and water were simultaneously injected into the fracture and attempts were made to attain steady state flow. Saturation measurements were not made. Plots of relative permeability as a function of mass flow rate ratio and gas relative permeability versus water relative permeability showed that significant phase interference occurred.

Mc Donald et al. **[8]** reported non-linear relative permeability measurements made on a naturally fractured limestone core using nuclear magnetic resonance techniques.

Babadagli and Ersaghi **[9]** introduced the concept of effective fracture relative permeability. They suggested that the rate dependent effective fracture relative permeabilities could be used to model a dual porosity system as a fracture network model where the matrix is assumed to have like a sub-system of the network just supplying oil to the fracture by countercurrent capillary imbibition (the effects of gravity were not included).

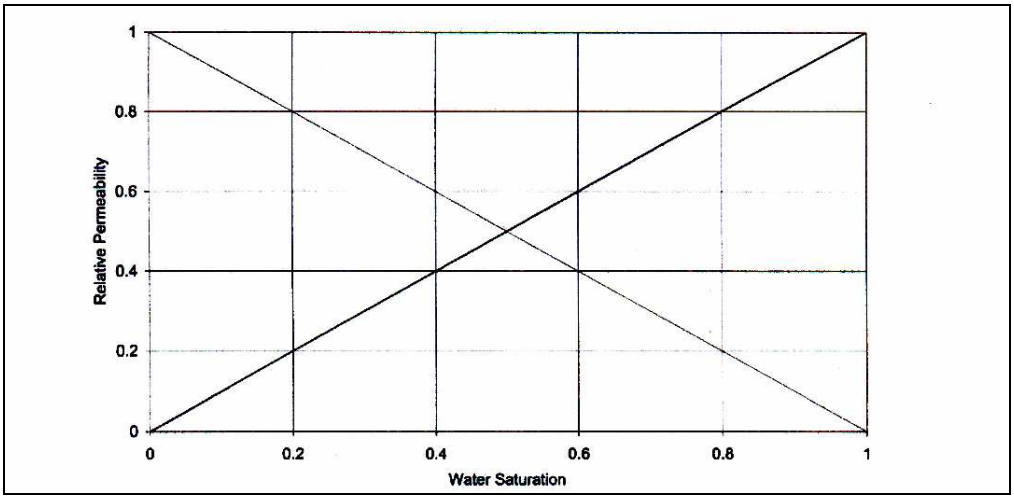

Figure 1. Romm's fracture relative permeabilities suggestion **[1]**

1.2 Capillary Interaction in Fracture/Matrix Systems

Much of the research on flow through fractured porous media is centered around single phase flow **[10]**.

Romm **[1]** reported the measured liquid-liquid permeabilities of parallel plates simulating the fractures.

In 1979, Saidi et al **[11]** questioned the single block concept in the simulation of fractured petroleum reservoir. The single-block concept assumes that the matrix blocks drain independently. Saidi et al. questioned the single block concept in the simulation of fractured petroleum reservoir. The single-block concept assumes that the matrix blocks drain independently. Saidi et al. suggested that the matrix

blocks interact. They attributed the interaction between blocks to the reimbibition process and capillary continuity between the adjacent blocks through liquid bridges. In their history match of North Sea Ekofisk fractured reservoirs, Thomas **[12]** observed that the use of a measured matrix gas-oil capillary pressure function resulted in excess GOR production. They were forced to set this function to zero to match the gas oil ratio. They interpreted this as a sign of capillary continuity across the fractures in the Ekofisk field and reasoned the capillary continuity requires a few sites across the fractures.

In a more recent paper, Festoy and Van Golf-Racht **[13]** incorporated continuity across a stack of two matrix blocks by assuming a limited contact area between the two blocks. They used a conventional single-porosity numerical model to simulate the drainage rate as a function of the contact-area size and location for this system. They concluded that the partial physical connection between the two blocks drastically improved the final recovery when compared with another case where the two blocks have no physical connection.

The reasoning of Kazemi **[14]** mentioned that to maintain gravity capillary-equilibrium, the maximum capillary pressure in the matrix and fracture must be set equal. They also stated, however, that in a two phase process, both phases should be mobile for the entire range of saturations for the fractures. In their last publication on dual porosity simulators, Gilman and Kazemi **[15]** however mentioned that horizontal fractures would reduce recovery and cause capillary discontinuity between matrix blocks.

1.3 Effects of Rock Properties

Relative permeability-saturation relations are not identical for all reservoir rocks, but may vary from formation to formation and from one portion to another of a heterogeneous formation.

Stone **[16]** have shown that the fluid flow behavior in uniform porosity carbonate samples is similar to fluid flow behavior in consolidated sandstones, but the difference becomes pronounced as the rock heterogeneity increases.

Muskat et al. **[17]** suggested that it is necessary to know the pore geometry of a reservoir rock before fluid movement through it can be analyzed.

Morgan and Gordon **[18]** found that pore geometry and surface area per unit volume influenced water-oil relative permeability curves. They have shown that rocks with large pores and correspondingly small surface areas have low irreducible water saturation and therefore have a relatively large amount of pore space available for the flow of fluids. This condition allows high relative permeability end points to exist and allows a large saturation change to occur during two-phase flow. Correspondingly, rocks with small pores have larger surface areas per unit volume and they have irreducible water saturations that leave little room for the flow of hydrocarbons. This condition creates a low initial oil relative permeability as well as a limited saturation range for the two-phase flow.

Gorring **[19]** demonstrated that oil in a larger pore can be surrounded and blocked off when it is encircled by smaller pores which imbibe the displacing water by capillary forces. He concluded that both pore size distribution and pore orientation have a direct effect on non-wetting residual equilibrium saturation. Goring also identified the size of channels occupied by non-wetting phase as an important factor influencing relative permeability.

Crowell et al. **[20]** indicated that higher initial water saturation yields a higher probability for the non-wetting phase to be in larger channels so that it can be recovered efficiently during wetting-phase imbibition.

1.4 Effect of Wettability

Wettability is a term used to describe the relative attraction of one fluid for a solid in the presence of other immiscible fluids. It is the main factor responsible for the microscopic fluid distribution in porous media and it determines to a great extent the amount of residual oil saturation and the ability of a particular phase to flow. The relative affinity of a rock to a hydrocarbon in the presence of water is often described as ‘water wet’, ‘intermediate’, or ‘oil wet’.

Early experimenters thought that all oil-bearing formations were strongly water wet because an aqueous phase was always the fluid initially in contact with reservoir rock; furthermore, silica and carbonates are normally water-wet in their clean state. Subsequent studies suggested that many oil reservoirs are not strongly water-wet and that the presence of crude oils containing natural surface-active agents, such as asphaltic or wax type material readily adsorbable by solid-liquid interfaces, can render the solid surface oil-wet. **[21]** Other studies provide evidence that reservoir rock wetting performance may cover a broad spectrum.

The microscopic distribution of fluids in a porous medium is greatly influenced by the degree of rock preferential wettability. The fluid distribution in virgin

reservoirs under strongly water-wet and strongly oil-wet conditions has been described by Pirson. In a strongly water-wet reservoir, most of the water resides in dead-end pores, in small capillaries, and on the grain surface. In strongly oil wet reservoirs, water is in the center of the large pores as discontinuous droplets, while oil coats the surfaces of the grains and occupies the smaller capillaries.

Under strongly water-wet conditions the effective permeability to the non-wetting phase at irreducible water saturation is approximately equal to the absolute permeability of the rock. In strongly water-wet reservoirs, water traps oil in the larger pores as it advances along the walls of the pore, while in strongly oil-wet reservoirs, water moves in large pores and oil is trapped close to the walls of the pores.

Some investigators have found that relative permeability becomes progressively less favorable to oil production as a rock becomes less water-wet. The residual oil saturation increases as a rock becomes less water-wet. Others have shown that weakly water-wet cores have more favorable relative permeability curves and lower residual oil saturations than strongly water-oil-wet rocks. Conceptually, this latter behavior seems to be reasonable since the capillary forces in strongly water-wet cores are strong. The oil may be by-passed and trapped in larger pores by the tendency of a water wet core to imbibe water into the smaller capillaries. The by-passed oil in the large pores is then surrounded by water and is immobile except at very high pressure gradients. The saturation interval for two-phase flow under this condition is probably short.

As the capillary forces are reduced by the reduction of preferential water-wettability of a rock, the tendency toward rapid imbibitional trapping of oil in large pores by movement of water through small pores should also diminish. The

zone of two-phase flow should become broader and oil displacement to a lower residual saturation should be possible **[22].**

Relative permeability-saturation relations are not unique functions of saturation for a given core, but are subject to hysteresis, that is, the relative permeability to a fluid at a given saturation depends on weather that saturation is obtained by approaching it from a higher value or lower value. The type relative permeability curve that is representative of flow characteristics through the formation in the reservoir depends on the mechanism by which the reservoir is depleted **[23].**

If other factors remain constant, higher flow rates and lower interfacial tensions are conducive to higher oil recovery, these are changes that diminish the ratio of capillary forces to viscous forces. In a two-phase system, hysteresis is prominent in relative permeability to the non-wetting phase than in relative permeability to the wetting phase **[24, 25].** The hysteresis in wetting phase relative permeability is believed to be very small and thus, sometimes difficult to distinguish from normal experimental error.

These curves describe relative permeability when the flow reversal occurs at one of the saturation end points.

The water (wetting phase) relative permeability curve is essentially the same in strongly water-wet rock for both drainage and imbibition process **[26].**

However at a given saturation, the non-wetting phase relative permeability of a consolidated rock is usually less for an imbibition cycle than for a drainage cycle **[27, 28, 29, 30].**

The amount of trapped oil in water-wet porous media is given approximately by the area between the drainage and imbibition oil relative permeability curves **[31].**

It is believed that the occurrence of hysteresis is possibly related to the pore size distribution and cementation of a rock. As water is progressively imbibed into oil-filled pores of different sizes, oil is ejected from them. The ejection process continues as long as continuous escape paths through pores still containing oil are available. These escape paths appear to be lost at oil saturations which greatly exceed those which occur at the onset of continuity of a non-wetting phase, (e.g., gas) on the drainage cycle. Thus, the residual oil saturation which results from water flooding a water-wet rock is much greater than the critical gas saturation that characterizes the same rock. Apparently oil is trapped on the imbibition cycle. A similar behavior is observed if a preferentially water-wet rock containing free gas is water flooded.

1.5 Effects of Overburden Pressure

Wilson **[32]** reported that a 5000 psi laboratory simulation of overburden pressure at reservoir temperature reduces the core effective permeabilities to oil and water by about the same extent as it reduces the single-phase permeability of that core. Consequently, the water and oil relative permeability of a natural core, under 5000 psi overburden pressure, show only a moderate change from the relative permeability measured under atmospheric conditions. . Wilson also pointed out that an overburden pressure that can produce over 5% reduction in a porosity of a

core can also produce a sufficiently large change in pore size distribution to affect the relative permeability of the core.

Merliss et al. **[33]** concluded that the effect of overburden pressure on relative permeability was primarily due to changes in interfacial tension.

1.6 Effects of Temperature

Several early studies **[34, 35]** indicated that irreducible water saturation increased with increasing temperature and that residual oil saturation decreased with increasing temperature, all of these studies employed a dynamic displacement process.

Difficulties in evaluating these results include possible wettability changes, due to the core cleaning procedure **[36],** possible changes in absolute permeability and clay migration **[34,37,35].**

Miller and Ramey **[38]** performed dynamic displacement experiments at elevated temperatures on unconsolidated sand packs, and a Barea core. Their results indicated that changes in temperature do not cause relative permeability changes, but that changes in the flow capacity at elevated temperatures are due to clay interactions, change in pore structure, etc. The only change that they observed was an increase in oil relative permeability at irreducible water saturation and this parameter is relatively unimportant for predicting two-phase flow behavior.

1.7 Effects of Interfacial Tension and Density

Moore and Slobod **[39]** reported a reduction in waterflood residual oil saturation of a water-wet core at lower values of interfacial tension.

Pirson **[40]** stated that the drainage relative permeability is independent of the interfacial tension.

Bardon and Longeron **[41]** found that a reduction in interfacial tension reduced oil relative permeability at constant gas saturation in an oil-gas drainage cycle.

The effect of liquid density on relative permeability has been found to be insignificant **[42].**

1.8 Effects of Viscosity

Sanbderg et al. **[43]** found that oil and water relative permeabilities of a uniformly saturated core are independent of the oil viscosity in the range of 0,398 to 1,683 cp.

Donaldson et al. **[44]** and Geffen et al. **[45]** also concluded that relative permeability is independent of viscosity as long as the core wettability is preserved.

Wilson **[32]** found that a 5000 psi fluid pressure which caused kerosene viscosity to increase from 1,7 to 2,7 cp and water viscosity to increase by1% did not produce any significant effect on water and oil relative permeability values.

Muskat et al. **[46]** reported that the effect of viscosity on relative permeability of unconsolidated sand was very small and within the limits of experimental accuracy.

Yuster **[47]** concluded that relative permeability values for the systems he studied were markedly influenced by variation in viscosity ratio, increasing with an increase of the ratio. This conclusion was later supported by the work of Morse et al. **[48].** Odeh **[49]** expanded Yuster's work and concluded that the non-wetting phase relative permeability increases with an increase in viscosity ratio. He found that the magnitude of the effect on relative permeability decreases with increase in single-phase permeability. Odeh found that the deviation in non-wetting phase relative permeability is increased as the non-wetting phase saturation is increased, with the deviation reaching a maximum at the non-wetting phase residual saturation. He also concluded that the wetting-phase relative permeability is not effected by variation in the range of 0, 5 to 74, 5 on water and oil relative permeability curves. Odeh stated that the effect of viscosity ratio on relative permeability could be ignored for samples with single-phase permeabilities greater than 1 D.

Yuster's and Odeh's results have been criticized by other investigators **[50].** Downie and Crane **[51]** reported that oil viscosity could influence the oil effective permeability of some rocks. Later, they qualified their statement by saying that once an increased relative permeability is obtained by employment of high viscosity oil; it may not be lost by replacing this oil with one of the lower

viscosity. They explained this phenomenon qualitatively in terms of the movement of colloidal particles at oil-water interfaces.

Pirson **[40]** stated that the importance of the effect of viscosity ratio on the imbibition non-wetting phase relative permeability is of second-order magnitude. Ehrlich and Crane **[52]** concluded that the imbibition and the drainage relative permeabilities, under a steady state condition of flow, are independent of viscosity ratio. However, they found that the irreducible wetting phase saturation following steady-state drainage, when the interfacial effect predominated over viscous and gravitational effects, decreases with an increase in the ratio of non-wetting to wetting-phase viscosities.

Perkins **[53]** concluded that flow in a porous body is governed by relative permeability and viscosity ratio when the ratio of capillary pressure to the applied pressure is negligible.

Pickell et al. **[54]** concluded that only a large variation in viscous forces could have any appreciable effect on residual oil saturation.

Levebwre du Prey **[55]** made a systematic study of the effect of this ratio on relative permeability by simultaneously varying the interfacial tension, viscosity and velocity. He found that the relative permeability decreases as the ratio $\sigma \cos\theta / \mu v$ increases. He also concluded that the relative permeability curve is influenced by the viscosity ratio when the wetting phase is displaced by the non-wetting phase.

An assumption that the relative permeability values are independent of viscosity implies that the system can be represented by a bundle of parallel, non-

interconnected capillary tubes, each of which is filled with either the wetting or the non-wetting phase alone. Thus, the non-wetting phase flows through the larger channels while the wetting phase flows through the smaller capillaries. However, this model probably does not completely represent the conditions in porous media. An alternative model is the simultaneous flow of two immiscible fluid phases in larger capillaries.

A flow picture more compatible with the present knowledge of fluid behavior is a combination of the two models described above, with one dominating over the other depending primarily on wettability.

Odeh **[56]** believed that the fluid phases did not flow in separate capillaries in porous media as Leverett postulated and further stated that the wetting phase moves microscopically in a sort of sliding motion imparted to it by the shear force caused by motion of the non-wetting phase. From this model he concluded that a decrease in interstitial wetting phase saturation can be developed as a result of an increase in viscosity, thereby affecting the relative permeability values.

In view of the diverse opinions which have been expressed by various investigators concerning the influence of viscosity on relative permeability, it seems best to conduct laboratory relative permeability experiments with fluids which do not differ greatly in viscosity from the reservoir fluids.

1.9 Effects of Initial Wetting Phase Saturation

The amount of initial interstitial water affects the oil-water relative permeability values. Caudle et al. **[57]** investigated this relationship.

McCaffery and Bennion investigated the effect of varying the amount of initial water saturation on water and oil relative permeability. According to their study; not only the starting points, but also the shape of the relative permeability curves vary with the amount of initial interstitial water **[58].**

Sarem **[59].** found that the presence of initial water saturation tended to shift water-oil relative permeability ratio curves toward the region of lower oil saturation. The difference in the residual oil saturation caused by this shift was reported to be about half the difference in initial water saturation. Thus, a lower oil saturation is obtained at higher values of initial water saturation.

Other investigators have suggested that even though the immobile connate water does not appreciably affect the relative permeability ratio, the amount and distribution of the interstitial water may influence the relative permeability.

1.10 Effects of Other Factors

The effects of displacement pressure, pressure gradient, and flow rate on the shape of relative permeability curves have long been a controversial subject in petroleum-related literature. Some authors believe that the effect of displacement pressure and pressure gradient may be due to the changes imposed on viscosity, interfacial tension or other fluid or rock properties. Others believe that the

changes in relative permeability, which appear to result from changes in displacement pressure and pressure gradient, are actually due primarily to an ‘end effect’ developed during laboratory tests.

End effect or boundary effect refers to a discontinuity in the capillary properties of a system at the time of relative permeability measurement. In a stratum of permeable rock, the capillary forces act uniformly in all directions, and thus negate each other. In a laboratory sample, however, there is a saturation discontinuity at the end of a sample. When the flowing phases are discharged into an open region under atmospheric pressure, a net capillary force persists in the sample; this force tends to prevent the wetting phase from leaving the sample. The accumulation of the wetting phase at the outflow face of the sample creates a saturation gradient along the sample which disturbs the relative permeability measurements. For example, a large difference, in saturation at the displacement front causes a large capillary pressure gradient, which in turn causes the water to advance ahead of the flood front and to reduce the capillary pressure gradient in the measured region. The advancing water can not be produced when it reaches the outflow face of a core, because the pressure in the water just inside the core is lower than the pressure in the oil-filled space around the outflow face. This difference in pressure is equal to the capillary pressure for the existing saturation at the outflow face. Therefore, water accumulates at the outflow end of the core, causing a reduction in the capillary pressure. The water will not be produced until the capillary pressure is overcome and the residual oil saturation (at the outflow face of the core) is reached. The calculation of relative permeability based on the average saturation of the sample produces enormous results in this case, since the relative permeability varies throughout the core due to the saturation gradient created by the wetting phase accumulation at the outflow face of the core.

Owens et al. **[60],** , Kyte and Rappoport **[61]** and Perkins **[53]** believe that the most convenient way of minimizing the boundary effect is the adjustment of capillary forces to insignificant values, as compared to the viscous forces. This is usually done by a flow adjustment. However, the adjusted rate must be low enough so that fluid mixing is enhanced. An equation has been developed **[62]** to predict the extent that a core can be disturbed by boundary effect, at a given rate. Another convenient way of minimizing the boundary effect at the outflow end of a core is to use a more viscous oil in a longer core **[62].**

Sandberg et al. **[43]**, Richardson et al. **[62]**, found that the drainage relative permeability is independent of the flow rate as long as a saturation gradient is not introduced in the core by the internal forces.

Pirson **[40]** concluded that relative permeability is not rate-sensitive in drainage processes.

Moore and Slobod **[63]** reported that waterflood recovery from a water-wet core was practically independent of flooding rate. However they observed that a significant recovery increase may be obtained at extremely high rates. Huppler **[64]** stated that the waterflood recovery from cores with the significant heterogeneity was sensitive to flooding rate.

Crowell et al. **[20]** studied the effect of core dimensions on laboratory measurement of relative permeability. They found that the residual gas saturation in water-gas systems was almost independent of length of the core, within the limits of the laboratory-scale models used. They also examined cylindrical and rectangular samples, and observed that a 100-fold change in the ratio of core length to core cross-sectional area of Barea and Boise sandstones did not alter the residual gas saturation of the samples.

Moore and Slobod **[63]** also found that fluid recovery from water-wet cores was not affected by the sample length.

When a mobile fluid is displaced by a more mobile fluid, the displacement is unstable and the flood front may cause fingers. Heterogeneity aids the fingering process. **[65]**

An unstable displacement leads to premature breakthrough and a longer period of two-phase flow at the outlet. Fingered displacement is no longer one dimensional and the JBN technique is no longer strictly applicable to such a displacement. The effects of fingering and capillarity can not be suppressed simultaneously. At low rates, fingering is small, but the capillary end effect is high. At high rates, fingering is large, but the capillary end effect is low **[66].**

Most naturally occurring porous media are heterogeneous, and the relative permeabilities of different regions need not be the same. Huppler **[64]** studied the effect of permeability heterogeneity on water flooding numerically, where the relative permeabilities of all the regions were identical. Huppler recommends for oils that are not too viscous (viscosity smaller than 20 cp), water flooding at low rates for water-wet rocks and at field rates for mixed-wet and weakly water-wet rocks. This recommendation does not account for capillary end effects.

If the rock is heterogeneous and the viscosity ratio between oil and water is large, then the fingering process is amplified by the heterogeneity **[65].** In such cases, unsteady displacements can be dominated by fingering; especially if the rock is mixed-wet. It is not clear how the unsteady recovery and pressure-drop data can be interpreted to obtain the actual relative permeabilities.

Perhaps the heterogeneity of the core should be evaluated from an independent test (i.e. single phase tracer displacement), and then the unsteady-displacement should be matched by a simulation that accounts for both capillarity and heterogeneity **[65].**

1.11 Effect of Polymer on Oil Recovery

In Figure 2**,** the influence of viscosity ratio on oil recovery is shown. This figure clearly demonstrates the improvement in oil recovery related to the viscosity of the displacing phase. The irreducible oil saturation or residual oil saturation after a sufficiently high number of flooded pore volumes, should, however, be the same for all viscosity ratios.

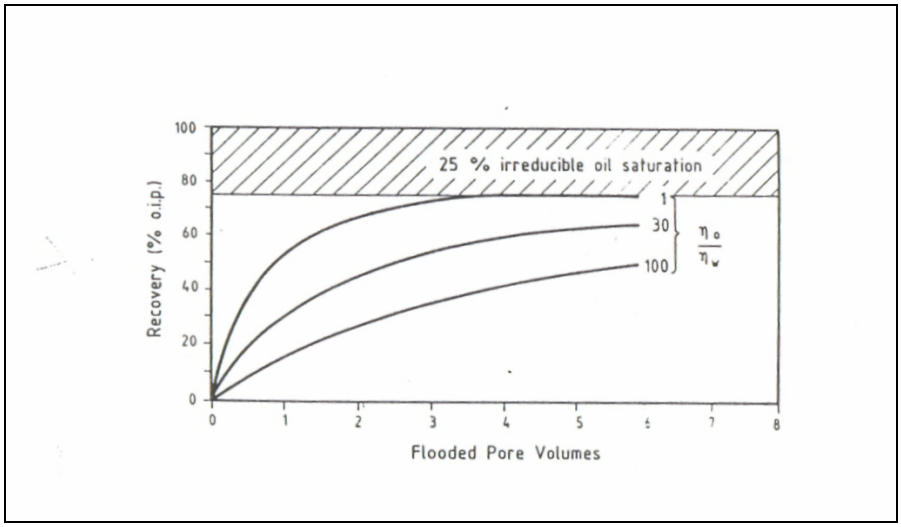

Figure 2. Influence of viscosity ratio on oil recovery process according to Tunn **[67]**

Figure 3 shows the mobility ratio curves of an experimental study performed by Welge. It can be seen that the mobility ratio in a water flood at low water saturations may also be below 1 and that at high saturations the mobility ratio for the polymer flood may become greater than 1.

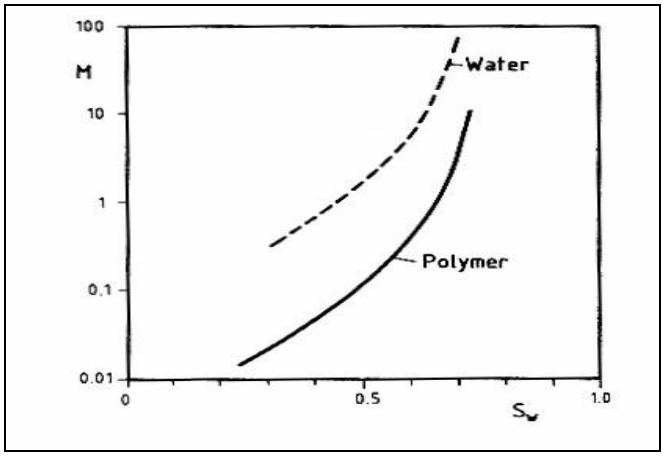

Figure 3. Mobility ratio for the displacement of oil by water and polymer solution as a function of saturation of the displacing phase **[67]**

CHAPTER 2

STATEMENT of the PROBLEM

Mainly to see how additional oil can be recovered at carbonate reservoirs by polymer flooding, and to see the effects of some production parameters such as flow rate and horizontal fracture, an experimental set-up was formed. The experimental data was collected for the carbonate cores belonging to Midyat Formation. Distilled water was used, and hexane, representing oil, and a cross -linked polymer polyvinylpyrrolidone was used in the core flood experiments.

Within the limits of the experimental set-up, the probability of an additional oil recovery was investigated for a carbonate reservoir by polymer flooding. In addition, influence of some factors on flooding parameters was investigated using, artificial neural networks and reservoir simulation.

CHAPTER 3

THEORY

Introduction

In the theory chapter of the thesis, basic concepts and measurement of relative permeability were introduced. In addition, ANN and reservoir simulation, which are powerful data analysis tools used in the thesis, were introduced briefly.

3.1 Relative Permeability

3.1.1 Permeability

The ability of a formation to conduct fluids is named as permeability. In other words, fluid conductance capacity of a formation is called permeability. Below will be discussed the derivation of Darcy's Law.

In the introduction to API Code 27 it is stated that permeability is the property of the porous medium and is a measure of the capacity of the medium to transmit fluids. The measurement of the permeability, then, is a measure of the fluid conductivity of the particular material.

Poiseuille's equation for viscous flow:

$$v = \frac{d^2 \Delta P}{32 \rho L} \quad \textbf{(1)}$$

Fanning's equation for viscous and turbulent flow:

$$v^2 = \frac{2d\Delta P}{f\rho L} \quad \textbf{(2)}$$

A more convenient form of Poiseuille's equation is

$$Q = \frac{\pi r^4 \Delta P}{8 \mu L} \quad \textbf{(3)}$$

where r is the radius of the conduit in centimeters, Q is the volume rate of flow in cubic centimeters per second, and the other terms are as previously defined.

If the reservoir system is considered to be a bundle of tubes such that the flow could be represented by a summation of the flow from all the tubes, then the total flow would be

$$Q_t = n \frac{\pi r^4 \Delta P}{8 \mu L} \quad \textbf{(4)}$$

where n is the number of tubes of radius r. If the block consists of a group of tubes of different radii, then

$$Q_T = \sum_{j=1}^{k} n \frac{\pi r_j^{\ 4}}{8\mu L} \quad \textbf{(5)}$$

where n_j= number of tubes of radius r_j

k = number of groups of tubes of different radii

The previous equation reduces to

$$Q_t = \frac{\pi \Delta P}{8\mu L} \sum_{J=1}^{k} n_j r_j^4 \quad \textbf{(6)}$$

If $\frac{\pi}{8} \sum n_j r_j^4$ is treated as a flow coefficient for particular grouping of tubes, the equation reduces to

$$Q_t = C \frac{\Delta P}{\mu L} \quad \textbf{(7)}$$

where $C = \frac{\pi}{8} \sum_{j=1}^{k} n_j r_j^4$ **(8)**

If the fluid conducting channels in a porous medium could be defined as to the dimension of the radii and the number of each radii, it might be possible to use Poiseuille's flow equation for porous media. As there are numerous tubes and radii involved in each segment of porous rock, it is an impossible task to measure these quantities on each and every porous rock sample.

In the attempt to use Poiseuille's flow equation to define flow in a porous rock, it was assumed that a series of tubes of length L comprised the flow network. If these tubes are interconnected, and are not individual tubes over the length L, then the derivation would have to account for the interconnection of the flow channels.

For unconsolidated sands, it was found that an expression of the friction factor f could be obtained in terms of Reynolds number. But for consolidated sandstones it was found that a different relationship existed between the friction factor and Reynolds number for each sample investigated. If a single relationship could have been obtained for consolidated sandstones as was obtained for unconsolidated sandstones, then it would have been necessary to classify rocks only as to average grain diameter and weather consolidated or unconsolidated. As this is not possible, it again becomes evident that another method of expressing fluid conductance of rocks must be used.

The preceding attempts to determine a means of calculating the conductance of rock were made to augment for or made to supplant the empirical relationship of permeability as developed by Darcy. The pore structure of rocks does not permit simple classification, and therefore empirical data are required in most cases. In 1856, Darcy investigated the flow of water through sand filters for water purification. His experimental apparatus is shown schematically in **Figure 4**. Darcy interpreted his observations so as to yield results essentially as given in **Equation 9.**

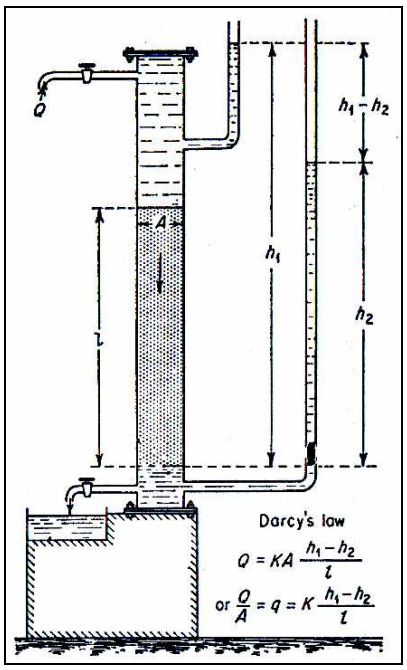

Figure 4. Hubbert's Schematic drawing of Henry Darcy's experiment **[68]**

$$Q = KA\frac{h_1 - h_2}{L} \qquad \textbf{(9)}$$

Here Q represents the volume rate of flow of water downward through the cylindrical sand pack of cross-sectional area A and height l. h_1 and h_2 are the heights above the standard datum of the water in manometers located at the input and output faces respectively and represent the hydraulic head at points 1 and 2. K is a constant of proportionality and was found to be characteristic of the sand pack.

Darcy's investigations were confined to flow of water through sand packs which were100 percent saturated with water. Later investigators found that Darcy's law could be extended to other fluids as well as water and that the constant of proportionality K could be written as k/μ where μ is the viscosity of the fluid and k is a property of the rock alone. The generalized form of Darcy's law as presented in API Code 27 is **Equation 10**.

$$v_s = -\frac{k}{\mu}\left(\frac{dP}{ds}\frac{\rho g}{1{,}0133}\frac{dz}{ds}x10^{-6}\right) \qquad \textbf{(10)}$$

where s = distance in direction of flow and is always positive, cm

v_s = volume flux across a unit area of the porous medium in unit time along flow path s cm/sec

z= vertical coordinate, considered positive downward, cm

ρ= density of the fluid, gr/cc

g= acceleration of gravity, 980,665 cm/ sq sec

dp/ds= pressure gradient along s at the point to which v_s refers, atm/cm

μ= viscosity of the fluid, centipoises

k= permeability of the fluid, darcys

$1{,}0133x10^{-6}$ = dynes/(sq cm)(atm)

dz/ds can be expressed as $sin\theta$ where θ is the angle between s and the horizontal. v_s can further be defined as Q/A where A is the average cross-sectional area perpendicular to the lines of flow. The coordinate system applicable to **Equation 9** is shown in **Figure 5**.

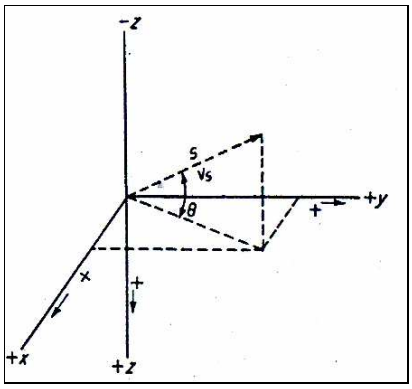

Figure 5. Coordinate system to which generalized Darcy's law is referred **[68]**

Horizontal, rectilinear steady-state flow is common to virtually all measurements of permeability. Consider a block of porous medium as in **Figure 6**. Here *Q*, the volume rate of flow, is uniformly distributed over the inflow face of area *A*.

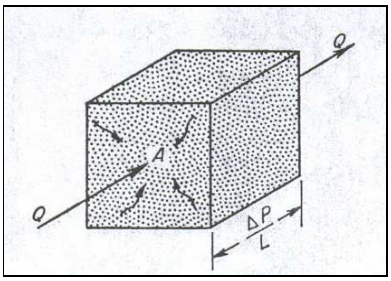

Figure 6. Sand model for rectilinear flow of fluids. **[68]**

If the block is 100% saturated with an incompressible fluid and is horizontal, then *dz/ds=0*, *dP/ds= dP/dx* and **Equation 9** reduces to

$$v_x = -\frac{k}{\mu}\frac{dP}{dx} = \frac{Q}{A} = \frac{k}{\mu}\frac{dP}{dx} \qquad \textbf{(11)}$$

$$\frac{Q}{A}dx = -\frac{k}{\mu}dP \qquad \textbf{(12)}$$

Integrating between the limits 0 and L in x and P_1 and P_2, where P_1 is the pressure at the inflow face and P_2 is the pressure at the outflow face. The following equation is obtained for the horizontal flow.

$$Q = \frac{kA(P_1 - P_2)}{\mu L} \qquad \textbf{(13)}$$

Darcy's law holds only for conditions of viscous flow (i.e. the rate of flow is

sufficiently low to be directly proportional to the pressure gradient). Furthermore, the medium must be 100 % saturated with the flowing fluid and the fluid must not react with the porous medium. **[68]**

3.1.2 Effective and Relative Permeability

In petroleum reservoirs, the rocks are usually saturated with two or more fluids, such as interstitial water, oil and gas. It is necessary to generalize Darcy's law by introducing the concept of effective permeability to describe the simultaneous flow of more than one fluid. In the definition of effective permeability each fluid phase is considered to be completely independent of the other fluids in the flow network. The fluids are considered immiscible, so that Darcy's low can be applied to each individually. Thus Darcy's law can be restated as follows:

$$v_{os} = -\frac{k_o}{\mu_o}\left(\frac{dP_O}{ds} - \rho_o g \frac{dz}{ds}\right) \quad \textbf{(14)}$$

$$v_{gs} = -\frac{k_g}{\mu_g}\left(\frac{dP_g}{ds} - \rho_g g \frac{dz}{ds}\right) \quad \textbf{(15)}$$

$$v_{ws} = -\frac{k_w}{\mu_w}\left(\frac{dP_w}{ds} - \rho_w g \frac{dz}{ds}\right) \quad \textbf{(16)}$$

In the above equations, the subscripts *o, g* and *w* refer to oil, gas and water, respectively.

The effective permeability is a relative measure of the conductance of the porous medium for one fluid phase when the medium is saturated with more than one fluid. This definition of effective permeability implies that the medium can have a distinct and measurable conductance to each phase present in the medium.

Experimentation has established that effective permeability is a function of the prevailing fluid saturation, the rock wetting characteristics and the geometry of the pores of the rock. It becomes necessary, therefore, to specify the fluid saturation when stating the effective permeability of any particular fluid in a given medium. The effective permeability is stated as some numerical value at some given saturation conditions. Just as *k* is the accepted symbol for the permeability, k_o, k_w and k_g are the accepted symbols for the effective permeability to oil, water and gas, respectively. The saturations, if known, should be specified to define completely the conditions at which a given effective permeability exists. Unlike the previously defined permeability, many values of effective permeability exist, one for each particular condition of fluid saturation. Symbolically $k_{o(60,13)}$ is the effective permeability of the medium to oil when the fluid saturations are 60% oil and 13% water and 27% gas. The saturation succession given above, that is, oil and water, is always followed. The gas saturation is understood to be the difference of the sum of oil and water from 100 per cent.

Effective permeabilities are normally measured directly in the laboratory on small core samples. However, owing to many possible combinations of saturation for a single medium, laboratory data are usually summarized and reported as relative permeability. Relative permeability is defined as the ratio of the effective permeability of a fluid at a given value of saturation to the effective permeability of that fluid at 100 per cent saturation. It is normally assumed that the effective permeability is the same for all fluids at 100 per

cent saturation, this permeability being denoted as the permeability of the porous medium. Thus, relative permeability can be expressed symbolically as

$$k_{ro(50,30)} = \frac{k_{o(50,30)}}{k} \quad \textbf{(17)}$$

$$k_{rw(50,30)} = \frac{k_{w(50,30)}}{k} \quad \textbf{(18)}$$

$$k_{rg(50,30)} = \frac{k_{g(50,30)}}{k} \quad \textbf{(19)}$$

which are the relative permeabilities to oil, water and gas, respectively, when the medium is saturated with 50 per cent oil, 30 per cent water, and 20 per cent gas, and *k* is the permeability at 100 per cent saturation of one of the fluid phases. **[68]**

If we define relative permeability as the ratio of effective permeability to absolute permeability, Darcy's law may be restated for a system which contains three fluid phases as follows:

$$v_{os} = -\frac{kk_{ro}}{\mu_o}\left(\frac{dP_O}{ds} - \rho_o g \frac{dz}{ds}\right) \quad \textbf{(20)}$$

$$v_{gs} = -\frac{kk_{rg}}{\mu_g}\left(\frac{dP_g}{ds} - \rho_g g \frac{dz}{ds}\right) \quad \textbf{(21)}$$

$$v_{ws} = -\frac{kk_{rw}}{\mu_w}\left(\frac{dP_w}{ds} - \rho_w g \frac{dz}{ds}\right) \quad \textbf{(22)}$$

where the subscripts *o, g* and *w* represent oil, gas and water, respectively.

Note that k_{ro}, k_{rg} , k_{rw} are the relative permeabilities to the three fluid phases at the respective saturations of the phases within the rock.

Darcy's low is the basis for almost all calculations of fluid flow within a hydrocarbon reservoir. In order to use the law, it is necessary to determine the relative permeability of the reservoir rock to each of the fluid phases; this determination must be made throughout the range of fluid saturations that will be encountered.

In two-phase systems, the relationships are expressed as functions of saturation as shown in **Figure 7**. The subscripts w and nw refer to wetting and non-wetting phases respectively. $S_{w(\max)}$ occurs in a two-phase system when the non-wetting phase reaches the residual non-wetting phase saturation. Similarly, $S_{w(\min)}$ represents the irreducible wetting phase saturation.

The effect of saturation history on relative permeability is illustrated in **Figure 8**. If the rock sample is initially saturated with the wetting phase and the relative permeability data are obtained by decreasing the wetting phase saturation while flowing non-wetting and wetting fluids simultaneously in the core, the process is classified as drainage or desaturation. If the data are obtained by increasing the saturation of the wetting phase, the process is termed imbibition or resaturation. The process used in obtaining relative permeability data in laboratory must correspond to the reservoir process to which these data shall be applied.

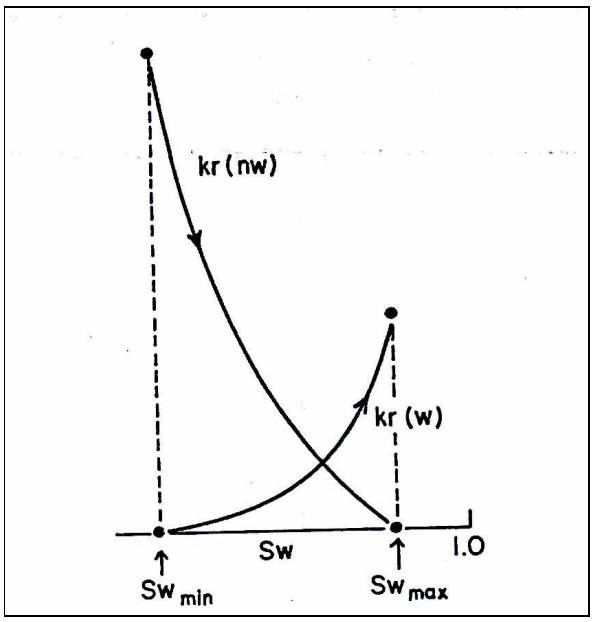

Figure 7. Representation of Relative Permeability **[65]**

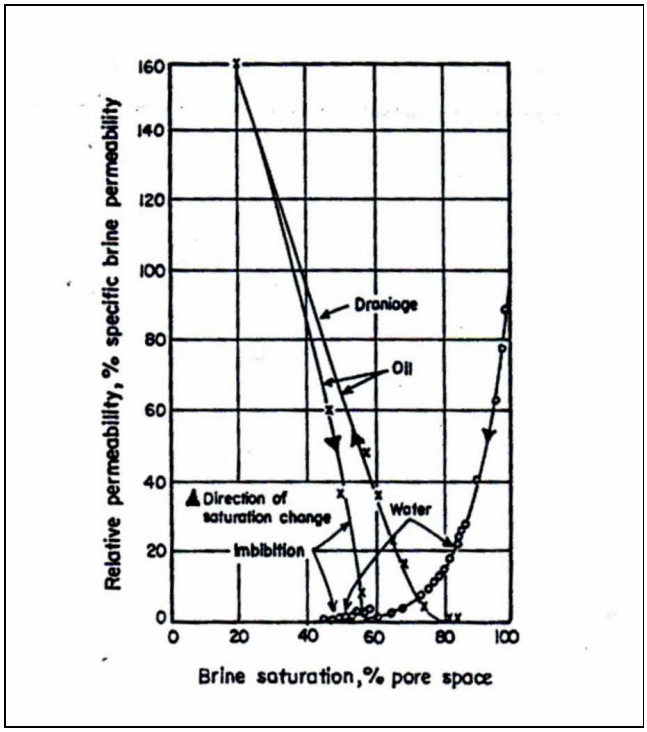

Figure 8. Oil Water Flow Characteristics **[65]**

The difference in the two processes of measuring relative permeability can be seen by observing **Figure 8**. It is noted that the imbibition technique causes the non-wetting phase (oil) to lose its mobility at higher values of saturation than does the drainage technique. The two methods have similar effects on the wetting phase (water) curve. The drainage method causes the wetting phase to lose its mobility at higher values of wetting phase saturation than does the imbibition method. **[65]**

3.1.3 Fracture Permeability

For flow through slots of fine clearances and unit width Buckingham reports that

$$\Delta P = \frac{12\mu v L}{h^2} \quad \textbf{(23)}$$

where h is the thickness of the slot. By analogy to Darcy's law, where

$$\Delta P = \frac{\mu v L}{k} \quad \textbf{(24)}$$

then

$$k = \frac{h^2}{12} \quad \textbf{(25)}$$

where h is in cm and k is in d.**[73]**
The permeability of the slot is given by

$$k = 84{,}4 * 10^6 h^2 \quad \textbf{(26)}$$

It is obvious that in-situ fractures and solution cavities contribute substantially to the productivity of any reservoir. **[65]**
There are several alternatives for modeling the flow in a fractured porous medium. The discrete fracture network model assumes that the capillary forces are dominant with respect to viscous forces and gravity forces, and evaluates the flow paths of the invading phase based on the capillary-driven distribution of the phases. The theory is similar to that presented by Pruess and Tsang **[6]**.

One of the most widely used techniques to model multi-phase flow in a

fractured porous medium is the conventional continuum model that uses approximations of governing equations and constitutive relationships to build a numerical model. In continuum models, the reservoir is discretized into two collocated continua, one called the matrix, and the other called the fracture. One major assumption is that the matrix continuum is comprised of matrix blocks that are separated by fractures. The dimensions of these matrix blocks can be variable throughout the reservoir and are a function of fracture spacing, orientation and width. Four different continuum models, each describing the flow in a fractured reservoir differently, are reported in the literature. The first one is the standard dual porosity model where fluid flow is through the reservoir takes place through the fracture network Warren and Root **[74]**. The matrix blocks act as a source and sink terms. A schematic diagram of connectivity for the standard dual porosity model in that each matrix block is connected to both the fracture blocks and the surrounding matrix blocks, **Figure 9**. Dual permeability model of Kazemi **[14]**, differs from the standard dual porosity model in that each matrix block is connected to both the fracture blocks and the surrounding matrix blocks, **Figure 9**. In this model flow occurs through both the fracture network and the matrix blocks. The multiple-interacting continua (MINC) model introduced by Pruess and Narasimhan **[70]** uses a nested discretization of the matrix blocks. The nested structure of the matrix-fracture transfer allows very efficient representation of the transient flow regime that is often neglected in the standard dual porosity model. One disadvantage with MINC model is that even though it can represent the pressure, viscous and capillary forces, it neglects the effects of the gravity force. The subdomain model by Fung and Collins **[71]** is a variation of the standard dual porosity model and it allows the refinement of the matrix blocks in the vertical direction to represent the gravity drainage process from the matrix block to fracture more accurately. Each matrix block is refined by a fixed number of subdivisions in order to more accurately represent the fluid pressures and saturations within the matrix blocks.

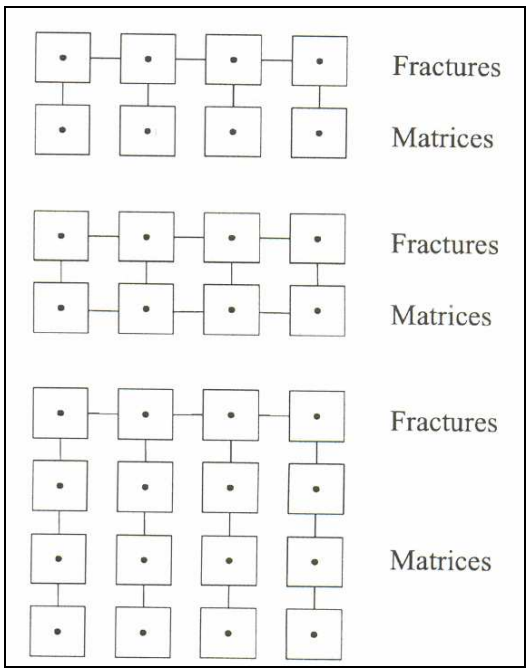

Figure 9. Schematic diagrams of connectivity for the standard dual porosity model (top), the dual-permeability model (middle), and the MINC model (bottom) **[72]**

Dual porosity simulations require two sets of relative permeability data, one for matrix and one for the fracture system. If matrix relative permeability is known from a separate measurement, then it is possible to estimate fracture relative permeability by history matching experimental pressure, production and saturation profiles with a mathematical model. One approach is to use least-squares minimization for history matching. The fracture relative permeability for both phases can be estimated by minimizing an objective function *j*, defined as the difference between the measured and model calculated data at different times. For a typical displacement experiment, the measured data might be pressure drop across the core sample, ΔP, the cumulative volume of displaced phase recovered, *Q,* and the internal saturation profiles, *S*. Then the objective function, *J,* can be expressed as

$$J = \sum_{i=1}^{N} W_{pi}(\Delta P_i^{obs} - \Delta P_i^{cal}) + \sum_{i=1}^{N} W_{qi}(Q_{ti}^{obs} - Q_{ti}^{cal})^2 + \sum_{k=1}^{M}\sum_{i=1}^{n} W_{si}(S_{i,k}^{obs} - S_{i,k}^{cal})^2) \quad \textbf{(27)}$$

where W_i's are the inverses of the variances of the experimental measurement errors which will give the maximum-likelihood/minimum-variance estimate of the parameters. Note that addition of time dependent saturation distribution along the core to the estimation process greatly improves the uniqueness of the solution as stated by Akin and Demiral **[73]**.

In non-linear parameter estimation or curve fitting, it is important to have good initial estimates for the model parameters. Different fracture relative permeability types reported in the literature could be used as a starting point: (a) Romm's relative permeability description. The power-law relative permeability model presented with the following equations reduces to a linear relative permeability model and Corey model when the exponent, *n* is selected as 1 and 4, respectively.

$$S_e = \frac{S_w - S_{wc}}{1 - S_{or} - S_{wc}} \quad \textbf{(28)}$$

$$k_{rw} = k_{rw}^0 S_e^n \quad \textbf{(29)}$$

$$k_{ro} = k_{ro}^9 (1 - S_e)^n \quad \textbf{(30)}$$

The goodness of the fit between different models could then be evaluated by comparing the sum of square residual values given by **Equation 27** for each case. **[72]**

The basics of permeability established in the case of a conventional reservoir remain valid in the case of a fractured reservoir. But in the presence of two systems, (matrix and fractures), permeability may be redefined as matrix permeability, fracture may be redefined as matrix permeability, fracture

permeability and system permeability.

The permeability of a fracture-matrix system may be represented by the simple addition of the permeabilities of matrix k_m and k_f,

$$k_t = k_m + k_f \quad \textbf{(31)}$$

By using conventional cylindrical cores and a conventional parameter the permeability, based on Darcy's equation, is expressed by,

$$k_t = \frac{Q\mu L}{A\Delta P} \quad \textbf{(32)}$$

through which is obtained as the total permeability of the system, and not the single permeabilities of matrix and fractures.

It is generally difficult to obtain representative values of the three terms of permeability - k_t, k_m, k_f in a fractured core. Under certain idealized conditions, the core (shown in **Figure 10**), measurements from vertical and horizontal flow may result in

$$k_{tv} = k_m + k_f \quad \textbf{(33)}$$

$$k_{th} = k_m \quad \textbf{(34)}$$

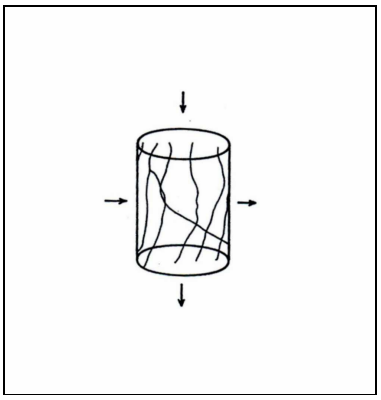

Figure 10. Oriented fractures in cylindrical core **[70]**

The difference between overburden pressure and pore pressure p is called net overburden pressure and increases during reservoir depletion since reservoir pressure p declined. The increasing net overburden pressure and its consequences on fractured reservoir permeability and porosity has been examined in a series of experimental works. **[74,75,76]**. The behavior of the whole bulk volume (matrix+ fracture) was examined through triaxial cell tests. The following has been deduced from the experimental results. Fracture permeability is very much reduced with the increase of confining pressure, which is equivalent to the increasing net overburden pressure. Total rock permeability k_t, as defined in **Equation 31** is expressed by the summation of the two relative permeabilities, k_m and k_f, but fracture permeability compared with matrix permeability is very sensitive to modification of the effective pressure.

In fractured reservoirs, the recovery mechanisms are basically fluid expansion, pore volume contraction, displacement of oil from the matrix, convection and diffusion. For simplicity, the investigators have restricted themselves to waterflood. The idealized element of a fractured reservoir is illustrated in **Figure 11**. Sudation refers to the combined effect of two sets of forces which play a role in the substitution of oil within the matrix by the

water or gas in the surrounding fractures. Gravity forces due to difference in densities between oil and water (or gas), and capillary forces due to interaction of surface forces within the pores.

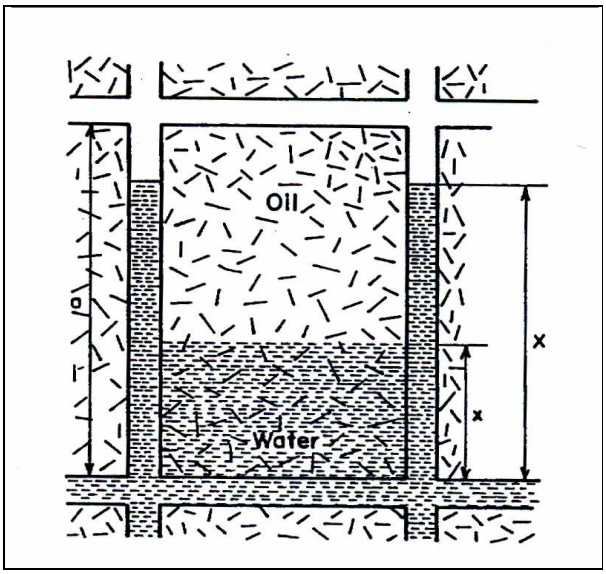

Figure 11. Sudation from a matrix element **[65]**

The flood front moves more rapidly in the fracture network, and bypasses the oil in the matrix: sudation intervenes, and some of the matrix oil is interchanged with water from the fractures, so that an oil/water mixture flows in the network of channels. The oil in the fracture migrates upward under the influence of gravity. The multiple flow is described using the relative permeability concept.

Relative permeabilities in a conventional reservoir are obtained from core analysis. In a fractured reservoir, evaluation of relative permeability curves is complicated because of the nature of the double porosity system, where the fracturing plane between two matrix units develops a discontinuity in the multi-phase flowing process. In the literature, the relative permeability of a specifically fractured reservoir is seldom examined, but the influence of

heterogeneity within a porous media on relative permeability was studied in detail.

Since the behavior of relative permeability versus heterogeneity may be used as a basic approach of a fractured reservoir, it is interesting to examine the influence of flooding rate, core length, and wettability on the laboratory results in a heterogeneous reservoir. **[64,77,78]** Evaluation of relative permeability in heterogeneous rocks through water flooding presents the risk of inaccuracy if an earlier water breakthrough has taken place. This means that the results become uninterruptible if the water breakthrough through fractures or vugs is ahead of the main advancing front in the matrix. The fracture matrix relative permeability curve in this case will resemble an anomalously shaped curve **(Figure 12)** as a result of piston like displacement in some fractures, but not in the fracture-matrix system**. [79]**

Laboratory work **[80]** has shown that: a) For a single fracture, the fluids have a strong tendency to interfere with each other and relative permeabilities reflect a decrease in total mobility. b) For a connected network of fractures, the fluids segregate and flow in different channels: overall mobility is not affected. c) Segregation takes place rapidly as compared to the time scale involved in field operations.

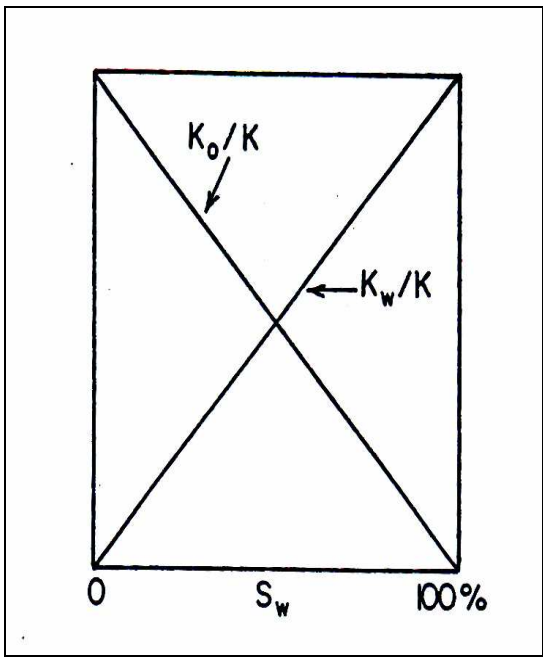

Figure 12. Anomalously shaped relative permeability curve with fracture along core axis**[65]**

The relative permeabilities used for flow in the fracture network are therefore straight lines, and the absence of capillary phenomenon in the fractures means that their end points at water saturations of 0 and 100% are both close to one **(Figure 12). [81]**

Relative permeability is basically associated with intergranular pores. In an intergranular system, the fluid arrangement in pores is controlled by the capillary forces and, therefore, saturation in fluids will depend on the relationship between the wetting and non-wetting phases of all fluids which fill the pores. The wetting phase will occupy the larger pores as a result of the relationship between the wetting and non-wetting phases of all fluids which fill the pores. The wetting phase will occupy the larger pores as a result of the relationship between fluid saturation and pore size distribution. Thus, relative permeability curves will be influenced by the pore frequency curve as well as

by the saturation history **[75].**

If three phases do coexist, the relative permeability of each phase will be influenced by the saturation of the other phases **[82]** in the following ways:

a) k_{rw} will only depend on mobile water, $S_w - S_{wi}$, but remains independent of oil and gas saturation.

b) k_{rg} will only depend on gas saturation. S_g, but is independent of oil and water saturations.

c) k_{ro} depends on oil saturation but is also indirectly dependent on the range of pore size in which there is oil saturation. k_{ro} will be larger if , for example, $S_w = 0{,}45$ and $S_g = 0{,}05$ than if $S_{wi} = 0{,}3$ and $S_g = 0{,}2$, because at the same saturation, in oil, $S_o = 0{,}5$ in the second case oil will be located in smaller pores while in first case the oil will be located in larger pores**.[65]**

3.1.3.1 Capillary Interaction in Fracture/Matrix Systems

The effect of capillary forces in a multi-phase flow process in a fractured porous medium is accounted fro both matrix and fracture capillary pressures. Defining the matrix blocks of a fractured petroleum reservoir as discontinuous block is appropriate only if the fracture capillary pressure is assumed as zero. No reason exists, however, to believe that the assumption of zero fracture capillary pressure is appropriate **[82].** On the contrary, theoretical analysis **[83]** and examination of the field performance of some fractured reservoirs **[84, 85]** indicate a degree of capillary continuity between the matrix blocks.

Three models to represent the capillary pressure of the fracture, P_{cf}, are hypothesized.

$$a - P_{cf} = 0 \quad \textbf{(35)}$$

$$b - P_{cf} = const \quad \textbf{(36)}$$

$$c - P_{cf} = P_{cf}(S_w) \quad \textbf{(37)}$$

The first model has been widely used in the numerical simulation of fractured reservoirs, but a zero fracture capillary pressure does not have a sound basis.

The second model is based on the relationship between the capillary pressure and the distance between the two flat parallel plates.

The third model assumes that the fracture-capillary-pressure curve has a shape similar to that of a porous medium but with major differences in curvature. **Figure 13** shows that the ultimate recoveries of a tall matrix block and a stack of three small matrix blocks where each small block height is equal to a third of the tall block. If the capillary pressure in the fractures between the small matrix blocks is assumed to be zero, most of the oil will be kept inside the matrix. The existence of vertical continuity between the matrix blocks in the stack, however, may cause the ultimate oil recovery to increase substantially to the extent that it matches the recovery from the tall matrix block **[86].**

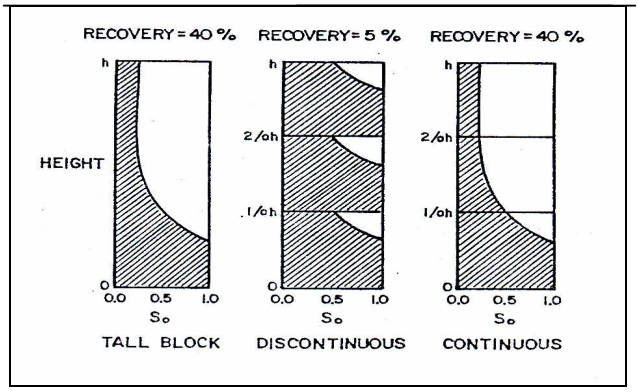

Figure 13. Effect of fracture capillary pressure on the ultimate oil recovery of various blocks

3.1.4 Measurement of Relative Permeability

The relative permeability of a rock to each fluid phase can be measured in a core sample by either 'steady state' or 'unsteady state' methods **[22].** There are numerous steady state methods which can be used to in the laboratory to measure relative permeability, but essentially, all of them depend upon the following technique. A small core sample is chosen and prepared for the test. It is mounted either in Lucite or in a pressurized rubber sleeve. Either the flow system is designed for a high rate of flow and large pressure differential, or each end of the sample is suitably prepared with porous disks and test sections to minimize end effects.

The phases, oil and gas, oil and water, or gas and water which are to be used in the test are introduced simultaneously at the inlet end through different piping systems. Most tests are started with the core sample at 100 per cent

saturation in the wetting phase, and the tests are known as desaturation tests. The two fluids are introduced at a predetermined fluid ratio and are followed through the core until the produced ratio is equal to the steady-state flow condition and the existing saturations are considered to be stable.

The saturation of the various fluids are determined in one of three fashions: (1) Electrodes have been inserted in the test section and the saturations are determined by measurement of the core resistivity; (2) the core section is removed and weighed to determine the saturation conditions; or (3) a volumetric balance is maintained of all fluids injected and produced from the sample. Once the saturation has been measured by one of the above methods, the relative permeability of the two phases at these saturation conditions can be calculated. The injected ratio is increased, removing more of the wetting phase, until once again the system is flowing in steady state condition. The process is continually repeated until a complete relative permeability curve is obtained.

An alternate method is to use the resaturation process where the test section is originally 100 per cent saturated by the non-wetting phase. The results obtained using the desaturation and resaturation processes illustrate a hysteresis effect of the same type discussed earlier in connection with capillary-pressure curves **[68].**

In the steady state method, the primary concern in designing the experiment is to eliminate and reduce the saturation gradient which is caused by capillary pressure effects at the outflow boundary of the core. Steady-state methods are preferred to unsteady state methods by some investigators for rocks of intermediate wettability, although some difficulty has been reported in applying the Hassler **[87]** steady-state method to this type of rock.

In the capillary pressure method, only the non-wetting phase is injected into the core during the test. This fluid displaces the wetting phase and the saturations of both fluids change throughout the test. Unsteady-state techniques are now employed for most laboratory measurements of relative permeability. Some of more commonly used laboratory methods for measuring relative permeability are described below.

3.1.4.1 Steady State Methods

3.1.4.1.1 Penn State Method

In order to reduce end effects due to capillary forces, the sample to be tested is mounted between two rock samples which are similar to the test sample. This arrangement also promotes through mixing of the two fluid phases before they enter the test sample. The laboratory procedure is begun by saturating the sample with one fluid phase (such as water) and adjusting the flow rate of this phase through the sample until a predetermined pressure gradient is obtained. Injection of a second phase, (such as a gas) is then begun at a low rate and flow of this first phase is reduced slightly so that the pressure differential across the system remains constant. After an equilibrium condition is reached, the two flow rates are recorded and the percentage saturation of each phase within the test sample from the assembly and weighing it. This procedure introduces a possible source of experimental error, since a small amount of fluid may be lost because of gas expansion and evaporation. One authority recommends that the core be weighed under oil, eliminating the problem of obtaining the same amount of liquid film on the surface of the core for each weighing.

The estimation of water saturation by measuring electrical resistivity is a faster procedure than weighing the core. However, the accuracy of saturations obtained by a resistivity measurement is questionable, since resistivity can be influenced by fluid distribution as well as fluid saturations. The four-electrode assembly was used to investigate water saturation distribution and to determine when flow equilibrium has been attained. Other methods which have been used for *in situ* determination of fluid saturation in cores include measurement of electric capacitance, nuclear magnetic resonance, neutron scattering, X-ray absorption, gamma-ray absorption, volumetric balance, vacuum distillation, and microwave techniques.

After fluid saturation in the core has been determined, the Penn-State apparatus is reassembled, a new equilibrium condition is established at a higher flow rate for the second phase, and fluid saturations are determined as previously described. This procedure is repeated sequentially at higher saturations of the second phase until the complete relative permeability curve has been established.

The Penn-State method can be used to measure relative permeability at either increasing or decreasing saturations of the wetting phase and it can be applied to both liquid-liquid and gas-liquid systems. The direction of saturation change used in the laboratory should correspond to field conditions. Good capillary contact between the test sample and the adjacent downstream core is essential for accurate measurements and the temperature must be held constant during the test. The time required for a test to reach an equilibrium condition may be 1 day or more.

3.1.4.1.2 Single-Sample Dynamic Method

The apparatus and experimental procedure differ form those used with Penn-State technique primarily in the handling of end effects. Rather than using a test sample mounted between two core samples, the two fluid phases are injected simultaneously through a single core. End effects are minimized by using relatively high flow rates, so the region of high wetting phase saturation at the outlet face of the core is small. The theory which was presented by Richardson et al. for describing the saturation distribution within the core may be developed as follows. From Darcy's law, the flow of two phases through a horizontal linear system can be described by the equations

$$-dP_{wt} = \frac{-Q_{wt}\mu_{wt}dL}{k_{wt}A} \tag{38}$$

$$-dP_{n} = \frac{-Q_{n}\mu_{n}dL}{k_{n}A} \tag{39}$$

where the subscripts wt and n denote the wetting and non-wetting phases, respectively. From the definition of capillary pressure, P_c, it follows that,

$$dP_c = dP_n - dP_{wt} \tag{40}$$

These equations may be combined to obtain

$$\frac{dP_c}{dL} = \left(\frac{Q_{wt}\mu_{wt}}{k_{wt}} - \frac{Q_n\mu_n}{k_n}\right) / A \tag{41}$$

where dP_c / dL is the capillary pressure gradient within the core. Since

$$\frac{dP_c}{dL} = \frac{dP_c}{dS_{wt}} \frac{dS_{wt}}{dL} \quad \textbf{(42)}$$

it is evident that

$$\frac{dS_{wt}}{dL} = \frac{1}{A}\left(\frac{Q_{wt}\mu_{wt}}{k_{wt}} - \frac{Q_n\mu_n}{k_n}\right)\frac{1}{dP_c / dS_{wt}} \quad \textbf{(43)}$$

Richardson et al. **[23]** concluded from experimental evidence that the non-wetting phases saturation at the discharge end of the core was at the equilibrium value, (i.e., the saturation at which the phase becomes mobile). With this boundary condition, **Equation 43** can be integrated graphically to yield the distribution of the wetting phase saturation throughout the core. If the flow rate is sufficiently high, the calculation indicates that this saturation is virtually constant from the inlet face to a region a few centimeters from the outlet. Within this region, the wetting phase saturation increases to the equilibrium value at the outlet face. Both calculations and experimental evidence show that the region of high wetting-phase saturation at the discharge end of the core is larger at low flow rates than at high rates.

Although the flow rate must be high enough to control capillary pressure effects at the discharge end of the core, excessive rates must be avoided. Problems which can occur at very high rates include non-laminar flow.

3.1.4.1.3 Stationary Fluid Methods

Leas et al. **[88]** described a technique for measuring permeability to gas with

the liquid phase held stationary within the core by capillary forces. Very low gas flow rates must be used, so the liquid is not displaced during the test. Rapoport and Leas **[88]** employed a similar technique using semi permeable barriers which held the gas phase stationary while allowing the liquid phase to flow. Corey et al. extended the stationary fluid method to a three phase system by using barriers which are permeable to water but impermeable to oil and gas.

3.1.4.1.4 Hassler **[89]** Method

Semi permeable membranes are installed at each end of the Hassler test assembly. These membranes keep the two fluid phases separated at the inlet and outlet of the core, but allow both phases to flow simultaneously through the core. The pressure in each fluid phase is measured separately through a semi-permeable barrier. By adjusting the flow rate of the non-wetting phase, the pressure gradients in the two phases can be made equal, equalizing the capillary pressures at the inlet and outlet of the core. This procedure is designed to provide a uniform saturation throughout the length of the core, even at low flow rates and thus eliminate the capillary end effect. The technique works well under conditions where the porous medium is strongly wet by one of the fluids, but some difficulty has been reported in using the procedure under conditions of intermediate wettability. The Hassler method is not widely used at this time, since the data can be obtained more rapidly with other laboratory techniques.

3.1.4.1.5 Hafford **[23]** Method

In this method the non-wetting phase is injected directly into the sample and wetting phase is injected through a disc which is impermeable to non-wetting phase. The central portion of the semi-permeable disc is isolated from the remainder of the disc by a small metal sleeve. The central portion of the disc is used to measure the pressure in the wetting fluid at the inlet of the sample. The non-wetting fluid is injected directly into the sample and its pressure is measured through a standard pressure tap machined into the Lucite surrounding the sample. The pressure difference between the wetting and non-wetting fluid is a measure of the capillary pressure in the sample at the inflow end. The design of the Hafford **[23]** apparatus facilitates investigation of boundary effects at the influx end of the core. The outflow boundary effect is minimized by using a high flow rate.

3.1.4.1.6 Dispersed Feed Method

The technique is similar to the Hafford **[23]** and single-sample dynamic methods. In the dispersed feed method, the wetting fluid enters the test sample by first passing through a dispersing section, which is made of a porous material similar to the test sample. This material does not contain a device fro measuring the input pressure of the wetting phase as does the Hafford **[23]** apparatus. The dispersing section distributes the wetting fluid so that it enters the test sample more or less uniformly over the inlet face. The non-wetting phase is introduced into radial grooves which are machined into radial

grooves which are machined into the outlet face of the dispersing section, at the junction between the dispersing material and the test sample. Pressure gradients used for the tests are high enough so the boundary effect at the outlet face of the core is not significant **[22].**

3.1.4.2 Unsteady State Methods

Unsteady-state relative permeability measurements can be made more rapidly than steady-state measurements, but the mathematical analysis of the unsteady-state procedure is more difficult. Welge's **[90]** theory can be used to calculate the ratio of relative permeabilities, whereas, the individual relative permeabilities can be obtained using Johnson et al. technique. The latter is the modified form of Johnson et al. **[91]** technique.

Johnson et al. theory assumes two conditions which must be achieved before the method is applicable. They are that the flowing velocity be high enough to achieve what has been termed stabilized displacement, and that the flow velocity is constant at all cross sections of the linear porous body. In stabilized displacement, the flowing pressure gradient is high compared with the capillary pressure difference between the flowing phases. The high pressure drop insures that the portion of the core in which capillary effects predominate will be compressed to a negligibly small fraction of the total pore space. The assumption of constant flow velocity at all cross sections require that the phases behave as immiscible incompressible fluids. **[22]**

Heaviside and Black **[92]** states that the concept of relative permeability is truly applicable to drainage displacement where as the concept is not strictly

valid for the imbibition process.

3.1.4.3 Capillary Pressure Methods

The techniques which are used for calculating relative permeability from capillary pressure data were developed for drainage situations, where a non-wetting phase (gas) displaces a wetting phase (oil or water). Therefore use of the techniques is generally limited to gas-oil or gas water systems, where the reservoir is produced by a drainage process. Although it is possible to calculate relative permeabilities in a water oil system from capillary pressure data, accuracy of this technique is uncertain; the displacement of oil by water in a water-wet rock is an imbibition process rather than a drainage process.

Data obtained by mercury injection are customarily used when relative permeability is estimated by the capillary pressure technique. The core is evacuated and mercury (which is the non-wetting phase) is injected in measured increments at increasing pressures. Approximately 20 data points are obtained in a typical laboratory test designed to yield the complete capillary pressure curve, which is required for calculating relative permeability by the methods described below.

Several investigators have developed equations for estimating relative permeability from capillary pressure data. Purcell **[93]** presented the equations

$$k_{rwt} = \frac{\int_{0}^{Swi} dS / p_c^n}{\int_{0}^{1} dS / p_c^n} \quad \textbf{(44)}$$

$$k_{rnwt} = \frac{\int_{Swi}^{1} dS / p_c^n}{\int_{0}^{1} dS / p_c^n} \quad \textbf{(45)}$$

where the subscripts wt and nwt denote the wetting and non-wetting phases, respectively and n has a value of 2,0**.** Fatt and Dykstra **[94]** developed similar equations with n equal to 3, 0.

A slightly different result is obtained by combining the equations developed. The results are

$$k_{rwt} = \left(\frac{S_L - S_{wi}}{1 - S_{wi}}\right)^2 \frac{\int_{Swi}^{S_L} dS_w / P_c^2}{\int_{Swi}^{1} dS_w / P_c^2} \quad \textbf{(46)}$$

$$k_{rwt} = \left(\frac{S_L - S_{wi}}{1 - S_{wi}}\right)^2 \frac{\int_{S_L}^{1} dS_w / P_c^2}{\int_{Swi}^{1} dS_w / P_c^2} \quad \textbf{(47)}$$

where S_L is the total liquid saturation.

3.1.4.4 Centrifuge Methods

Centrifuge techniques for measuring relative permeability involve monitoring liquids produced from rock samples which were initially saturated uniformly with one of or two phases. Liquids are collected in transparent tubes connected to the rock sample holders and production is monitored throughout the test. Mathematical techniques for deriving relative permeability data from these measurements are described in **[95,96,97].**

Although the centrifuge methods have not been widely used, they do offer some advantages over alternative techniques. The centrifuge methods are substantially faster than the steady-state techniques and they apparently are not subject to the viscous fingering problems which sometimes interfere with the unsteady-state measurements. On the other hand, the centrifuge methods are subject to capillary end effect problems and they do not provide a means for determining relative permeability to the invading phase.

O'mera and Leas **[97]** describe an automated centrifuge which employs a photodiode array in conjunction with a microcomputer to image and identify liquids produced during the test. Stroboscobic lights are located below the rotating tubes and movement of fluid interfaces is monitored by the transmitted light. Fluid collection tubes are square in cross section, since a cylindrical tube would act as a lens and concentrate the light in a narrow band along the major axis of the tube.

3.1.4.5 Calculation from Field Data

Below will be mentioned the disadvantages of working with the field data.

1) The core on which relative permeability is measured may not be representative of the reservoir in regard to such factors as fluid distributions, secondary porosity, etc.

2) The technique customarily used to compute relative permeability from field data does not allow the pressure and saturation gradients which are present in the reservoir, nor does it allow for the fact that wells may be producing from several strata which are at various stages of depletion.

3) The usual technique for calculating relative permeability from field data assumes that cumulative gas oil ratio at any pressure is constant throughout the oil zone. This assumption can lead to computational errors if gravitational effects within the reservoir are significant.

4) When relative permeability to water is computed from field data, a common source of error is the production of water from some source other than hydrocarbon reservoir. These possible sources of extraneous water include casing leaks, fractures that extend from the hydrocarbon zone into an aquifer, etc. **[22]**

3.2 Factors That Effect Relative Permeability

3.2.1 Effects of Saturation States

At low saturations of the fluid that preferentially tends to wet the grains of a rock, the wetting phase forms doughnut-shaped rings around the grain contact points. These are called pendular rings. The rings do not communicate with each other and pressure cannot be transmitted from one pendular ring to another. Sometimes such a distribution may occupy an appreciable fraction of

the pore space. The amount depends upon the nature and shape of individual grains, distribution as well as degree and type of cementation.

Above the critical wetting-phase saturation, the wetting phase is mobile through a tortoise path under a pressure differential and as the wetting phase saturation increases, the wetting phase relative permeability increases as well. The wetting phase saturation distribution in this region is called funicular and up to a point, the relative permeability to the wetting phase is less than the relative permeability to the non-wetting phase due to the adhesion force between the solid surface and wetting fluid, and the grater tortuosity of the flow path for the wetting phase. The non-wetting phase moves through the larger pores within this range of saturation, but as the saturation of the wetting phase further increases, the non-wetting phase breaks down and forms a discontinuous phase at the critical non-wetting phase saturation. This is called an insular state of non-wetting phase saturation.

Fluid flow studies have shown that when immiscible fluids flow simultaneously through a porous medium, each fluid flows its own flow path. This flow network changes for different ranges of saturation and as the non-wetting phase saturation reduces, the network for this phase breaks down and becomes discontinuous; the remaining stationary islands of the non-wetting phase cannot be displaced at pressure gradients encountered in hydrocarbon reservoirs. This condition is referred to as residual non-wetting phase saturation. Similarly, as the wetting phase saturation decreases, the network through which this phase flows breaks down and becomes discontinuous and immobile. This is referred to as an irreducible wetting phase saturation.

In preferentially oil wet systems, the oil phase relative permeability is found to be strictly a function of oil saturation while in water-wet rocks, the oil phase relative permeability is found to depend on both water and oil saturation. Donaldson and Dean **[98]** have pointed out that under two phase

flow, relative permeability to water was increased when oil, rather than gas was the non-aqueous phase, indicating that water relative permeability is not solely a function of water saturation.

3.3 Polymer Injection

3.3.1 Purposes

The production history of a petroleum reservoir may be divided into different phases. The first, where oil is flowing freely from the reservoir to the production well is the best known, but in most cases, also the shortest. Very early in the life of a reservoir energy must usually be supplied to the porous medium which bears the crude oil so that it continues to flow to the producing wells. This energy is brought into the reservoir by injection of water or gas. With these secondary methods, about 30 to 40 percent of the original oil in place may be recovered, while the rest must be left in the earth. In order to recover some of this oil as well, tertiary methods have been developed which are still the subject of research **[99].**

Polymer flooding consists of adding polymer to the water of a water flood to decrease its mobility. The resulting increase in viscosity, as well as a decrease in aqueous phase permeability that occurs with some polymers, causes a lower permeability ratio. This lowering increases the efficiency of the water flood through greater volumetric sweep efficiency and lower swept zone oil saturation. Irreducible oil saturation does not decrease although the remaining oil saturation does approaching a certain value for both water flooding and polymer flooding. The greater recovery efficiency constitutes the economic

incentive for polymer flooding when applicable. Generally, a polymer flood will be economic only when the water flood mobility ratio is high, the reservoir heterogeneity is high, or a combination of these two occurs.

Polymers have been used in oil production in three modes.
Firstly as near well treatments to improve the performance of water injectors or watered-out producers by blocking-off high conductivity zones.
For many years, relative permeability modifiers (RPMs) have received a great deal of attention from the oil and gas production industry. Because of the completion techniques used in many wells, it is not always practical or cost-effective to protect hydrocarbon interval properly during a water-shutoff treatment. RPMs offer the option of bullheading a treatment without zonal isolation, which is designed to decrease water production with little or no decrease in oil or gas production.

Controlling water production has been an objective of the oil industry almost since its inception. Produced water has a major economic impact on the profitability of a field. Producing 1 bbl of water requires as much or more energy as producing the same volume of oil. Often, each barrel of produced water represents an equal amount of unproduced oil. In addition, water production causes other problems such as sand production, the need for separators, disposal and handling concerns, and the corrosion of tubulars and surface equipment.

Two broad categories of chemical systems are available for reducing water production:
a) Nonsealing systems that allow the flow of fluids through a porous medium.
b) Sealing systems that completely block the flow of fluids in a porous medium.

Non sealing systems are typically dilute solutions of water-soluble polymers.

These polymers most likely reduce effective water permeability by means of a 'wall effect' **[100]** wherein the polymer adsorbs onto the formation, creating a layer of hydrated polymer along the pore throat that inhibits water flow.

Sealing systems are porosity-fill materials that can be valuable when a water-producing zone can be mechanically or chemically isolated. However, in many situations, a target zone can not be isolated, and the sealing system sometimes penetrates zones that should not be treated. Although there are claims that sealing systems will reduce water permeability more than they reduce oil permeability, **[101]** it is extremely risky to pump such a system without zonal isolation. Although some sealants do reduce the permeability to water more than to hydrocarbons, the pressure required for the hydrocarbons to breakthrough the sealant may be so high that hydrocarbon production after the treatment is unlikely.

The lack of non-mechanical methods to selectively place a sealing system and the high costs for gel placement have increased interests in developing chemical systems that selectively reduce the effective water permeability, do not decrease oil permeability , do not require special placement techniques. **[102]**

Secondly, as agents that may be cross-linked in situ to plug high-conductivity zones at depth in the reservoir.

These processes require that polymer be injected with an inorganic metal cation that will cross-link subsequently injected polymer molecules with ones already bound to solid surfaces.

Third, as agents to lower water mobility or water-oil mobility ratio.

The first mode is not truly polymer flooding since the actual oil-displacing

agent is not the polymer. Certainly most polymer EOR projects have been in the third mode.

3.3.2 Polymer Types

Several polymers have been considered for polymer Flooding: Xanthan gum, hydrolised polyacrilamide (HAPM), copolymers (a polymer consisting of two or more different types of monomers) of acrylic acid and acrylamide, copolymers of acrylamide and 2-acrylamide 2-methyl propane sulfonate (AM/AMPS), hydroxyethylcellulose (HEC), carboxymethylhydroxyethylcellulose (CMHEC), polyacrylamide (PAM), polyacrylic acid, glukan, dextran, polyethylene oxide (PEO), and polyvinyl alcohol. Although only the first three have actually been used in field, there are many potentially suitable chemicals, and some may prove to be more effective than those now used.

3.3.2.1 Polyacrylamides

These are polymers whose monomeric unit is the acrylamide molecule. As used in polymer flooding, polyacrylamides have undergone partial hydrolysis, which causes anionic (negatively charged) carboxyl groups to be scattered along the backbone chain. The polymers are called partially hydrolyzed polyacrylamides (HPAM) for this reason. Typical degrees of hydrolysis are 30%-35% of the acrylamide monomers; hence the HPAM molecule is negatively charged, which accounts for its physical properties.

This degree of hydrolysis has been selected to optimize certain properties

such as water solubility, viscosity and retention. If hydrolysis is too small, the polymer will not be water soluble. If it is too large, its properties will be too sensitive to salinity and hardness.

The viscosity increasing feature of HPAM lies in its large molecular weight. This feature is accentuated by the anionic repulsion between polymer molecules and between segments of the same molecule. The repulsion causes the molecule in solution to elongate and snag on others similarly elongated, and effect that accentuates the mobility reduction at higher concentrations.

If the brine salinity or hardness is high, this repulsion is greatly decreased through ionic shielding since the freely rotating carbon-carbon bonds allow the molecule to coil up. The shielding causes a corresponding decrease in the effectiveness of the polymer since snagging is greatly reduced. Virtually all HPAM properties show a large sensitivity to salinity and hardness, an obstacle to using HPAM in many reservoirs. On the other hand, HPAM is inexpensive and relatively resistant to bacterial attack, and it exhibits permanent permeability reduction.

3.3.2.2 Polysaccharides

These polymers are formed from the polymerization of saccharide molecules, a bacterial fermentation process. The polymer is susceptible to bacterial attack after it has been introduced into the reservoir. These disadvantages are offset by the insensitivity of polysaccharide properties to brine salinity and hardness.

The polysaccharide molecule is relatively non-ionic and, therefore, free of the

ionic shielding effects of HPAM. Polysaccharides are more branched to than HPAM, and the oxygen-ringed snagging and adding a more rigid structure to the solution. Polysaccharides do not exhibit permeability reduction.

Today, HPAM is less expensive per unit amount than polysaccharides, but when compared on a unit amount of mobility reduction, particularly at high salinities, the costs are close enough so that the preferred polymer for a given application is site specific. Both classes of polymers tend to chemically degrade at elevated temperatures.

3.3.2.3 Polymer Forms

The above polymers take on three distinctly different physical forms: powders, broths and emulsions. Powders, the oldest of the three, can be readily transported and stored with small cost. These are difficult to mix because the first water contacting the polymer tends to form very viscous layers of hydration around the particles, which greatly slow subsequent dissolution. Broths are aqueous suspensions of about 10% wt polymer in water and which are much easier to mix than powders. They have the disadvantage of being rather costly because of the need to transport and store large volumes of water. Broths are quite viscous so they can require special mixing facilities. In fact, it is the difficulty which limits the concentration of polymer in the broth. Emulsion polymers, the newest polymer form, contain up to 35 wt. % polymer solution, suspended through the use of a surfactant, in an oil carrier phase. Once this water-in-oil emulsion is inverted, the polymer concentrate can be mixed to with make-up water to the desired concentration for injection. The emulsion flows through roughly the same viscosity as the

oil carrier, which can be recycled.

3.3.3 Oil Trapping in Pores

The notion of a wetting phase residual saturation is consistent with our discussion of capillary pressure. Increasing pressure gradients force ever more of the non-wetting phase into pore bodies, causing the wetting phase to retreat into the concave contacts between the rock grains and other crevices in the pore body. At very high pressures, the wetting phase approaches monolayer coverage and a low residual saturation. Because of film instability, residual wetting phase saturation is theoretically zero when capillary pressure is finite.

A residual non-wetting phase saturation, on the other hand, is somewhat paradoxical. After all, the non-wetting phase is repelled by the rocks' surfaces and, given enough contact time, all the non-wetting phase would be expelled from the medium. Repeated experimental evidence has shown this not be the case, and, in fact, under most conditions, non-wetting phase residual oil saturation is as large as wetting phase residual oil saturation. The residual non-wetting phase is trapped in the larger pores in globules several pore diameters in length**.**

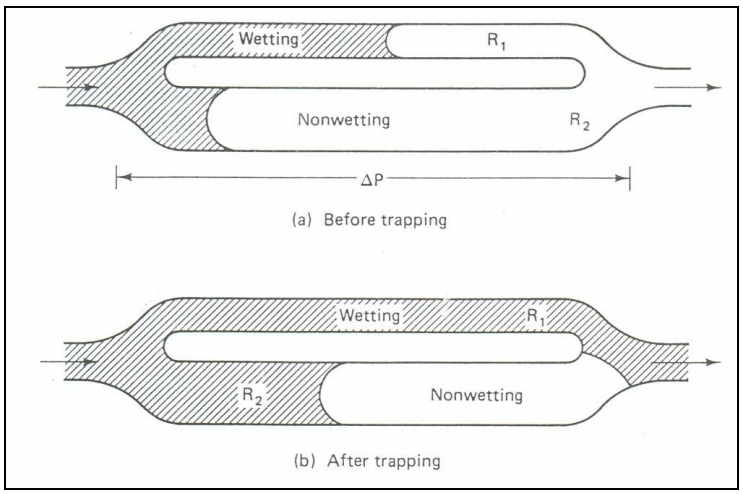

Figure 14. Schematic of pore doublet model **[102]**

The mechanism for a residual phase saturation may be illustrated through two simplified REV-scale models. **Figure 14** shows the double pore, or pore doublet model, a bifurcating path in the permeable medium, and **Figure 15** shows three versions of the pore snap-off model, as single flow path with variable cross-sectional area. Each model contains a degree of local heterogeneity. The pore doublet model shows different radii flow paths, and the pore snap-off model shows different cross-sectional areas in each of the flow paths. This local heterogeneity is needed for there to be a residual non-wetting phase saturation.

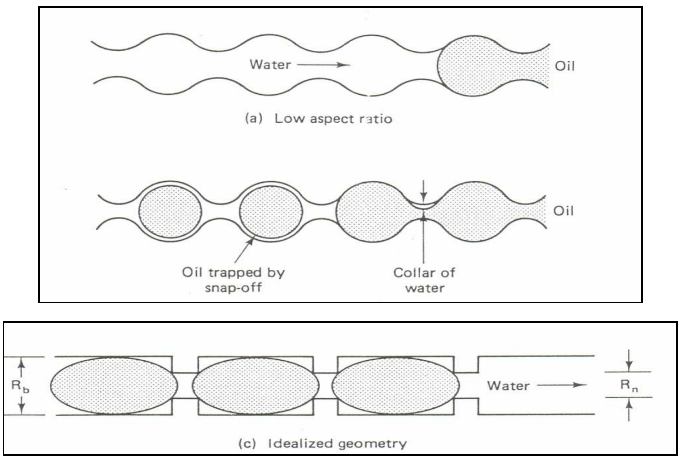

Figure 15. Various geometries of the pore snap-off model **[102]**

3.3.3.1 The Pore Doublet Model

This model assumes well-developed Poisseuille flow occurs in each path of the doublet, and the presence of the interface does not affect flow. Both assumptions would be accurate if the length of the doublet were much larger than the largest path radius and the flow were very slow. To investigate the trapping behavior of the doublet, the following ratio of the average velocities in flow paths can be examined.

$$\frac{v_1}{v_2} = \frac{4N_{vc} + (\frac{1}{\beta} - 1)}{\frac{4N_{vc}}{\beta^2} - \beta^2(\frac{1}{\beta} - 1)} \qquad \textbf{(48)}$$

where $\beta = R_2 / R_1$ is a heterogeneity factor, and

$$N_{vc} = \left(\frac{\mu L_1 q}{\pi R_1^3 \sigma \cos\theta}\right) \quad \textbf{(49)}$$

is a dimensionless ratio of viscous to capillary forces named as the local capillary number.

In the limit of negligible capillary forces, (large capillary number), the velocity in each path of the doublet is proportional to its squared radius. Hence the interface in the large-radius path will reach the outflow end before the small radius path, and the non-wetting phase will be trapped in small-radius path.

But if viscous forces are negligible, the small-radius path will imbibe fluid at a faster rate than is supplied at the doublet inlet. The interface velocity in the large-radius path is negative in the fluid-starved doublet, whereas the velocity in the large radius path is negative in the fluid starved doublet, whereas the velocity in the small-radius path is greater than that at the doublet inlet. The situation is in disagreement with the premises of the derivation: If the interface seals-off the small-radius path at the doublet inlet, the flow in the small-radius tube will be zero.

Though the extreme negligible viscous forces are hard to visualize, it is easy to imagine and intermediate case where viscous forces are small, but not negligible compared to capillary forces. Now the doublet is no longer starved for fluid, but the interface in the small-radius path is still faster than in the large radius path. The non-wetting phase is trapped in the large-radius path as shown in **Figure 14.**

Besides explaining how a non-wetting phase can become trapped at all, the simplified behavior of the pore doublet illustrates several qualitative observations about phase trapping.

1) The non-wetting phase is trapped in large pores, the wetting phase in cracks and crevices.
2) Lowering capillary forces will cause a decrease in trapping. This decrease follows from simple volumetric calculations since fluids trapped in small pores will occupy smaller volume fraction of the doublet than those in large pores.
3) There must be some local heterogeneity to cause trapping. In this case, the heterogeneity factor β must be greater than 1. Simple calculations with the pore doublet shows that increasing the degree of the heterogeneity increases the capillary number range over which the residual phase saturation changes.

But as a quantitative tool for estimating trapping, the pore doublet greatly overestimates the amount of residual non-wetting phase at low capillary number. At high capillary number, little evidence supports non-wetting phase trapping in the small pores. Most important, the capillary number defined by **Equation (49)** is difficult to define in actual media; hence the pore doublet model is rarely used to the REV scale.

3.3.3.2 Snap-Off Model

The snap-off model can readily translate the REV scale. The exact geometry of the model **(Figure 16)** is usually dictated by the ease of with which the resulting mathematics can be solved.

The snap-off model assumes as single flow path of variable cross-sectional area though which is flowing a non-wetting phase. The sides of the flow path are coated with a wetting phase so that a uniquely defined local capillary

pressure exists everywhere. But this capillary pressure varies with position in the flow path; it is large where the path is narrow and small where it is wide. For certain values of the potential gradient and pore geometry, the potential gradient in the wetting phase across the phase segment can be less than the capillary pressure gradient across the same segment. The external force is now insufficient to compel the non-wetting phase to enter the next pore constriction. The non-wetting phase then snaps off into globules that are localized in the pore bodies of the flow path. By this hypothesis, then, the condition for reinitializing the flow of any trapped globule is

$$\Delta\Phi_w + \Delta\rho g \Delta L \sin\alpha \geq \Delta P_c \qquad \textbf{(50)}$$

Where $\Delta\Phi_w$ and ΔP_c are the wetting phase potential and capillary pressure changes across the globule. ΔL is the globule size, $\Delta\rho = \rho_w - \rho_{nw}$ and α is the angle between the globule's major axis and the horizontal axis.

Equation 50 suggests a competition between external forces (viscous and gravity) and capillary forces that was also present in the pore doublet model though both models are quite different.

Of course, in any real permeable medium, local conditions approximating both the pore doublet and the snap-off model will occur. The theoretical treatment of the snap-off model again illustrates the basic requirements for non-wetting trapping: non-wetting trapping in large pores, the need for local heterogeneity, and strong capillary forces.

3.3.4 Trapping in Actual Media

We can now discuss the experimental observations of trapping in actual media. The most common experimental observation is a relationship between residual non-wetting and wetting phase saturations and a local capillary number. We call this relationship the capillary desaturation curve (CDC). **Figure 14** shows a schematic CDC curve. Typically these curves are plots of percent residual (non-flowing) saturation for the non-wetting or wetting phases on the y-axis versus a capillary number on a logarithmic x axis. The capillary number N_{vc} is a dimensionless ratio of viscous to local capillary forces, variously defined. At low N_{vc}, both wetting and non-wetting residual saturations are roughly constant at plateau values. At some N_{vc} designated as the critical capillary number $(N_{vc})_c$, a knee in the curves occurs, and the residual saturations begin to decrease. Complete desaturation – zero residual phase saturations – occurs at the total capillary $(N_{vc})_t$ number shown in **Figure 15**. Most water floods are well onto the plateau region of the CDC where, as a rule, the plateau residual wetting phase saturation is less than the residual non-wetting phase saturation. Frequently, the two CDC curves are normalized by their respective plateau values.

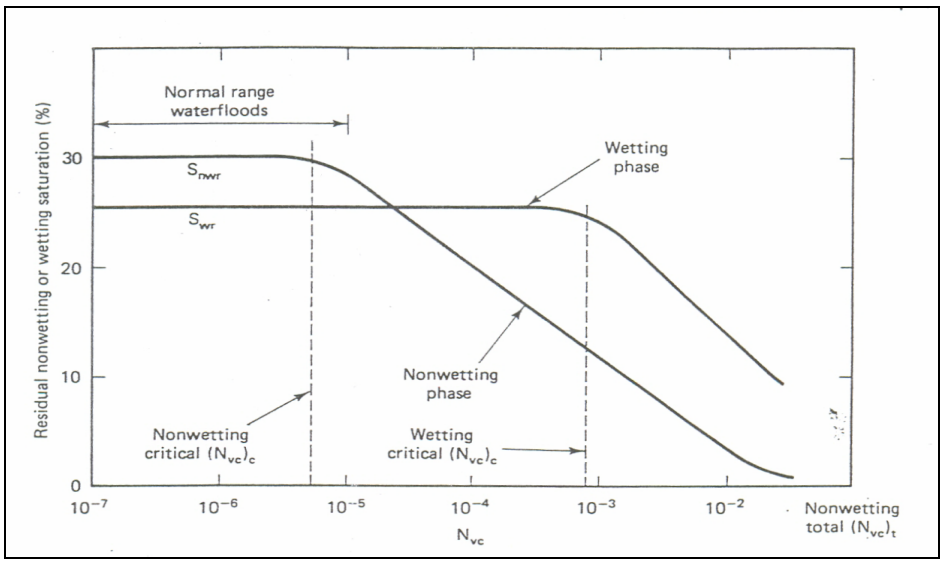

Figure16. Schematic capillary desaturation curve **[102]**

Summary of the results of experimentally determined CDC curves can be found in the list at Lake's book **[102]**.

No experimental data has been reported on actual reservoir permeable media; most experimental work has used pure hydrocarbons and synthetic brine. The plateau values of residual wetting and non-wetting phase saturations show considerable variation (there are more non-wetting phase measurements). The $(N_{vc})_c$ and $(N_{vc})_t$ for the non-wetting phase are less than the respective values for the wetting phase. For the non-wetting phase $(N_{vc})_c$ is in the 10^{-5} to 10^{-4} range whereas the $(N_{vc})_t$ is usually 10^{-2} to 10^{-1}. For the wetting-phase $(N_{vc})_c$ is roughly equal to the non-wetting $(N_{vc})_t$, whereas the wetting critical $(N_{vc})_c$ is 10^{-1} to 1. More precise conclusions are not warranted because of the variation in N_{vc} definitions and in the experimental conditions.

Three general observations based on the CDC curve are:

1) Wettability is important. The wetting phase normalized CDC curves should

be two to three factors of 10 to the right of a non-wetting phase CDC curve, however, intuitively; the two CDC curves should approach each other at some intermediate wetting condition.

2) Pore size distribution is also important. The critical-total N_{vc} range should increase with increasing pore size distribution for both wetting and non-wetting phases.

3) The critical-total N_{vc} range for the non-wetting phase should be greater than for the wetting phase with, again, a continuous shift between wettability extremes **[102].**

3.3.5 Mobility Ratio and Polymer Recovery Mechanisms

In order to appreciate how the situation for the flooding may be remedied using polymer, it is necessary to introduce the idea of mobility ratio, M, defined as:

$$M = \frac{\lambda_o}{\lambda_w} \frac{(\mu_o / k_o)}{(\mu_W / k_W)} \qquad \textbf{(51)}$$

where λ, μ and k are mobility, viscosity and effective permeability respectively and the subscripts o and w refer to oil and water. Oil is left behind in a water flood either because it is trapped by the capillary forces (residual oil) or because it is in someway by-passed. In order to remobilize this oil, it is necessary to increase greatly the viscous-to-capillary force balance between the water and oil phases in the displacement. This is characterized by the capillary number, N_c, which can be taken as *(vμ/σ),*

where v is the fluid velocity, μ is the fluid viscosity, and σ is the interfacial tension. To mobilize the residual oil, the quantity N_c must be increased by several orders of magnitude from the value it normally has in a water flood (N_c approximately equal to10^{-6}) and the only realistic way to achieve this is by drastically lowering the interfacial tension. This can be done by adding a surfactant (detergent) to the displacing fluid, and it is the recovery of this residual oil that is the target of low-tension surfactant flooding. However, in going from water to polymer flooding, the viscous forces *(μ)* are usually considered to be increased by up to one order of magnitude, which is not thought to be sufficient to mobilize residual oil. Thus, the target for polymer flooding is considered to be any oil that is bypassed in the water flood but does not include the residual oil.

As noted above, the bypassed oil may arise because of the unfavorable mobility ratio in the flood (μ_o / μ_w) or because there are large-scale heterogeneities such as stratification or channeling present in the reservoir. For linear (or one-dimensional, 1-D) floods, it is only necessary to consider the microscopic or local displacement efficiency of the water flood at higher mobility ratios (say M>1). For values of M≤1, the 1-D flow shows virtually piston-like displacement with almost full recovery of oil at water breakthrough. Thus there is little point in considering polymer to improve the situation, and it is only when M≥5 that polymer (in 1-D) would be seriously considered. At these unfavorable M values, the theory of immiscible displacement predicts a lower water saturation shock front with a considerable 'tailing' period of two phase (oil/water) production after breakthrough. The role of the polymer is to improve the microscopic displacement efficiency in such cases by lowering the effective M, mainly by increasing the water viscosity, μ_w, but to some extent, also by lowering the aqueous phase permeability, k_w (pore blocking). Thus, when polymer is added, to the drive brine, in a linear flood where the water flood M is high, it effectively reduces

M and leads to a more piston-like displacement with higher front heights and hence higher recovery efficiency. However, the situation is a little more complex in linear polymer flooding because of the presence of a bank of (low-viscosity) connate water which is driven in front of the injected polymer. This leads to double shock front behavior**. [103]**

3.3.6 Mechanics of Polymer Flooding

Flooding petroleum reservoirs with water soluble polymers may be regarded as the most economic tertiary oil recovery method though by definition polymer flooding does not increase the microscopic sweep efficiency of the reservoir rock, the remaining volume of oil in the porous media is assumed to be the same after a polymer flood as after a water flood. Thus the physical laws derived for water flooding may be applied to the injection of polymer solutions. The two phase flow of crude oil and polymer solution may be described by using the relative permeability concept.

Figure 17 shows the mobility ratio curves of an experimental study performed by Welge. **[90]**. It can be seen that the mobility ratio in a water flood at low water saturations may also be below 1 and that at high saturations the mobility ratio for the polymer flood may become greater than 1.

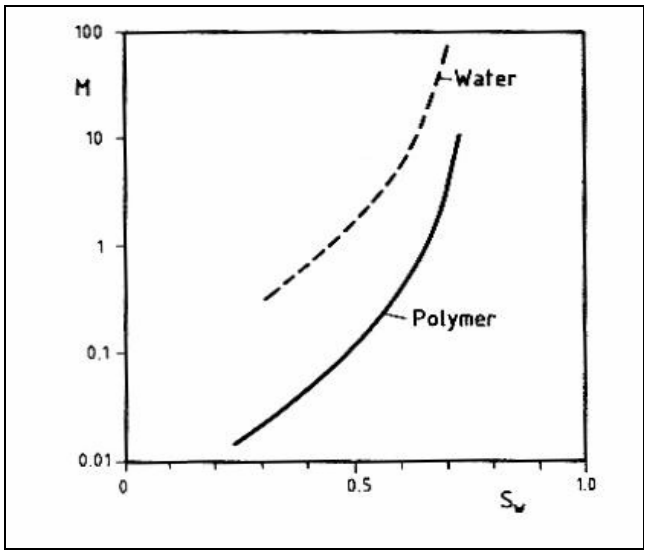

Figure 17. Mobility ratio for the displacement of oil by water and polymer solution as a function of saturation of the displacing phase according to Welge **[95]**.

3.3.7 Polymer Retention

When polymers are added to the displacement fluids, the objective is usually to viscosify the injection brine using the properties of the transported polymer. However there may be significant interactions between the transported polymer and molecules and the porous medium. Such interactions will cause the polymer to be retained by the porous medium and will lead to the formation of a bank injection fluid wholly or partially denuded of polymer. Clearly, this bank of fluid will have a viscosity which is much lower than the injected polymer solution and this will generally lead to a reduction in the efficiency of the polymer flood. However, this polymer retention on the porous medium may also cause some reduction of the rock permeability,

which can contribute to the oil recovery mechanism, as is discussed further below. However, overall, the retention of polymer tends to reduce oil recovery despite the permeability reduction contribution. In fact, it is the author's observation, that the level of polymer retention is one of the key factors in determining the economic viability of a polymer flood. Thus it is of great importance to establish the correct retention levels for a given proposed field polymer flood. The conditions under which such laboratory measurements should be made are extremely important so that for relevant figures for retention are available for the simulation assessment of the polymer flood. For example, the levels of polymer retention (and the accompanying permeability reduction) will vary in rocks of different permeability. If there is a certain amount of field core available, the 'most appropriate' core material on which to carry out retention experiments must be selected. Not all such experiments will be of equal value in assessing the polymer flood when the effects of polymer retention on oil recovery are quantified.

There are three main retention mechanisms which are thought to act when polymer solution flows through porous media. These are Polymer adsorption, mechanical entrapment and hydrodynamic retention.

3.3.7.1 Polymer Adsorption

Adsorption refers to the interaction between the polymer molecules and the solid surface— as mediated by the solvent (being aqueous). This interaction causes polymer molecules to be bound to the surface of the solid mainly by physical adsorption— Van der Waal's and hydrogen bonding—rather than by

chemisortpion in which full chemical bonds are formed between the molecule and the surface. Essentially, the polymer occupies surface adsorption sites, and the larger the surface area available, the higher the levels of adsorption that are observed. Adsorption is the only mechanism that removes polymer from the bulk solution if a free solid powder, such as silica sand or latex beads, is introduced into the bulk solution and stirred until equilibrium is reached.

3.3.7.2 Mechanical Entrapment of Polymer

The two mechanisms of mechanical entrapment and hydrodynamic retention are related and occur in flow through porous media. They play no part in free powder/bulk solution experiments. Retention by mechanical entrapment is viewed as occurring when larger polymer molecules become lodged in narrow channels as shown in **Figure 18** along with the other retention mechanisms. This has been studied by several workers. When the effective size of polymer molecules (HPAM) in solution was examined, of molecular size, some of the HPAM molecules should be entrapped as they flow through certain Barea samples. This can be envisaged by imagining the complex pore structure as being a large interconnected network of with a vast number of possible 'routes' connecting the inlet and the outlet of a core. A certain fraction of the network of the elements would consist of narrow pore throats. Thus as the polymer solution passed through this complex network, the molecules would take various routes and some molecules would be trapped in the narrow pores. These would block, and flows in these elements would consequently reduce, probably trapping more molecules upstream of the blockage.

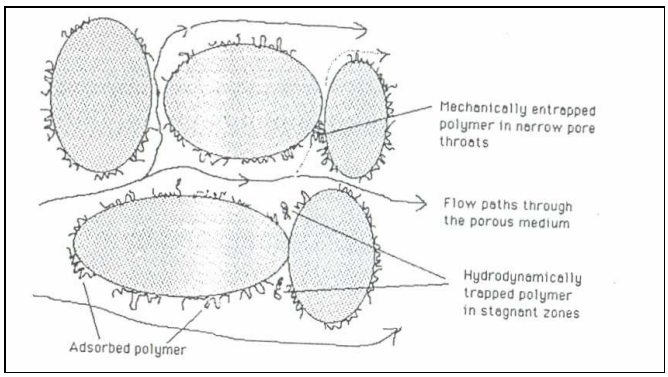

Figure 18. Schematic diagram of polymer retention mechanisms in porous media **[103]**.

If this physical picture of polymer mechanical entrapment is correct, then, there are several consequences that might be expected. Firstly, the concentration in the effluent of the core would either fail to reach full input concentration or would only do so after many pore volumes (pv) of fluid throughput. The latter situation would be the case where there were a small number of entrapment sites which had been fully blocked, thus all subsequent flow to be through the larger channels where no further entrapment occurred. Secondly, the distribution of mechanically entrapped polymer along the core should be largest close to the inlet and decrease approximately exponentially along the core. The third consequence of the deep-bed filtration model would be that, if there were above a critical number of 'entrapment sites', in the network, the core would ultimately block completely and the entrapment sites, and the permeability would fall to practically zero. Even for sub critical numbers of accompanying entrapment sites, there would be very large levels of retention and the accompanying permeability reduction would probably be unacceptable, since this effect would be largest close to the polymer injector. There is in fact experimental evidence, for the above predictions from the deep-bad filtration model.

3.3.7.3 Hydrodynamic Retention

Hydrodynamic retention of polymer is the least well defined and understood retention mechanism. The idea arose from the observation that, after steady state was reached in a polymer retention experiment in a core, the total level of retention changed when the fluid flow rate was adjusted to a new value.

The physical structure of the hydrodynamic retention mechanism that has been suggested is illustrated in **Figure 18**. Here, some of the polymer molecules are thought to be trapped temporarily in stagnant flow regions by hydrodynamic drag forces. In such regions it may be possible for the local polymer concentration to exceed that of the injected fluid. When the flow stops, these molecules may diffuse out into the main flow channels and, when the flow recommences, they are produced as a peak in polymer concentration. Although this mechanism for hydrodynamic retention is quite plausible, it is still not firmly established and alternative physical pictures may emerge when this phenomenon is studied further. Recently, a more detailed description of the physical phenomena involved in the hydrodynamic retention of macromolecules has been briefly discussed.

3.3.8 Degradation of Polymers

3.3.8.1 Mechanical Degradation

When a polymer solution is exposed to high shear conditions, the molecule

may be scissored. High shear conditions occur during mixing of polymer solutions or during the conveyance of a polymer solution in pumps and chokes or during injection in perforations, or in the formation near the well bore where the polymer solution is flowing at high velocities.

The chemical degradation of polymers in aqueous solutions is mainly affected by the presence of divalent ions and oxygen, and the temperature. Divalent hydrocarbons influence the hydrolysis of polyacrylamides and thus their formation brines. If from the handling at the surface, oxygen is introduced into such waters, the iron cation may be oxidized to Fe^{3+} which in turn may flocculate polyacrylamides as well as polysaccharides.

Biological degradation is mainly a problem of biopolymers, and preferentially at lower temperatures and salinities. By biological degradation is meant that the polymer molecule is destroyed by bacteria or chemical processes governed by enzymes **[67].**

3.3.9 Artificial Neural Networks

3.3.9.1 Definition of ANN

Neural computing is an alternative to programmed computing which is a mathematical model inspired by biological models. This computing system is made up of a number of artificial neurons and a huge number of interconnections between them. According to the structure of the connections, different classes of network architectures are identified **(Figure 19)**.

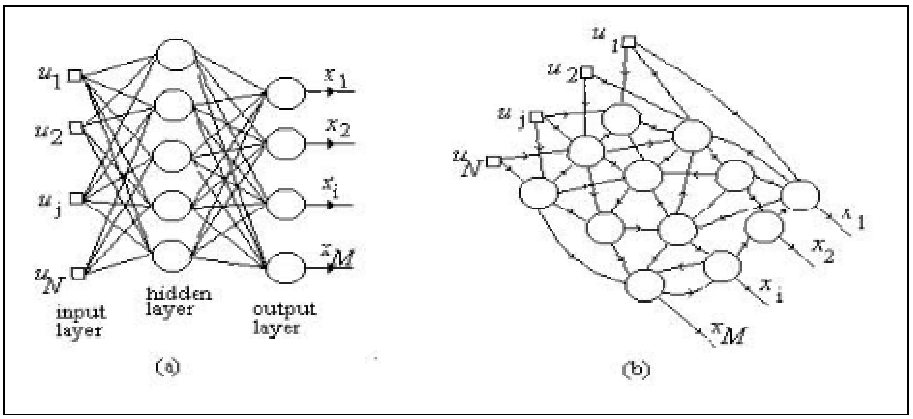

Figure 19. Layered feed-forward neural network, b) Non-layered recurrent neural network **[104]**

In feed-forward neural networks, the neurons are organized in the form of layers. The neurons in a layer get input from the previous layer and feed their output to the next layer. In this kind of networks connections to the neurons in the same or previous layers are not permitted. The last layer of neurons is called the output layer (right column) and the layers between the input and output layers are called the hidden layers. The input layer (left column) is made up of special input neurons, transmitting only the applied external input to their outputs. In a network if there is only the layer of input nodes and a single layer of neurons constituting the output layer then they are called single layer network. If there are one or more hidden layers (middle column), such networks are called multi layer networks. The structures, in which connections to the neurons of the same layer or to the previous layers are allowed, are called recurrent networks.

The lines represent weighted connections (i.e., a scaling factor) between processing elements. The performance of a network as shown in **Figure 20** is measured in terms of a desired signal and an error criterion. The output of the network is compared with a desired response to produce an error. An algorithm called back-propagation **[105]** is used to adjust the weights a small

amount at a time in a way that reduces the error. The network is trained by repeating this process many times. The goal of the training is to reach an optimal solution based on the performance measurement **[106].**

3.3.9.2 Application of ANNs in Geosciences

Within recent years there has been a steady increase in the application of neural network modeling in engineering. ANNs have been used to address some of the fundamental problems, as well as specific ones that conventional computing has been unable to solve, in particular when engineering data for design, interpretations, and calculations have been less than adequate. Also with the recent strong advances in pattern recognition, classification of noisy data, nonlinear feature detection, market forecasting and process modeling, neural network technology is very well suited for solving problems in the petroleum industry.

Ali **[107]** highlighted the key factors in the design or selection of neural networks and the limitations of the commonly used ANN models. Romeo et al. **[108]** used a simple multiplayer perceptron with 23 neurons to identify seismic data. Miller et al. **[109]** outlined the use of ANNs in classification of remote sensing data. Fletcher et al. **[110]** presented models that can predict oil well cement properties using an artificial neural network approach. Trained with diffuse reflectance Fourier Transform spectra of different cements, proposed ANN models correlated particle size distributions and cement thickening time with reasonable accuracy. Vukelic et al. **[111]** presented a case study of the development of a neural network that would decide if a reservoir would produce gas, liquid or nothing. Another implementation of ANNs, presented by Mohaghegh et al. **[112]**, was the

characterization of reservoir heterogeneity. The ANN was able to predict rock permeability, porosity, oil, water and gas saturations with accuracies comparable to actual laboratory core measurements. Aside from back-propagation ANNs, radial-basis-function (RBF) ANNs were also used to estimate porosity distribution **[113]**. In their study, Wang et al. **[113]** combined RBF ANNs with krigging techniques to estimate different yet equally probable porosity distributions. Other applications of ANNs in the petroleum industry include papers that employ ANN to pick the proper reservoir model for well testing purposes **[114]**, analyze and classify beam pumping unit dynamometer diagrams **[115]**.

3.3.9.3 Model Development

The ANN developed in this study is a back propagation layered feed forward network that consists of three layers: input, hidden, and output layer. The learning algorithm is simply composed of two sub-sequent steps; feed forward and error back propagation. The learning rate of the ANN could be adjusted by changing momentum factor (alpha) and learning rate modifier (eta).

3.3.10 Reservoir Simulation

3.3.10.1 General

Reservoir simulation is based on well known reservoir engineering equations

and techniques – the same equations and techniques the reservoir engineer has been using for years. In general simulation refers to the representation of some process by either a theoretical or physical model. Below well be considered the development and use of models that describe the reservoir performance under various operating conditions.

Reservoir simulation itself is not really new. Engineers have long used mathematical models in performing reservoir engineering calculations. Before the development of modern digital computers, however, the models were relatively simple. For example, when calculating the oil in place volumetrically, the engineer simulated the model by a simple model in which average values for the porosity, saturation and thickness were used.

Although simulation in the petroleum industry is not new, the new aspects are that more detailed reservoir features, and thus more accurate simulations, have become practical because of the capability afforded by the computers now available. The more detailed description, however, requires complex mathematical expressions **[116].**

Modeling a reservoir by dividing it into cells provides flexibility. High-speed computers permit multiple runs of a reservoir model to test different methods of field operations or to check the sensitivity of reservoir behavior to unknown rock or fluid properties.

The multicell models have many valid applications but they can also be misused because the model is only providing answers that the input data are forcing it to provide. Therefore a careful analysis and selection of input data is imperative. The engineer can usually obtain representative data on reservoir rock and fluid properties. The greater difficulty lies in properly selecting such items as relative permeability, vertical permeability and cell size.

3.3.10.2 Basic Analysis

If a reservoir is fairly homogeneous, average values of the reservoir properties, such as porosity, are adequate to describe it. The average pressure, time and production behavior of such a reservoir under a solution gas drive known, the material balance equation (MBE) is used.

The cumulative net withdrawal is the difference between the oil that leaves the reservoir and the oil that enters it. In this basic analysis, there is no oil entering the reservoir since the boundaries are considered impermeable to flow. Thus, the material balance reduces to its simplest form. Such a reservoir model is called the tank model **(Figure 20).** It is zero dimensional because, rock, fluid properties, and pressure values do not vary form point to point. Instead, they are calculated as average values for the whole reservoir. This tank model is the basic building block of reservoir simulators.

Consider a reservoir represented by sandbar. Let the two halves of the sandbars vary in lithology. The sandbar as a whole can not be represented by average properties, but each half can. Thus, the sandbar consists of two tank units, or cells, as they are normally called. The MBE describes the fluid behavior in each cell as in the previous tank model. However, the net withdrawal term of the MBE is more complicated because there can be migration of fluid from one cell to another, depending on the average pressure values of the two cells. This fluid transfer between the two cells is calculated by Darcy's law. The MBE together with Darcy's law describes the behavior of each cell. This model is not a zero-dimensional reservoir simulator since reservoir parameters may vary between the two cells. Instead, it is a one dimensional model, because it consists of more than one cell in one direction and of only one cell in the other two directions **(Figure 21).**

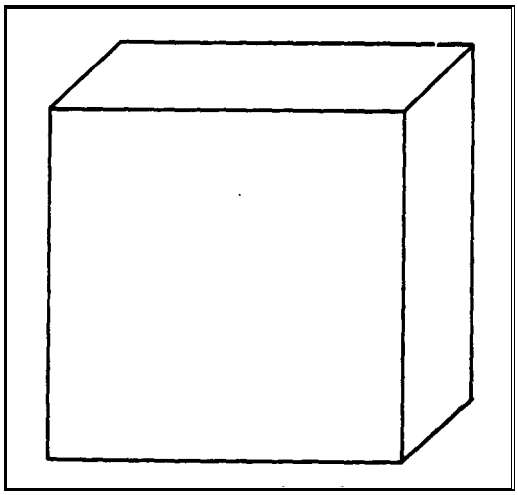

Figure 20. Tank model

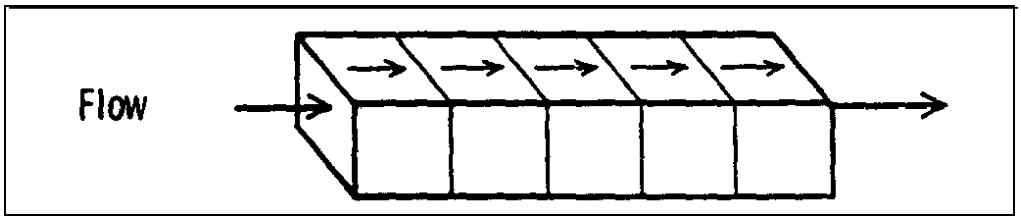

Figure 21. One-dimensional simulator

This analysis can be extended to reservoirs where properties as well as pressure values vary in two dimensions, and to other where the variation occurs in two dimensions. The simulators representing these reservoirs are called, respectively, two-dimensional and three-dimensional simulators, as illustrated in Figures 22 and 23. Thus a two dimensional reservoir simulator consists of more than one cell in two dimensions and one cell in the third dimension. And a three-dimensional simulator consists of more than one cell in all of the three dimensions.

Regardless of the number of dimensions used, the MBE is the basic equation

describing the fluid behavior within a cell; and Darcy's law describes the interaction between the cells. In one-, two-, and three dimensional models each cell, except the boundary cell, interacts respectively, 2, 4, and 6 cells. Since a simulator can consist of hundreds of cells, keeping account of the MBE for each cell is a formidable bookkeeping operation ideally suited to digital computation.

3.3.10.3 Types of Reservoir Simulators

There are several types of reservoir simulators. Choice of the proper simulator to represent a particular reservoir requires an understanding of the reservoir and a careful examination of the data available. A model that fits Reservoir A may not be appropriate for Reservoir B, in spite of apparent similarities between Reservoirs A and B. A reservoir model is useful only when it fits the field case.

One basis for classifying models as discussed earlier is the number of dimensions. The two dimensional model is the most commonly used. There are several two dimensional geometries, the most popular of which is the horizontal (x-y) geometry; but the vertical (x-z) and the radial (r-z) geometries are also used quite often.

Simulators can be classified also according to the type of reservoir or process they are intended to simulate. There are, for example, gas, black oil, gas condensate, and miscible displacement simulators. Moreover, there are one-, two-, and three-phase reservoir models. Furthermore, any of these simulators may or may not account for gravitational or capillary forces. It is not enough

to choose the proper simulator with respect to dimensionality; the simulator must represent the type of hydrocarbon and the fluid phases present.

After the type of model to use in a study has been selected, the next step is to divide the reservoir into a number of cells, as illustrated in **Figures 22 and 23**.

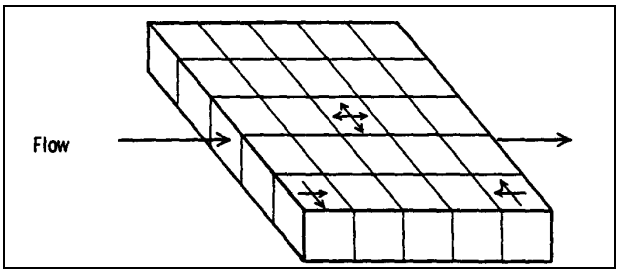

Figure 22. Two dimensional simulator

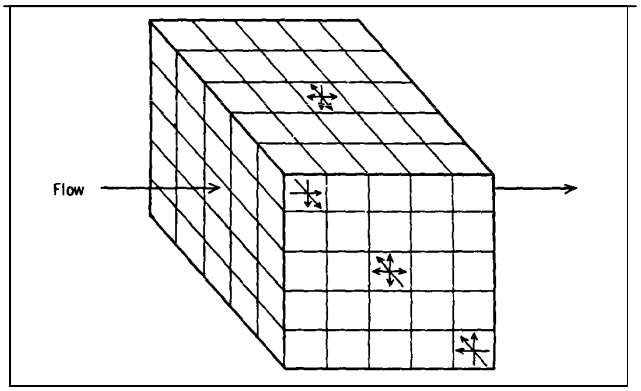

Figure23. Three-dimensional model

This is accomplished by laying out a gird system for the reservoir. In a two-dimensional study, the grid is established by drawing lines on a map of the reservoir. All grid lines must extend across the reservoir. Each cell is identified by its x, y, z coordinates. Then the flow conditions around the

perimeter of the reservoir are established. Normally the reservoir boundary is considered sealed, but influx or efflux at an assigned pressure or rate may also be specified.

The next step is to assign the following for each cell: rock properties, geometry, initial fluid distribution, and fluid properties. The rock properties consist of specific permeability, porosity, relative permeability and sometimes capillary pressure. The cell geometry includes the depth, thickness and locations of wells. Usually the wells are assumed to be located at the centers of the cells in which they fall. The initial fluid distribution consists of the oil, water and gas saturations at the beginning of simulation. Also, the average pressure of the cell at that time is assigned or calculated from known data. Fluid properties are specified by the usual PVT data. In addition, for each well it is necessary to provide a production schedule and a productivity index or a skin value (i.e., damage or improvement).

The engineer should scrutinize carefully these basic data for consistency and accuracy. For example, if pressure build-up data are available on a well, the permeability-thickness product of the cell where the well is located and the flow rate assigned to the well should be compatible with the build-up data. The time spent in examining the basic data is well spent, for it can lead to fewer simulation runs. Moreover, one must always remember that the answer is only as good as the input data.

3.3.10.4 History Matching and Performance Prediction

The main purpose of the reservoir simulation is to predict the rate of

hydrocarbon recovery for different methods of field operation. If adequate field data exist, reasonably accurate performance predictions can be made. If data are incomplete or suspect, simulators may be used only to compare semi-quantitatively the results of different ways of operating the reservoir. In either case, the accuracy of the simulator can be improved by history matching.
The first step in a history match is to calculate reservoir performance using the best data available. The results are compared with the field recorded histories of the wells. If the agreement is not satisfactory, such data has permeability, relative permeability, and porosity are varied from one computer run to another until a match is achieved. The simulator is then used to predict performance for alternative plans of operating the reservoir.

The behavior of the reservoir is influenced by many factors - permeability, porosity, thickness, saturation distributions, relative permeability, etc.- that are never known precisely all over the reservoir. What one arrives at is only a combination of these variables, which results in a match. This combination is not unique, so it may not represent precisely the condition of the reservoir. When the simulator, after a match, is used to predict, it is not certain that the physical picture of the reservoir described in the simulator will give predictions sufficiently close to the actual reservoir performance. In general, the longer the matched history period, the more reliable the predicted performance will be. It behooves the engineer to monitor periodically the predicted vs. the actual performance and to update his physical picture of the reservoir.

3.3.10.5 Basic Model Considerations

Stated simply, a multicell model simulates fluid flow in an oil or gas reservoir. Models can not describe flow exactly as it occurs, but they do give valid approximations. The mathematics of these models requires that the reservoir be treated as if it were composed of many individual segments. These segments are usually called cells, but are also referred to as grids, nodes, mesh points or a network. Models are made to represent reservoir fluid flow from cell to cell in one, two, or three dimensions as shown in **Figures 24, 25 and 26**, respectively.

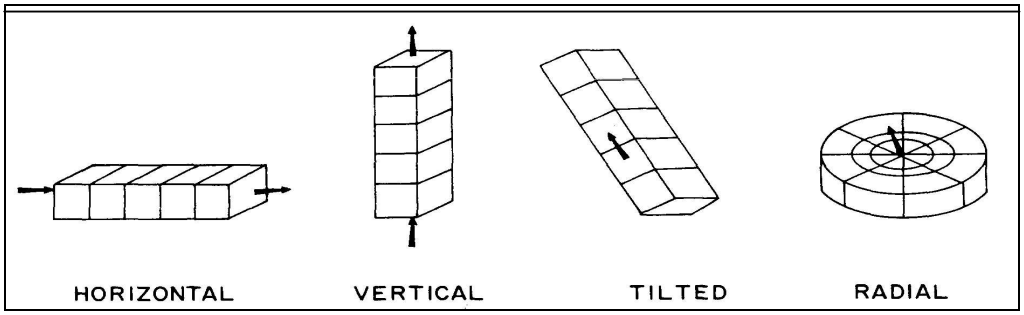

Figure 24. One dimensional models

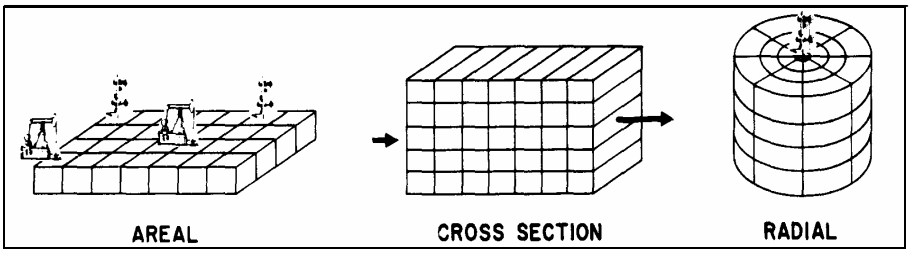

Figure 25. Two dimensional models

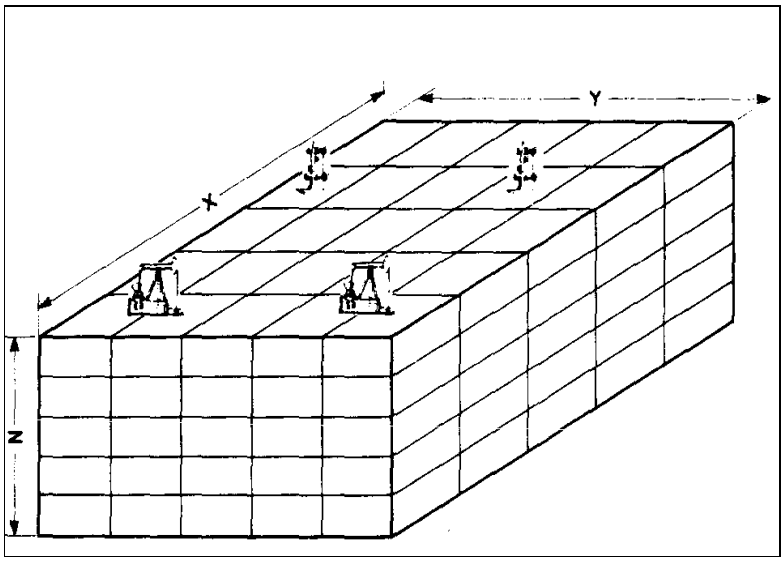

Figure 26. Three dimensional model

Each cell is assigned its specific reservoir properties of size, porosity, permeability, elevation, pressure, and fluid saturations. In addition to cell properties, well data must also be provided. These include location, productivity index, desired producing or injection rates, and limiting conditions such as economic limit, maximum water cut GOR, and minimum bottom-hole flowing pressure. General fluid and rock data must also be provided for the entire field or section of field being studied. These usually include PVT data for the oil, gas, and water, rock compressibility, and relative permeability for each flowing phase. Models using PVT data for oil, gas, and water are frequently referred to as 'black-oil models'. Special 'gas models' have been developed for the study of gas reservoirs. In some models the hydrocarbons are divided into components, in which case the term 'compositional model' is used. The reservoir engineer will rarely use a compositional model because it is more complex than is generally is necessary.

A system of mathematical equations is used to calculate the flow between

cells and the fluid saturation and volumes in each cell. The equations used are derived from: 1) The continuity equation or mass balance, 2) Darcy's law of flow through porous media, and 3) equation of state.

Finite- difference methods are used to solve the model equations. The methods do not give exact answers and are recognized as having some inherent error. The reservoir engineer should be aware of these potential errors, even though for the most part he will not be too concerned with them because the mathematical approaches in modeling are still generally more accurate then the engineer's ability to refine the input data.

3.3.10.6 How Models Work

A simplified calculation procedure used by a model would be as follows:

1) Start with the cells' having certain initial saturations and conditions given

2) Select a time step over which the model is to calculate.

3) Calculate or use an assigned production or injection for each well for the time period.

4) Calculate the flow between the cells during the time step and the new saturation for each cell.

5) Set a new time step and repeat the process until a model has calculated performance for the desired total time. High-speed computers are required for solving problems involved in a multicell model because of the extremely large number of calculations made in a typical study **[117].**

CHAPTER 4

EXPERIMENTAL SET-UP and PROCEDURE

4.1 Experimental Set-up

The experimental set-up is shown in the **Figure 27** below.

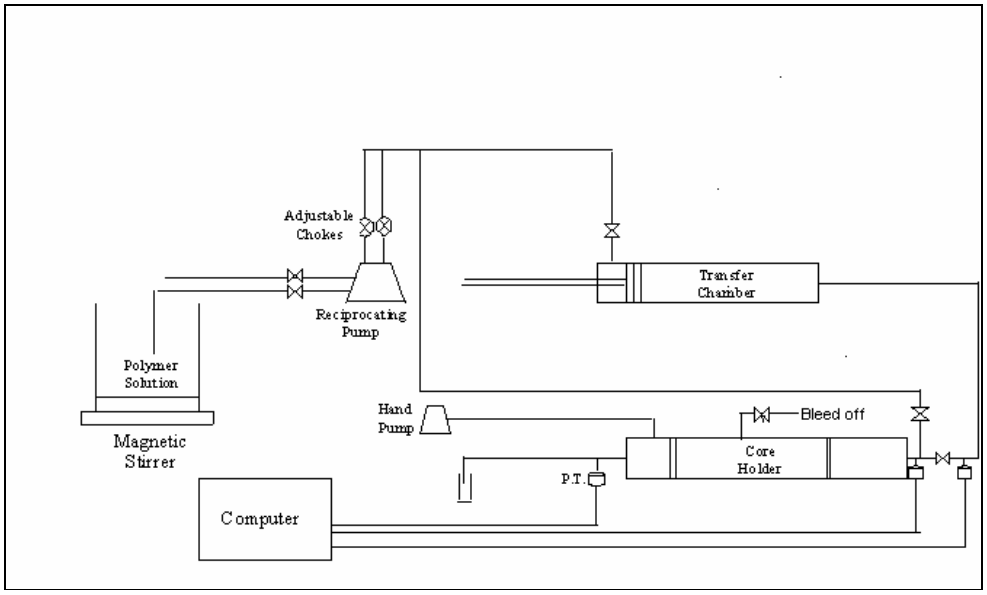

Figure 27. Experimental Set-up

The experimental set-up consists of a magnetic stirrer, a reciprocating pump, a core holder, a transfer chamber, hand pump, pressure transducers, and a computer as seen in the figure above.

The magnetic stirrer is used to both stirr and heat the polymer solution to a desired temperature.

The reciprocating pump has two suction lines and two discharge lines. The discharge rate of the pump can be controlled with adjustable chokes. Using the calibration table of the pump specified by the manifacturer, it is possible to adjust the flow rate. The pump is used to directly send the fluid to the core holder or pressure the transfer chamber and indirectly send the hexane to the core holder.

The core holder, as the name implies, contains the core. The confining pressure applied to the core at the holder is adjusted using the hand pump. The hand pump, having a reservoir with lubricator pressurises the holder to the desired pressure and the lubricator.

The transfer chamber has a piston and the piston is moved with the fluid pressured with the reciprocal pump. The hexane contained in the transfer chamber is displaced through the outlet of the chamber as the piston moves.

Inlet and outlet pressures of the core and the transfer chamber outlet pressures were measured with the transducers as shown in the figure above. The pressure transducers were connected to a data logger and were sending the pressure values in terms of milliamperes (mA). The pressure readings in mA are then converted to unit of atm. using the transducer calibration curves.

4.2 Experimental Procedure

The procedure of the experiment for water-hexane system is as follows:

1) Put the core in the core holder.

2) Adjust the confining pressure.

3) Connect the vacuum-pump to the outlet of the core. Let the vacuum-pump suck the lines and the core at least six hour to eliminate the occurrence of bubbles.

4) Adjust the flow rate to a low value such as 1 ml/min.

5) Increase the flow rate step by step and read the corresponding stabilized pressures. Continue saturating the core to about three pore volumes.

6) Re-adjust the flow rate to the specified value and start injecting hexane to the core.

7) Record the production values and the corresponding pressure values in every one or two minutes depending on the specified flow rate until about 3 pore volumes are injected to the system.

8) Start water injection and record the produced fluid volumes accumulating in the graduated cylinders together with the pressures.

9) Keep on injecting water till you are sure that the flow is in one phase and the cumulative injection reaches 3 pore volumes.

10) Bleed the core holder confining pressure lubricator, dismantle the core holder and put the core in the oven. Keep the core in the oven at least two days.

When polyvinylpyrrolidone solution is used at the experiments the procedure differs slightly:

1) Prepare a 0,05% by weight polyvinylpyrrolidone solution, heat it to 25 °C and stir the solution continuously

2) Put the core in the core holder.

3) Adjust the confining pressure.

4) Connect the vacuum-pump to the outlet of the core. Let the vacuum-pump suck the lines and the core at least six hour to eliminate the occurrence of bubbles.
5) Adjust the flow rate to a low value such as 1 ml/min.
6) Increase the flow rate step by step and read the corresponding stabilized pressures.
7) Continue saturating the core to about three pore volumes.
8) Re-adjust the flow rate to the specified value and start injecting hexane to the core.
9) Record the production values and the corresponding pressure values in every one or two minutes depending on the specified flow rate until about 3 pore volumes are injected to the system.
10) Then start injecting polymer solution and record the produced fluid volumes accumulating in the graduated cylinders together with the pressures.
11) Keep on injecting water till you are sure that the flow is in solution phase
12) Bleed the core holder confining pressure lubricator, dismantle the core holder and clean the core with toluene. Keep the core in the oven for at least two days.

When the cores are fractured, the procedure of the experiments is the same for water-hexane and polymer-hexane system.

The experiments are performed with water-hexane, then performed with water-polymer-hexane and then with fracture.

CHAPTER 5

RESULTS AND DISCUSSION

Introduction

The results of the experiments were analyzed and discussed in this chapter. The effects of the parameters were depicted with graphs and a further multivariate analysis was performed using Artificial Neural Networks (ANN). In addition, CMG Stars Simulator **[118]** was used for history matching and for the construction of the relative permeability curves. The basic concepts of the ANN and reservoir simulation were stated in Chapter 3 of the thesis.

5.1 Results

5.1.1 Porosity, Permeability and Viscosity

A total of 21 experiments was conducted. 16 of them have been started with absolute permeability determination and pump calibration curve construction purposes, and the results of the pump calibration are shown in **Figure 28**. All core plugs were from the same formation. The measured values of unfractured core permeabilities are between 72 md and 324 md.

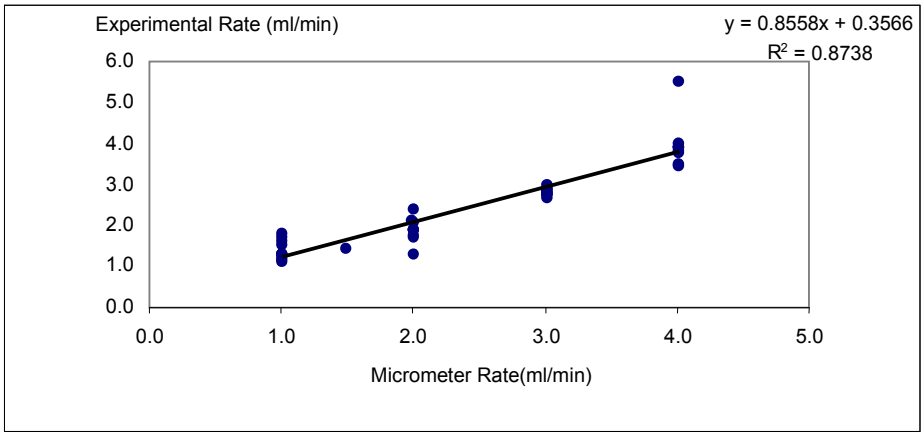

Figure 28. Pump calibration curve

The porosities are measured with the Helium Porosimeter and the values are tabulated below. With the horizontal fractures created at core-2 and core-3, the porosities increased to 20,43% and 19,54%, respectively. The porosities and the corresponding pore volumes can be seen in **Table 2**.

Table 2. Porosities and pore volumes

Core #	Porosity (%)	PV (cc)	Fracture
1	12,19	9,86	No
2	15,12	12,23	No
3	14,85	12,08	No
2	20,48	16,5	Yes
3	19,54	15,81	Yes

Heterogeneity of the cores was determined by taking thin sections. Thin sections taken perpendicular to the symmetry axis of the cylindrical cores are analyzed with an automated image analysis system and a microscope.

The viscosities of the polymer solution were measured using a cone and plate viscometer. The viscosity of the polymer solution (0,05 % by wt, polyvinylpyrrolidone + distilled water solution) was measured as 1,54 cp. Note that the viscosity of the distilled water is 1 cp and viscosity of hexane is

0,31 cp. The polymer solution could not be used at high rates (i.e. greater than 2ml/min) due to the performance decrease at the pump. The polymer, being insoluble in water, decreased the pump efficiency probably due to the suspended particles' resistance to gravity and blockage. As the water was ascending at the transparent tubing present at the suction line of the pump, the heavier suspended particles were descending. Due to these reasons, polymer injection rates and polymer concentration were kept low.

Porosity values were measured using a Helium Porosimeter and the capillary pressure was measured using the mercury pycnometer. The porosity values are tabulated in **Table 2**. The capillary pressure vs. saturation of mercury graph can be seen at **Figure 29**. The pore dimension distribution plot is shown in **Figure 30**. The binary number (Bin) is a statistical term and is defined with the minimum and maximum ranges of the samples and the number of samples.

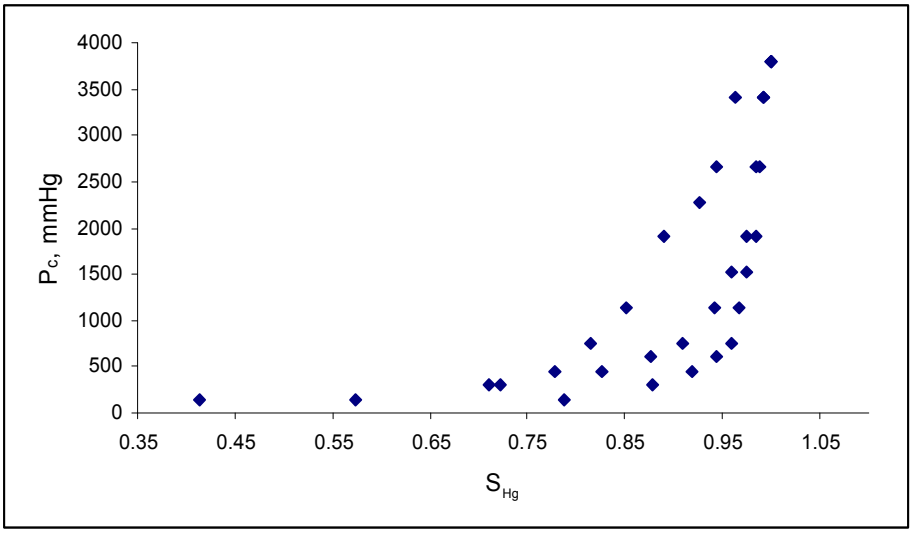

Figure29. Capillary pressure vs. mercury saturation from the pycnometer device for three cores of Midyat formation

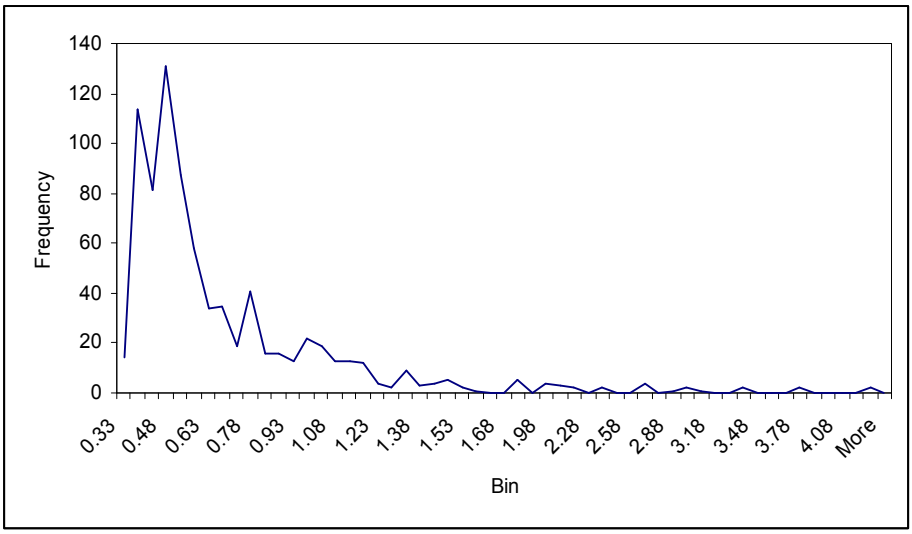

Figure 30. Pore dimension distribution plot for the Midyat Formation cores studied

Absolute water permeability values, construct the basis for the calculation of hexane end point relative permeabilities. Therefore, before totally saturating the cores with distilled water, the experimental values were checked in terms of repeatability. The experiments list can be seen at **Table A1.**

Using the adjustable flow controller present on the positive displacement injection pump, flow rates were varied to obtain the corresponding pressure losses. The pressure loss across the two ends of the core was measured by pressure transducers as stated in the previous chapter.

Permeability of a core plug was measured using Darcy's law. The ratios of *Q/A* vs. *DP/L* were plotted to obtain the permeability of the cores. The R-Squared values of the lines were attached to the top right of the graph window to give an idea about the accuracy of the best line. Besides, the equations of the lines are attached to each graph for permeability reading from the slopes.

Absolute water permeability measurements for core-1, core-2 and core-3 can be seen at **Table 3**.

Table 3. Absolute water permeability measurements

Core No	K(md)
1A	253
1C	134
1D	324,5
1E	316,2
2A	126,7
2B	256
2C	292
2D	72,2
2E	132
2F	2452
3A	200,2
3B	166
3C	109
3D	305,1
3E	258,3
3F	137

5.1.2 Calculation of Relative Permeability

JBN (Johnson, Bossler, Neumann) technique was tried for calculation of the relative permeability of the cores. The unsteady-state data were inserted in the calculation and since the results were unreasonable, it has been found unnecessary to tabulate the results. Specifically, saturation values were larger than unity, which is not possible.

The capillary pressure method is also used to calculate the relative permeabilities. And the results are plotted on **Figure 31**.

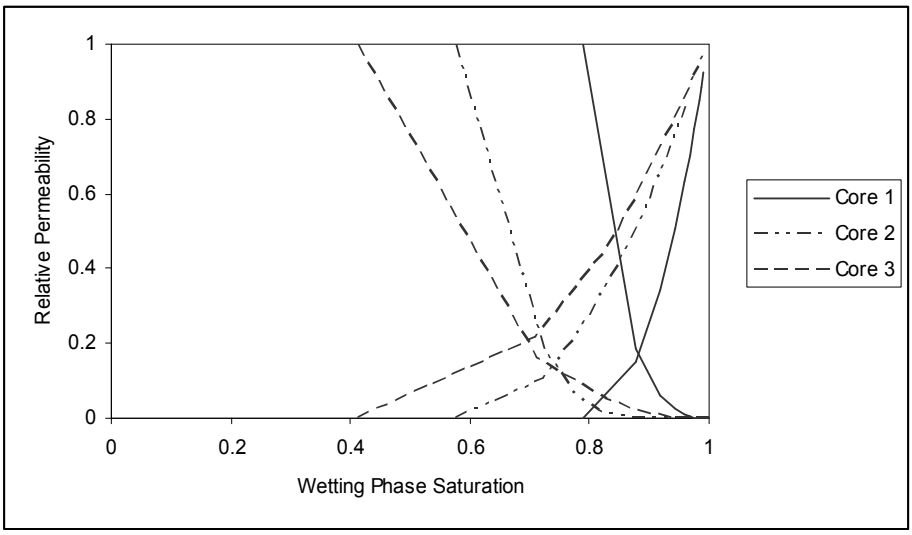

Figure31. Relative permeability vs. S_w graph for the cores1-2-3

5.1.3 Calculation of end point relative permeability to hexane

With the absolute permeabilities in hand, the end point relative permeabilities were calculated using **Equation 25**.

$$k_{rh}^{0} = \frac{QL\mu}{k_{abs}.A.\Delta P} \qquad \textbf{(25)}$$

where

k_{rh}^{0} : Relative permeability to hexane

Q: The flow rate, cc/min

L: Length of the core, cm.

μ: Viscosity, cp

k_{abs} : Permeability, Darcy

A: Cross sectional area, sq cm

ΔP: Pressure loss, atm

The values are tabulated in **Table 4.** As the absolute permeability values for the core flood experiments 12-19-20-21 for core-3 are not present, the measured absolute permeabilities were averaged for core-3. In the same manner, the absolute water permeability of core-2 is assumed as the averages of the ones measured before.

Table 4. End point relative permeability to hexane calculation

Experiment No	Core No	Q(cc/min)	L(cm)	M(cp)	A (cm^2)	ΔP(atm)	k_{abs} (d)	k^0_{rw}
1	1A	1,2124	7,1	1	11,4	28,19	0,253	0,105873
3	1C	1,6403	7,1	1	11,4	28,94	0,134	0,263435
4	1D	0,7845	7,1	1	11,4	24,88	0,325	0,060424
5	1E	0,7845	7,1	1	11,4	25,19	0,316	0,061381
7	2B	1,2124	7,1	1	11,4	29,25	0,256	0,10084
8	2C	1,2124	7,1	1	11,4	28,94	0,292	0,089355
9	2D	1,6403	7,1	1	11,4	32,125	0,072	0,441673
10	2E	0,7845	7,1	1	11,4	25,44	0,132	0,145497
13	3A	1,2124	7,1	1	11,4	29,38	0,2	0,128504
14	3B	1,2124	7,1	1	11,4	30,5	0,166	0,149139
15	3C	1,2124	7,1	1	11,4	29	0,109	0,238877
16	3D	1,2124	7,1	1	11,4	29,88	0,305	0,082855
17	3E	1,2124	7,1	1	11,4	25,06	0,258	0,116788
18	3F	0,7845	7,1	1	11,4	25,06	0,137	0,142313
11	2F	2,924	7,1	1	11,4	28,38	2,452	0,02617
12	2G	1,2124	7,1	1,54	11,4	29,81	0,175	0,222905
19	2H	1,2124	7,1	1,54	11,4	31,25	0,194	0,191809
20	3G	1,2124	7,1	1,54	11,4	32,56	0,194	0,184092
21	3H	2,0682	7,1	1,54	11,4	24,56	0,194	0,416329

5.2 Relative Permeability

In the literature, it was stated that the JBN analysis is not applicable to heterogeneous carbonate cores **[91]**. Although the method fails to give accurate results, the technique is tried for the calculation of relative permeability. The results of the analysis do not contradict with the information in the literature. Analysis performed on the three cores yielded unreasonable values such that hexane saturation values greater than unity were obtained which is physically impossible.

5.3 Rate Effect at Residual Oil Saturation (S_{or})

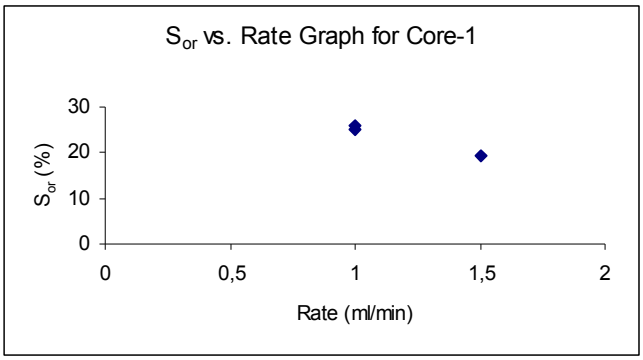

Figure 32. Rate effect at residual oil saturation for core-1

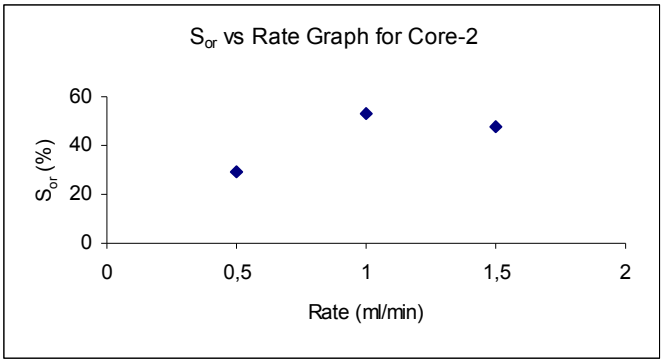

Figure 33. Rate effect at residual oil saturation for core-2

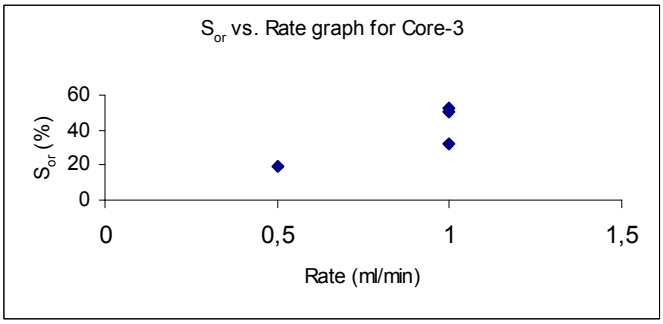

Figure 34. Rate effect at residual oil saturation for core-3

Figures 32, 33, and 34 were constructed to see the effect of rate at residual oil saturation. Referring to the plots, it is not possible to define any behavior.

5.4 Confining pressure effect at residual oil saturation

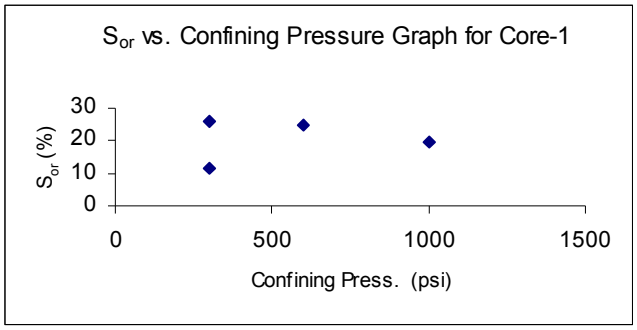

Figure 35. Effect of confining pressure on residual oil saturation for core-1

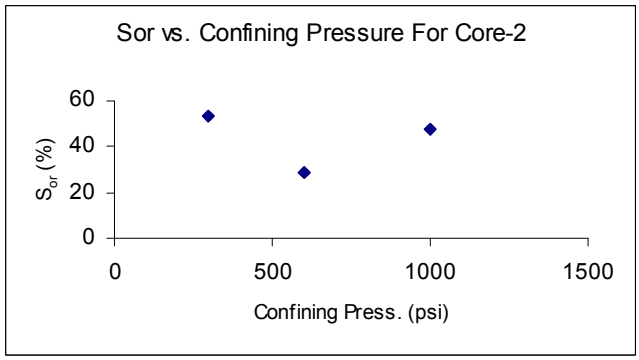

Figure 36. Effect of confining pressure on residual oil saturation for core-2

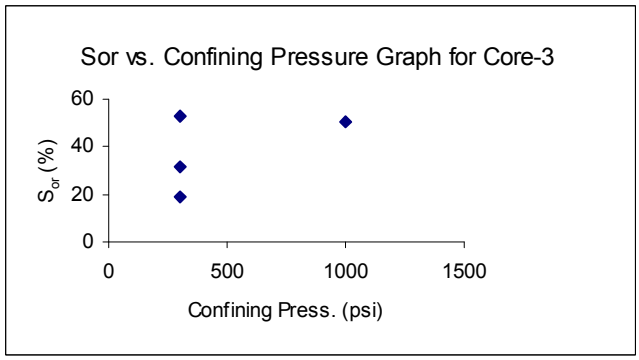

Figure 37. Effect of confining pressure on residual oil saturation for core-3

Figures 35, 36, and 37 demonstrate the behavior of residual oil saturation with confining pressure. From the plots, it is not possible to draw a conclusion but, note that Wilson **[32]** reported a 5% as the confining pressure was increased to 5000 psi. It is possible that for the range of confining pressures studied, no significant change has occurred.

5.5 Rate Effect at End Point Relative Permeability

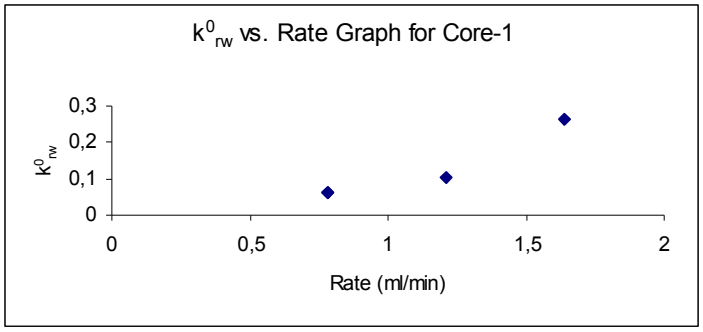

Figure 38. Rate effect at end point relative permeability for core-1

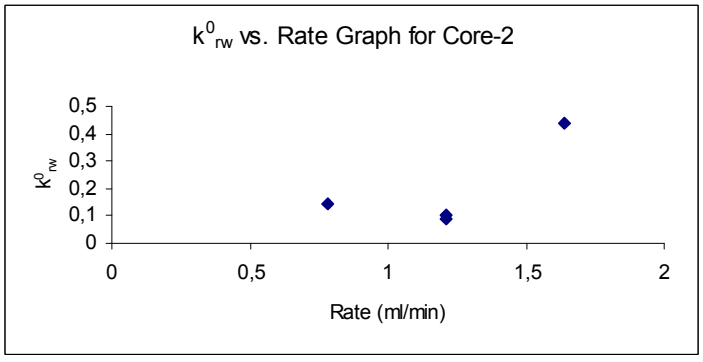

Figure 39. Rate effect at end point relative permeability for core-2

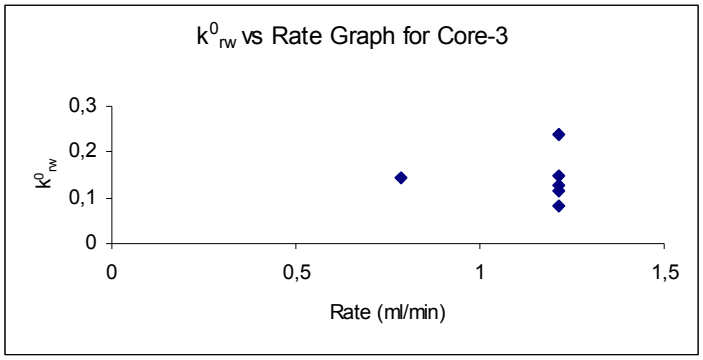

Figure 40. Rate effect at end point relative permeability for core-3

Figure 38, 39, and 40 show that end point relative permeability increases considerably when the flow rate is increased for core-1 and core-2, while it stays constant for core-3. The increase is due to decreasing absolute permeability and increasing flow rate in Equation 8. End point relative permeability to hexane increased as the injection rate was increased from 0,75 to 1,75 ml/min. This point is quite controversial to the literature. In the study of Akin and Demiral **[73]**, it was shown that end point relative permeabilities changed as the rate changed. As reported in the literature review section, several researchers **[83, 68, 69]** stated that as long as a saturation gradient is not present in the core it is possible that due to the heterogeneous nature of the core plugs, rate effects are considerable.

5.6 Confining Pressure Effect at End Point Relative Permeability

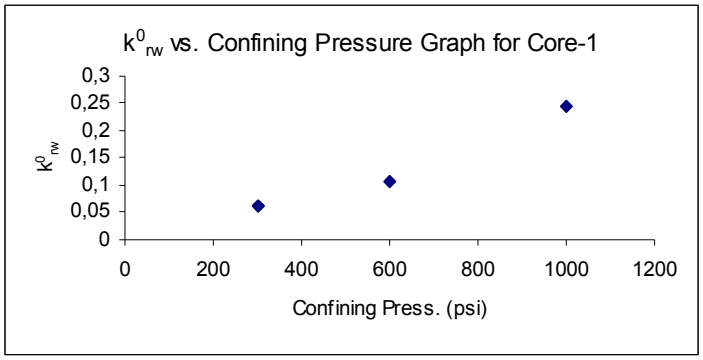

Figure 41. Confining pressure effect at end point relative permeability for core-1

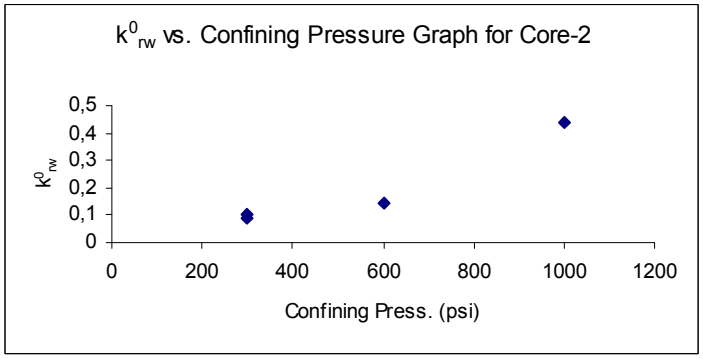

Figure 42. Confining pressure effect at end point relative permeability for core-2

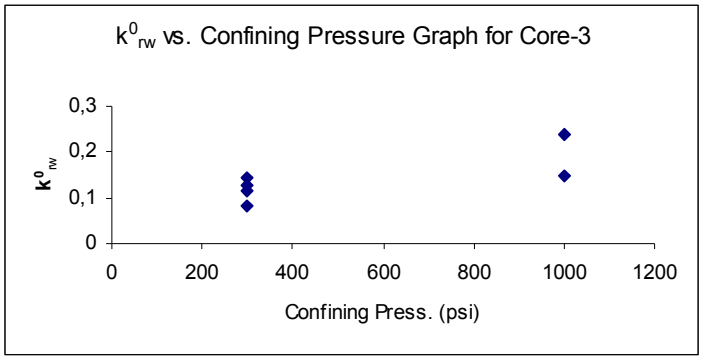

Figure 43. Confining pressure effect at end point relative permeability for core-3

Figures 41, 42 and 43 show the confining pressure effect. The behavior of end point relative permeability with increasing confining pressure and, the behavior of the relative permeability with increasing injection rate seem parallel. The result can be considered as the effect of injection rate rather than the effect of confining pressure. As the confining pressure increased form 300 psi to 1000 psi, end point relative permeability increased. This increase was somewhat more pronounced for core plugs 2 and 3 but less for core-1.

5.7 Effect of Fracture Presence on Residual Oil Saturation

Core-2, after being flooded with water and hexane for 6 experiments, is cut into two equal pieces for the core to represent a horizontally fractured dual porosity media. To eliminate the effect of flow rate on residual oil saturation, the flow rate was kept high, in fact, the highest of all flow rates, 3 ml/min. And from previous experiments, it was experienced that if the confining pressure is fixed at a low value such as 300 psi, the displacing fluid bypassed

almost the whole core and found a flow channel passing through the fracture. Therefore, the fracture aperture had to be decreased by exerting a higher pressure (1000 psi). As previously stated in section 8.3.8, the confining pressure has no impact on residual oil saturation. Shortly, the behavior of the residual oil saturation within a fractured medium was investigated with the other possible effects kept fixed. The related results are tabulated in Table A1**.** Fracture presence increases the residual oil saturation which can be attributed to the by-passed oil. In other words, displacing fluid tends to flow in fracture rather than the matrix.

Another way of understanding the effects is investigating the residual oil saturation values under the consideration of capillary number concept. If, for the same value of capillary number, there exist more than one saturation data, then the increase and decrease in residual oil saturation can be identified on the basis of the capillary number. The S_{or} vs. N_c (capillary number) data is shown in **Figure 44**. The void-type points are representing the polymer floods, the triangular-type black points are representing the polymer floods under the presence of a fracture. The off-point having the highest N_c value is representing experiment performed under fracture existence for core-2. To see the effect of polymer, vertical lines passing through polymer flood data points are drawn. Then the closest point to each line is determined. If the closest point's saturation value is higher than the polymer flood point's saturation value, then this means that the polymer flood decreases the residual oil saturation. In the same way, effect of fracture and polymer presence on residual oil saturation can also be observed from the capillary number plot. When referred to the **Figure 44,** it is not possible to draw a conclusion for the polymer flooding because two of the flood points are implying that the polymer flooding is increasing S_{or}, whereas one point is implying a decrease in S_{or}.

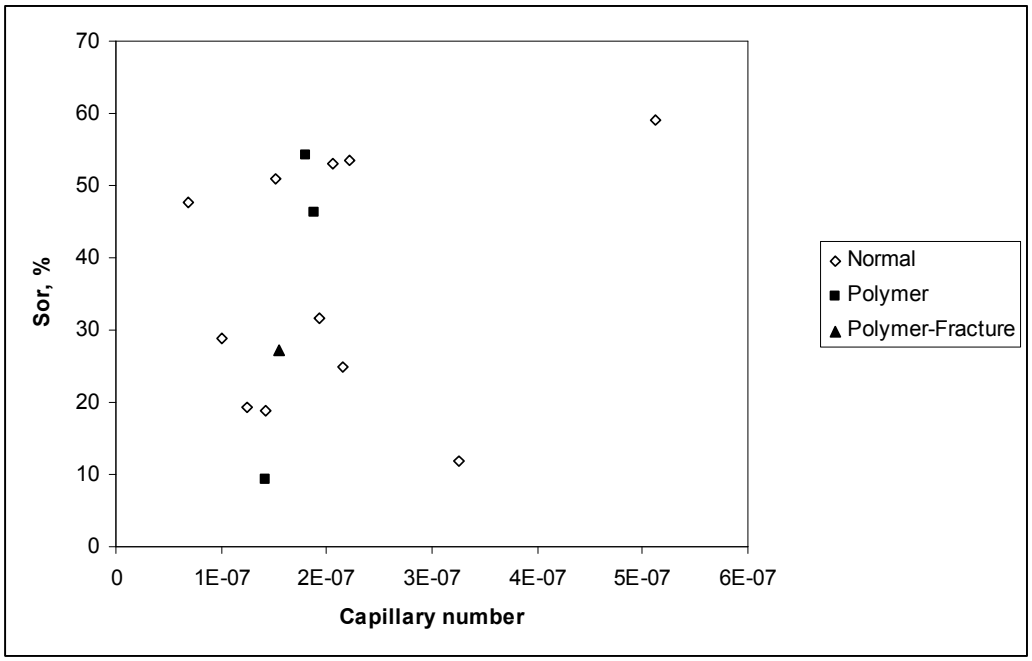

Figure 44. Residual oil saturation vs. capillary number graph

5.8 Effect of Polymer on End Point Relative Permeability

To see the effect, refer to **Table A1.** If the end point relative permeability 0,44 is considered as an off point and discarded for core-2, the polymer usage is causing an increase in the end point relative permeability. Moreover, when referred to the capillary number plot **(Figure 45)**, it is clearly seen that, end point relative permeability increases with polymer flooding. In the same manner, if a data is omitted from core-3 plot **(Figure 45)**, then polymer's effect can be noticed more clearly.

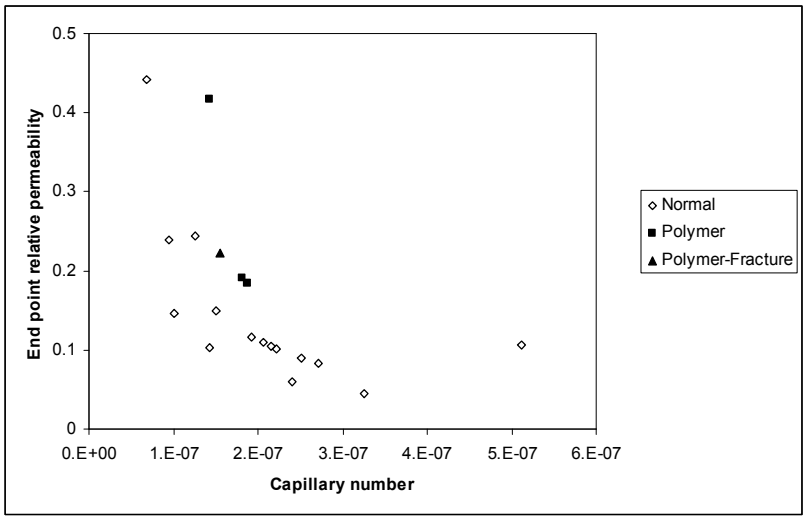

Figure 45. End point relative permeability vs. capillary number graph

5.9 Effect of Polymer and Fracture Coexistence on End Point Relative Permeability

If **Figure 45** considered, location of the points show that the coexistence of polymer and fracture causes an increase in the relative permeability. The triangular-shape point in the figure above, representing polymer and fracture coexistence is well above the points around.

5.10 Multivariate Analysis

Both in the literature and in the experiments, the results depicted a dependence on more than one variable. Namely, the parameters in interest, residual oil saturation, and end point relative permeability were thought to be affected by viscosity, confining pressure, absolute permeability and flow rate. To more clearly define the effects of these parameters, the endpoint k_r and S_{or} data were input into an artificial neural network.

The variables system, which is considered as multivariate was analyzed using Artificial Neural Networks (ANN). Inputs of the run were selected as flow rate, differential pressure, absolute permeability and viscosity. The output was defined as either S_{or} or k_r^0. The hidden layer size was selected as 20 for both networks. Number of training cycles (number of iterations) was set to 500, implying the number of iterations carried out to be 500. The training data were introduced into ANN sequentially. Data were partitioned as validation and training sets. The validation set was constructed by the software by randomly selecting 10% of the data.

5.10.1 Effect of parameters on S_{or} according to ANN Results

The mean square errors of the training set and the validation set were 0,008 and 0,009 respectively. These low errors show that the model is quite representative of the relationships among the variables. The mean square error can be seen at **Figure 45** below.

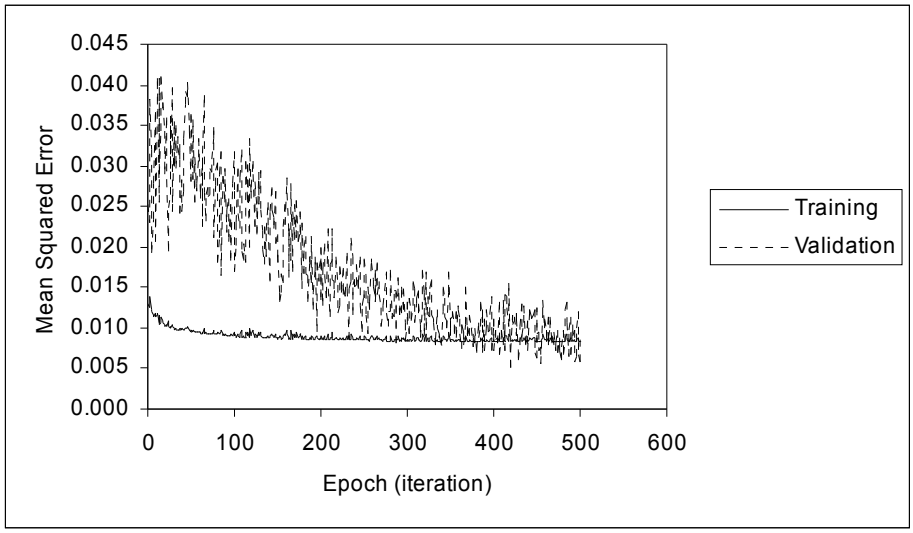

Figure 46. Mean square of the errors at training and validation sets for S_{or}

To see the effects of confining pressure and viscosity on residual oil saturation, other independent parameters, namely the flow rate and absolute permeability were kept constant at average values and the μ- S_{or} curves were constructed for different P_{conf} values as shown in **Figure 47** below.

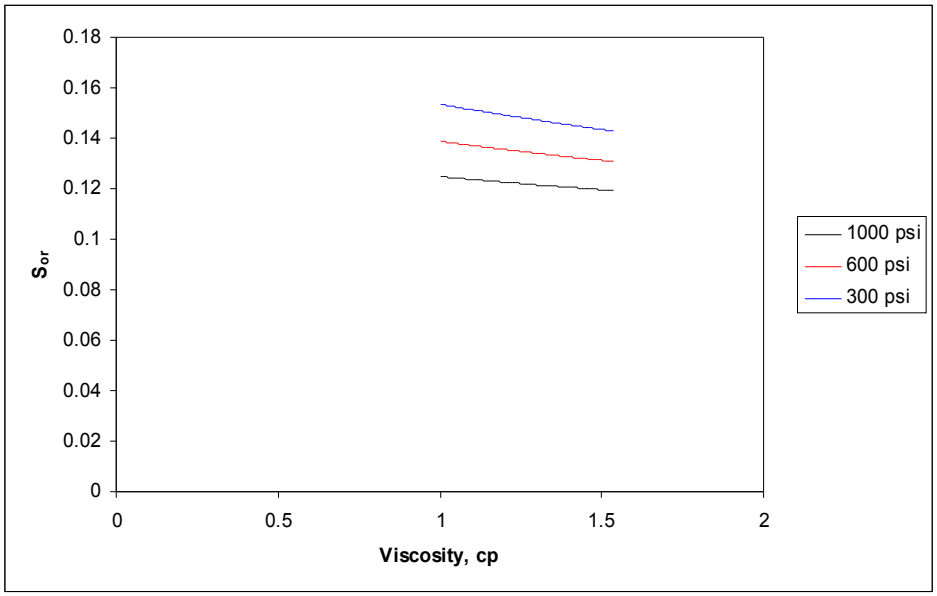

Figure 47. Residual oil saturation vs. viscosity curves for multiple confining pressures

From the figure above, it is clear that the viscosity and the residual oil saturation are inversely related. In addition, as the c

onfining pressure is decreased keeping the viscosity constant, the residual oil saturation increases.

For the relationship of absolute permeability-residual oil saturation-confining pressure, **Figure 48**, was formed. S_{or} increases non-linearly with increasing k_{abs} and decreases with increasing $P_{conf.}$ As discussed previously, the relationship between S_{or} and k_{abs} can be due to fingering, heterogeneity and the high fluid conductivity of the core.

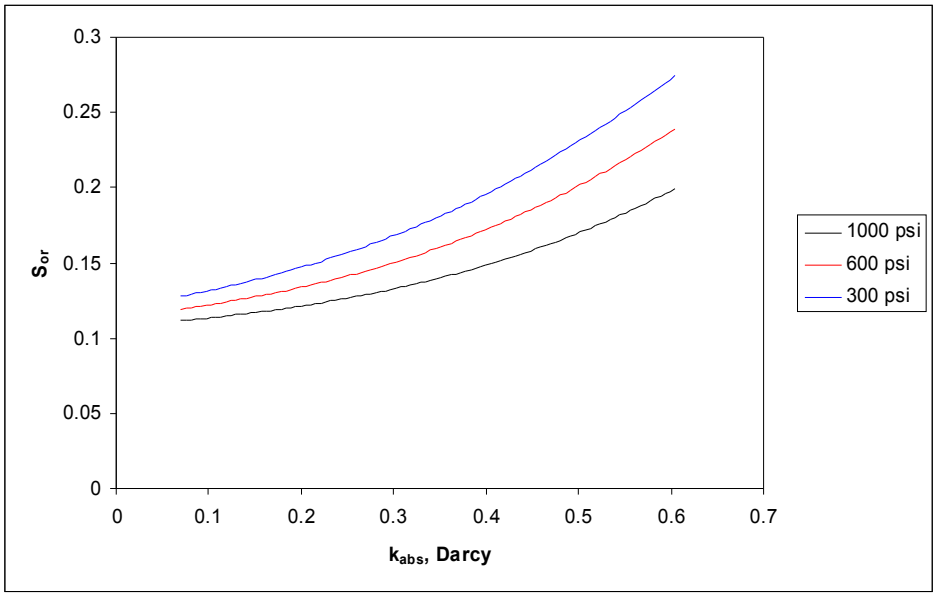

Figure 48. Residual oil saturation vs. absolute permeability curves for multiple confining pressures

Figure 49 shows the effect of differential pressure and confining pressure on residual oil saturation. Residual oil saturation is sensitive and directly related to differential pressure. S_{or} decreases as the confining pressure is increased.

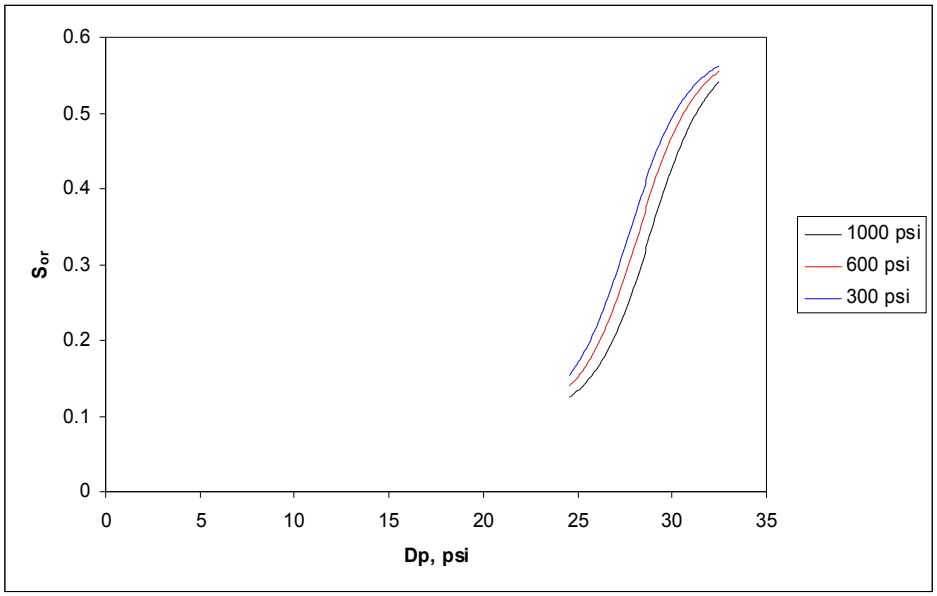

Figure 49. Residual oil saturation vs. differential pressure curves for multiple confining pressures

Influence of rate and confining pressure can be seen at **Figure 50.** As the flow rate increases, an increase in the residual oil saturation is seen, which may be an indication of fingering. In addition, it can be seen that, residual oil saturation increases as the confining pressure is decreased.

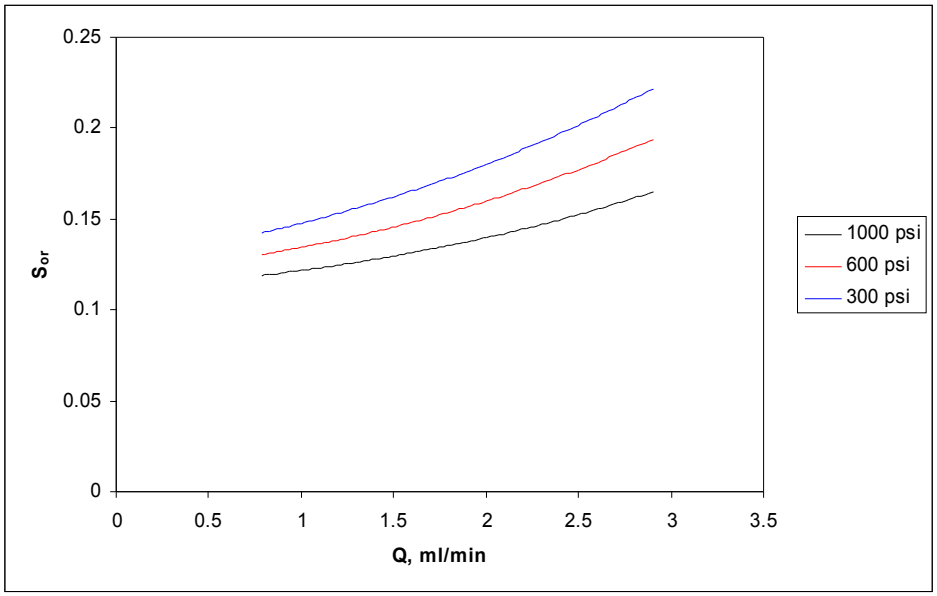

Figure 50. Residual oil saturation vs. flow rate curves for multiple confining pressures

The graph below **(Figure 51)** is demonstrating the influence of differential pressure and flow rate on residual oil saturation. For the same differential pressure, the corresponding residual oil saturation values seem close to each other, but as the flow rate is kept constant, the increase is sharp with a change in differential pressure.

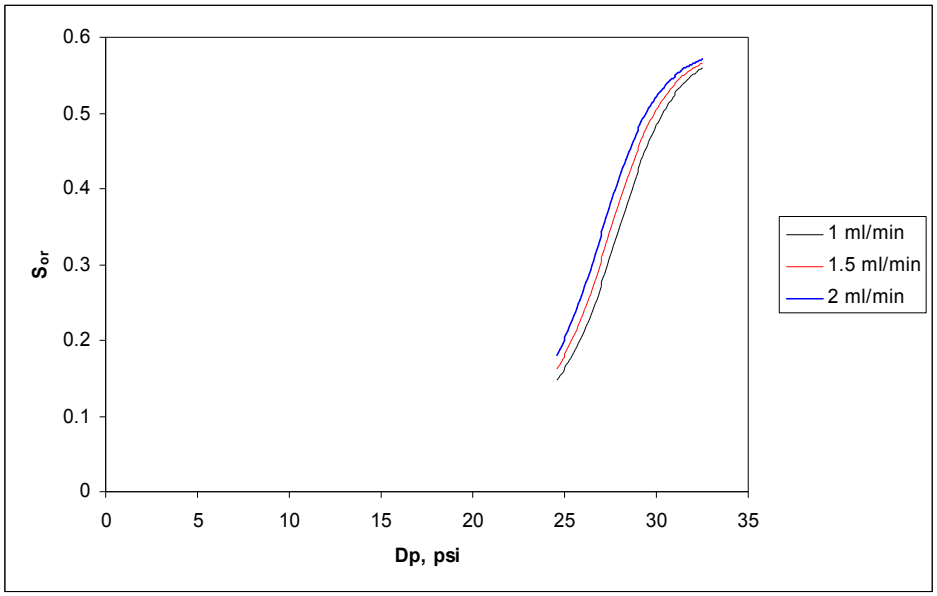

Figure 51. Residual oil saturation vs. differential pressure curves for multiple confining pressures

5.10.2 Effect of parameters on k_{rh}^{o} according to ANN Results

End point relative permeability to hexane, from the experimental data is affected by differential pressure, flow rate, viscosity and absolute permeability. In order to evaluate the effect of each parameter, the independent variables and the end point relative permeability were processed using an ANN similar to S_{or} relationship determination. The iterations were repeated 500 times and the other properties were kept the same. The mean square error plots at the iterations for both the validation and training sets are depicted in **Figure 52** below. Training errors were low starting from the very beginning of the iterations and eventually reached to the value of 0,001 for the validation set. The error increases in the first quarter of the iterations and then

starts to decrease and finally converges to 0,001 being the implication of a successful model.

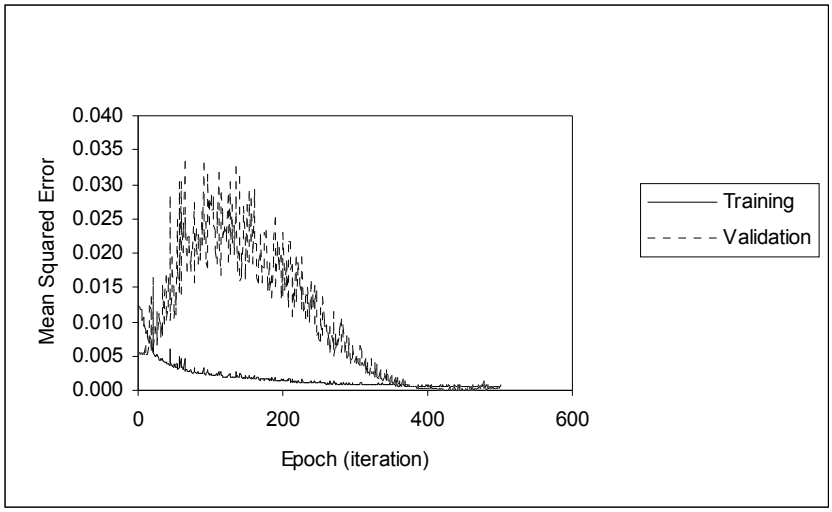

Figure 51. Mean square of the errors at training and validation sets for k_r^o

In **Figure 53**, viscosity and confining pressure effects are shown. k_r^0 increases as the viscosity increases, whereas k_r^0 decreases with increasing confining pressure. When **Figure 54** is considered, k_{abs} curves seem to coincide at high absolute permeabilities. The curves, when intersected with a vertical line representing a constant absolute permeability, k_r^0 readings are close.

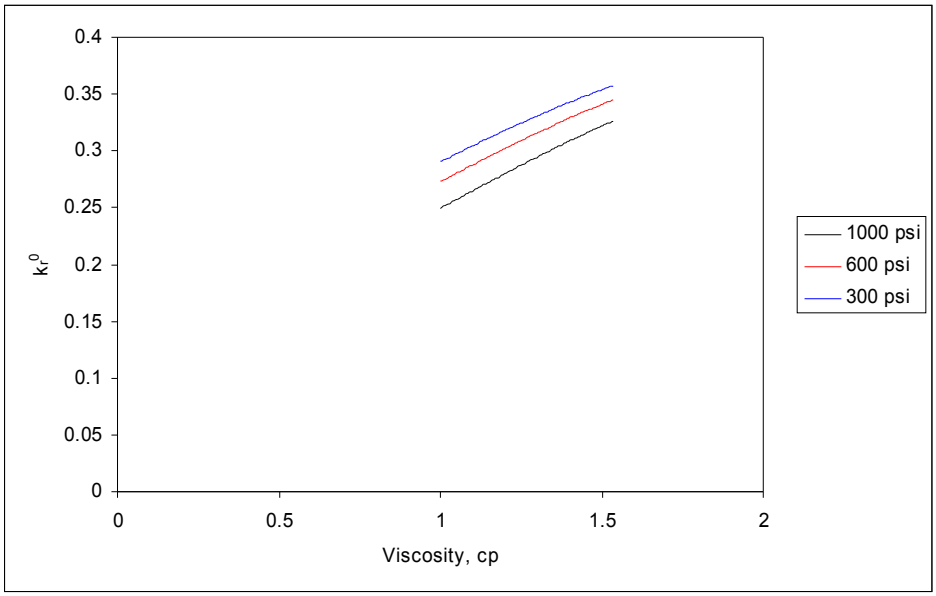

Figure 53. End point relative permeability vs. viscosity plots for various confining pressures

Absolute permeability- confining pressure, differential pressure- confining pressure, flow rate- confining pressure curves are given at **Figures 54,55** and **56**, respectively.

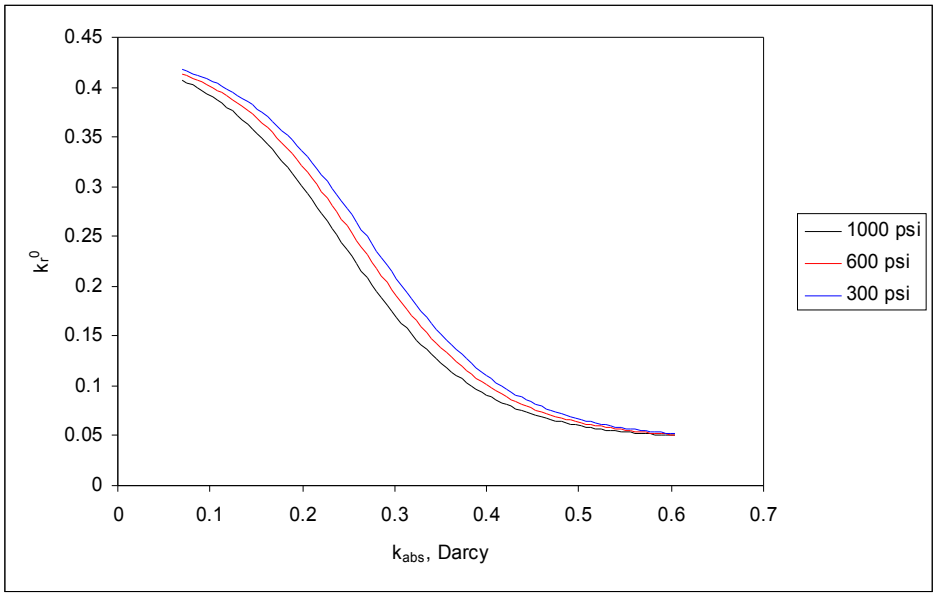

Figure 54. End point relative permeability vs. absolute permeability plots for various confining pressures

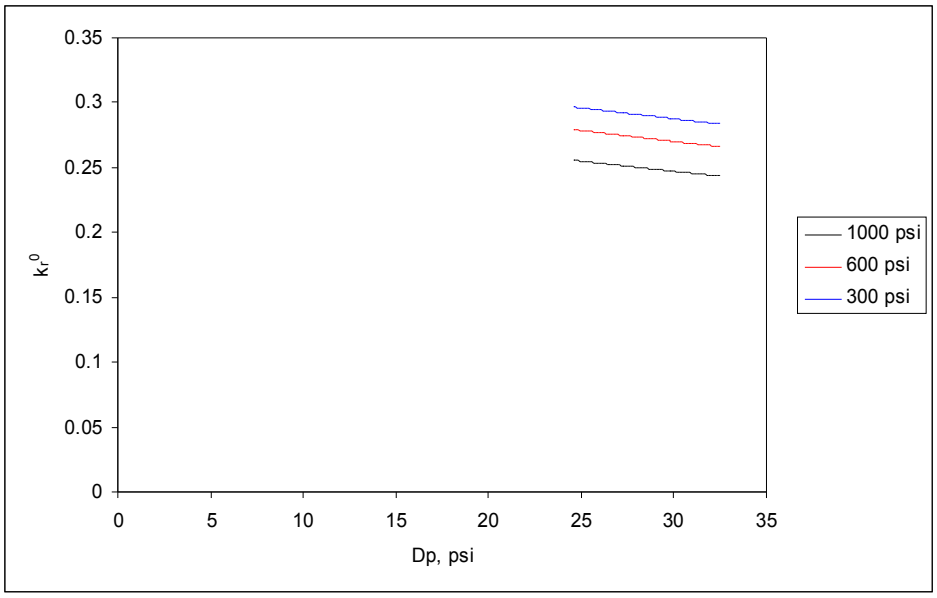

Figure 55. End point relative permeability vs. differential pressure plots for various confining pressures

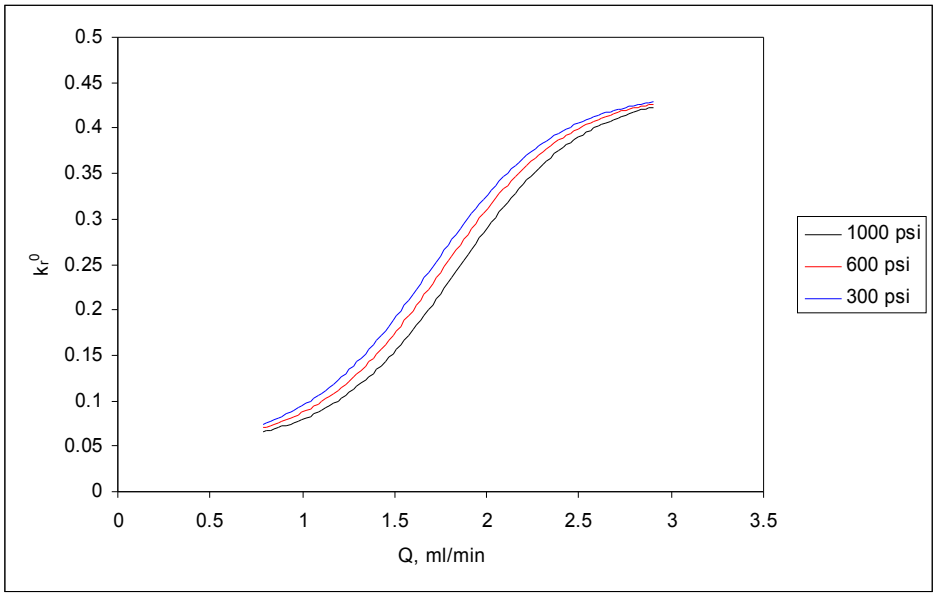

Figure 56. End point relative permeability vs. flow rate plots for various confining pressures

For the effect of differential pressure and flow rate on S_{or}, one can refer to **Figure 56**. Since the confining pressure curves are close to each other one can conclude that the S_{or} is not as sensitive to confining pressure as flow rate is. The differential pressure- S_{or} curves corresponding to various flow rates are steep and sensitive to differential pressure change.

5.11 Results of the Simulation Study

To observe the effect of polymer and fracture on relative permeability, CMG Stars Simulator was used. One dimensional model with 20 grids were chosen and the experimental pressure and production values were matched with the simulator results. The hexane and polymer production and pressure build-up

data were used in the history matching of the experiments. The end point relative permeabilities were fixed and the absolute permeability values were varied slightly to get a match.

The simulation was done for a core without polymer, then for a core with polymer and then for a core with polymer and fracture. The mathces for experiment 9 (where there is no effect of polymer and fracture either) are shown in **Figures 57**,**58**, and the simulation result is at **Figure 59**.

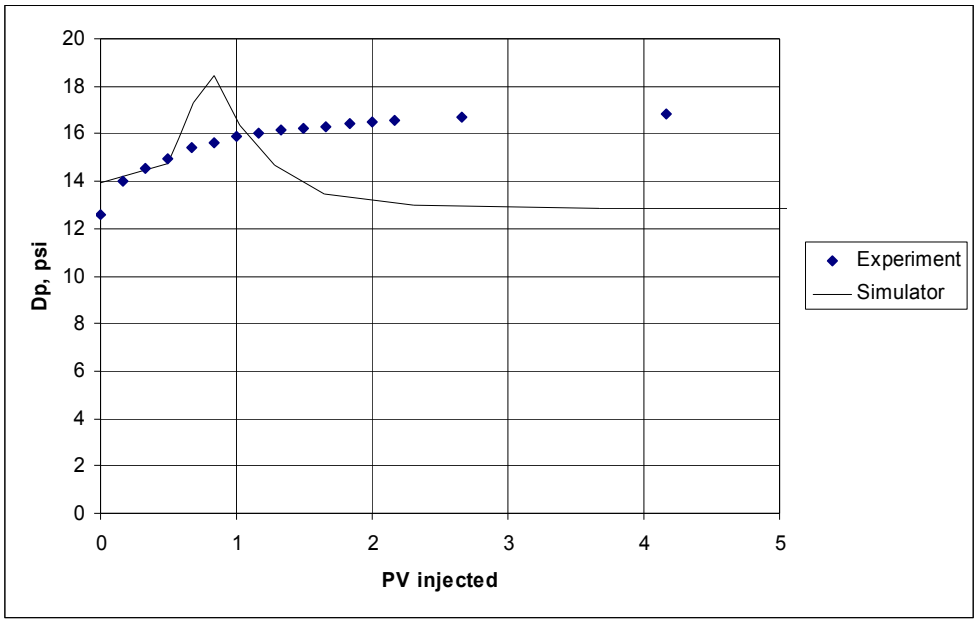

Figure 57. Pressure match for experiment 9

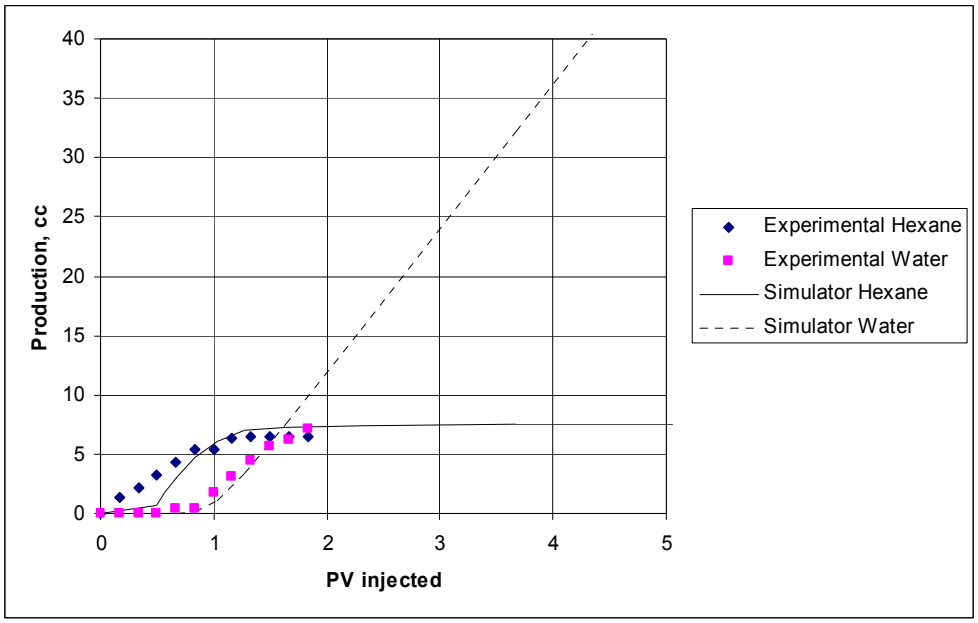

Figure 58. Production match for experiment 9

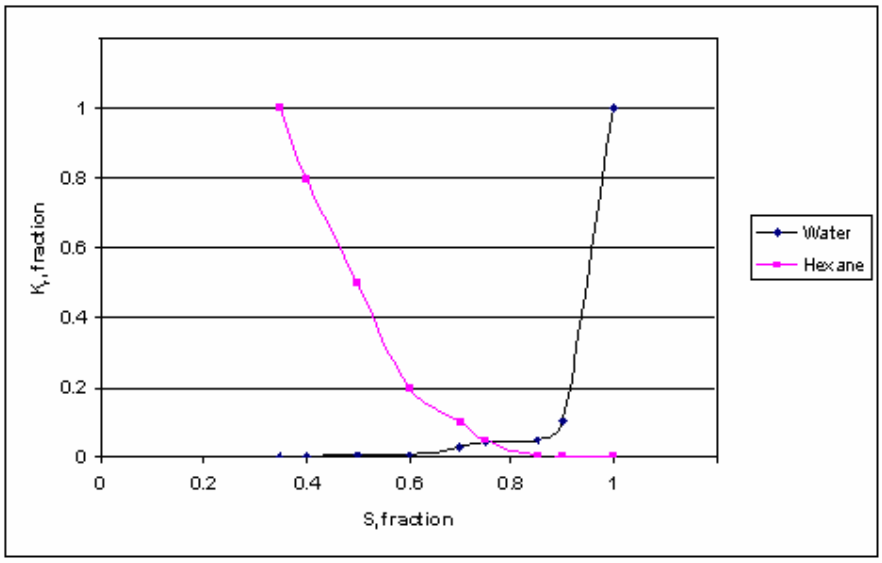

Figure 59. Simulator relative permeabilities for experiment 9

The history matching done on the pressure curve was quite poor for experiment 9. The same problem occurred while trying to match the pressures in the other experiments. The reason for the poor match is the sudden valve opening during the experiment. As the flow is changed from hexane injection to water injection, a hydraulic discontinuity is occurring as a valve is closed and another valve is opened. To eliminate this problem a pressure transducer was mounted to the outlet of the transfer chamber in order to observe the pressure at the inlet of the core and change the injection fluid observing the pressures. In spite of this modification on the experimental set-up, this problem could not be eliminated and is reflected in the pressure profiles.

To obsereve how polymer effets the end point relative permeability curves, Experiment 20 was simulated. The presure match, the production match and the relative permeability plots are shown in **Figures 60, 61,** and **62**, respectively.

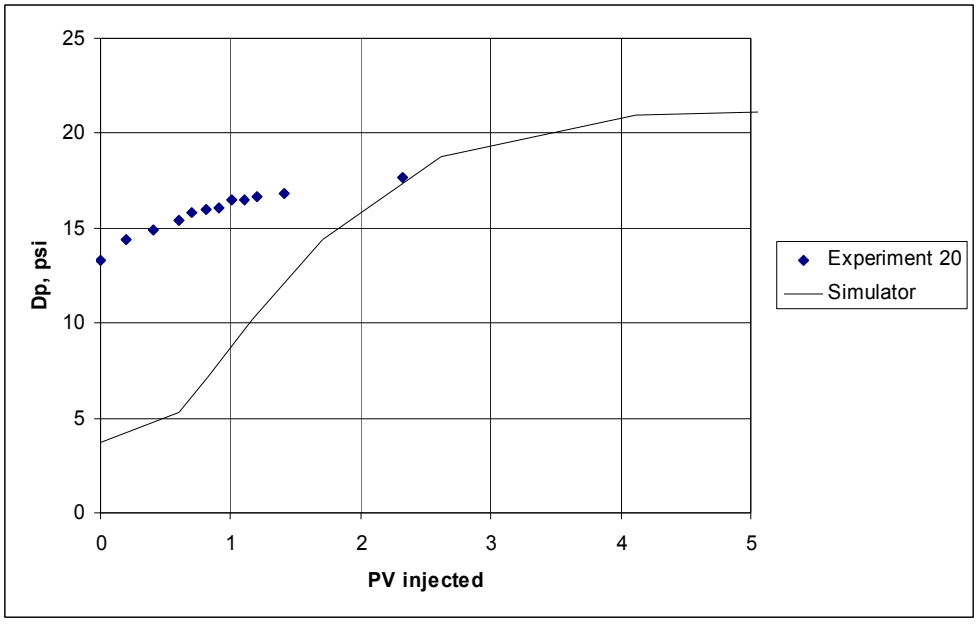

Figure 60. Simulator relative permeabilities for experiment 20

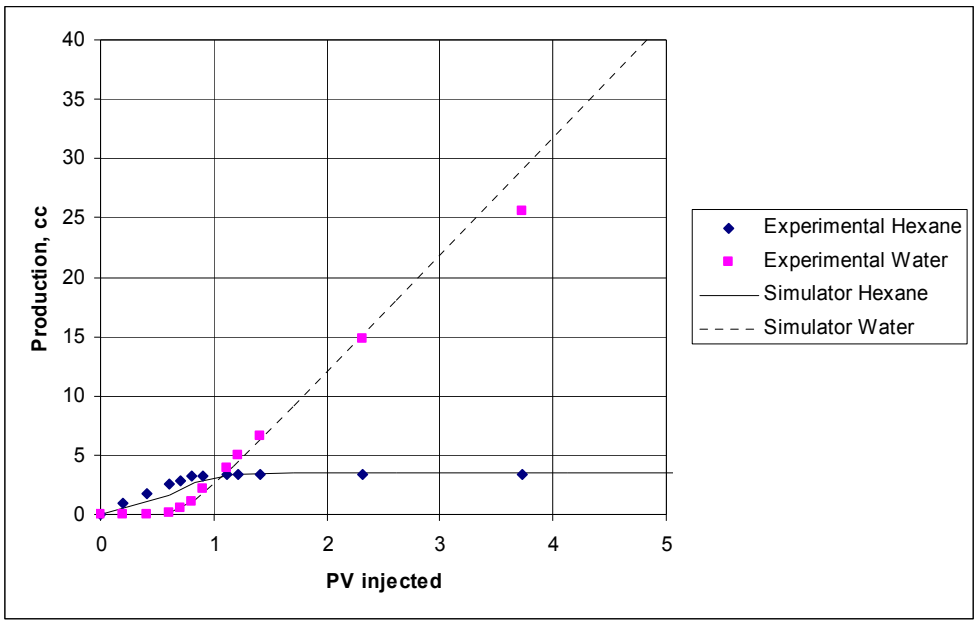

Figure 61. Production match for experiment 20

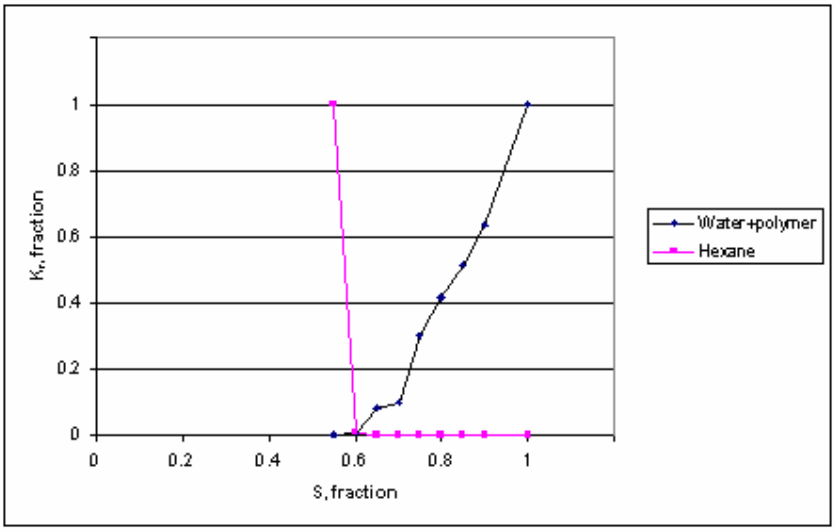

Figure 62. Simulator relative permeabilities for experiment 20

The pressure match for experiment 20, is much better than the one for experiment 9. Although there is not a one-to-one correspondence, the behavior of the curve seems the same as the experimental data if the simulator line could be shifted to the left horizontally. As stated before, in the previous simulation's discussion, the pressure discontinuity is the reason of the mismatch at the pressures. When the production profiles were considered, the matches for both the polymer and the water productions were quite successful. The behavior and the correspondence of the points are suitable.

Experiment 21 was performed with polymer and fracture together. To see how the type of the relative permeability curves change, the results of the simulation are depicted below with **Figures 63, 64**, and **65**.

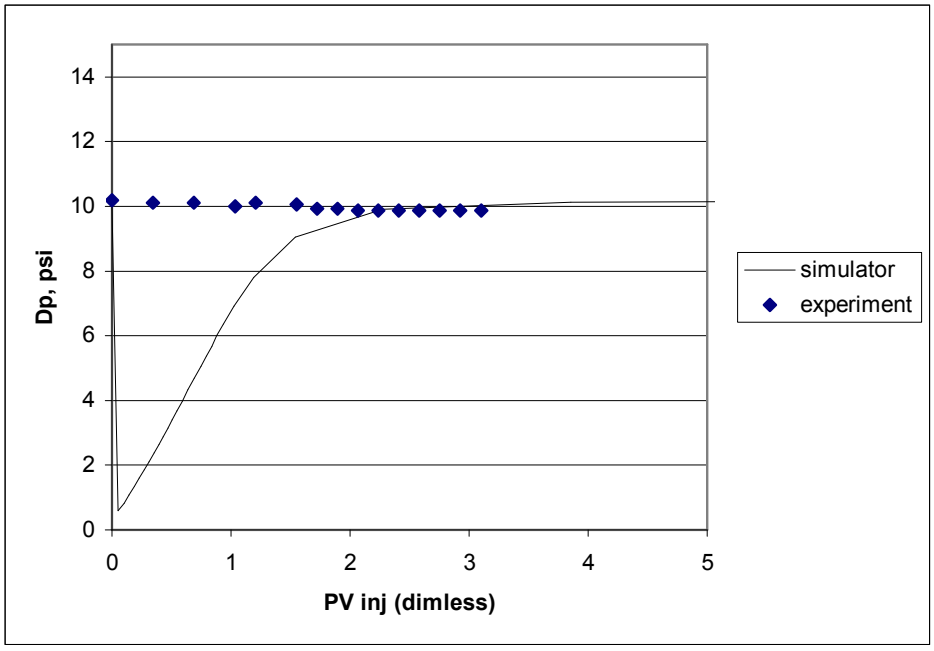

Figure 63. Pressure profile of experiment 21

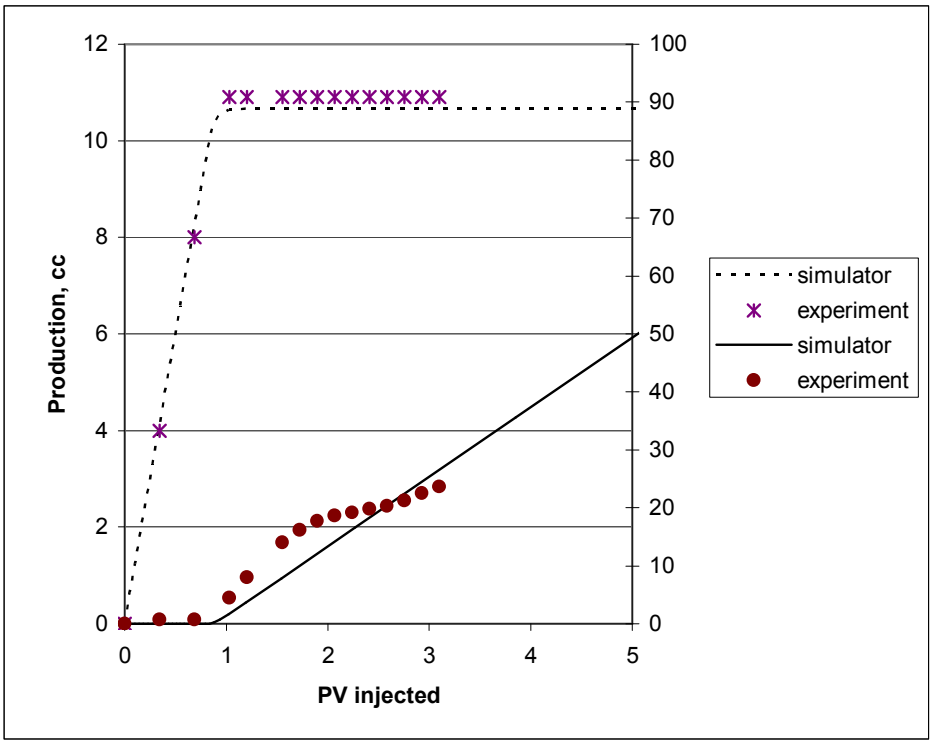

Figure 64. Production profile of experiment 21

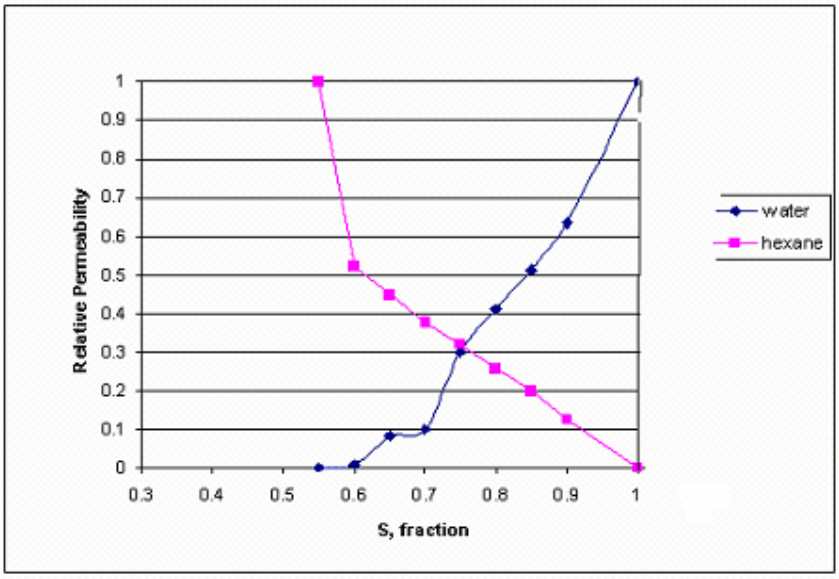

Figure 65. Simulator relative permeabilities for experiment 21.

When the three simulators' relative permeability graphs are considered, the effect of polymer and fracture can clearly be seen. It can be concluded that polymer flooding considerably shifts the curve and fracture presence changes the type of the curve.

Polymer effect, is clearly seen when the experiment 20 **(Figure 62)** is compared with experiment 9 **(Figure 59)** in which there is no influence of polymer. The relative permeability curve shifts right and the end point relative permeability to hexane increases.

Experiment 21 was performed under the presence of both fracture and polymer. The addition of a horizontal fracture influences both the position of the curve in the cartesian plane and the type of the curve. The curves for simulator relative permeabilities for experiment 9 **(Figure 59)** and experiment 20 **(Figure 62)** resembled a power-law type behavior, whereas the fractured experiment's curve is of type x-law type. This may be attributed to the dominancy of the fracture rather than the polymer. As stated before in the theory and in literature survey, the fractured relative permeability curves are of x-type like the one in **Figure 65**. In addition, the hexane end point relative permeability increases with the horizontal fracture.

CHAPTER 6

CONCLUSION

Considering the experimental study results and analysis, several conclusions were drawn. These are stated briefly below.

According to the simulation study, it can be concluded that the relative permeability curves change shape (from x-type to power-law type) with polymer usage and fracture existence.

In addition, from the experimental data analysis, it can be deduced that the polymer injection has a direct influence on end point relative permeability to oil at water wet carbonate cores in consideration. The end point relative permeability to hexane increases with polymer injection. Moreover, the end point relative permeability to hexane enhances considerably when the cores are horizontally fractured and rushed with polymer solution.

The investigation of the tertiary recovery technique of polymer injection was attempted for carbonate reservoirs of Midyat formation considering the concepts of residual oil saturation and relative permeability. Finally, it can be concluded that the polymer flooding may be applicable to Midyat formation residual oil and can improve the oil recovery further.

REFERENCES

1. Romm, E.S., 'Fluid Flow in Fractured Rocks', (in Russian), Nedra Publishing House, Moscow, 1962.
2. Merill, L.S., Jr, 'Two Phase Flow in Fractures', University of Denver, Denver CO, 1975.
3. Pieters, D.A., Graves, R.M., 'Fracture Relative Permeability: Linear or Non-linear Function of Saturation', SPE 28701, 1994.
4. Pan, X., Wong, R.C., 'Steady State Two Phase in a Smooth Parallel Fracture', 47th Annual Technical Meeting of the Petroleum Society in Calgary, Alberta, Canada, June 10-12.
5. Rangel-German, E., Akin, S., Castanier, L.M., 'Experimental and Theoretical Investigation of Multiphase Flow in Fractured Media', Geothermal Resources Council Ann. Meeting, San Diego, California, USA, Vol 22, pp 491-497, 1998.
6. Pruess, K., Tsang, Y.W., 'On Two Phase Relative Permeability and Capillary Pressure of Rough Walled Rock Fractures', Water Resour. Res, 1998.
7. Persoff, P., Pruess, K., Myer.L., 'Two Phase Flow Visualization and Relative Permeability Measurement in Transparent Replices of Rough-walled Rock Fractures', Sixteenth Workshop on Geothermal Reservoirs, Stanford University.
8. McDonald , A.E, Beckner, B.I., Chan, H.M., , T.A., Wooten., S.O., 'Some Important Considerations in the Simulation of Naturally Fractured Reservoirs', SPE 21814, SPE Meeting, Denver, Colorado, 1991.
9. Babadagli, T., Ersaghi, I., 'Improved Modeling of Oil Water Flow in Naturally Fractured Reservoirs Using Effective Fracture Relative Permeabilities', SPE 26076, Western Regional Meeting, Anchorage, AK, USA, 1993

10. Witherspoon, D. A., 'Validitiy of Cubic Law for Fluid Flow in a Permeable Rock Fracture', Water Resources Res., Dec 1980.
11. Saidi, A. M. , Tehrani, D. H., and Wit, K., 'Mathematical Simulation of Fractured Reservoir Performance Based on Physical Model Experiments', Proc, 10 th World Petroleum Congress, Moscow, 1979.
12. Thomas, L. K., 'Ekofisk Waterflood Pilot', JPT, Feb.1987.
13. Festoy, S. and Van Golf Racht, T.D., 'Gas Gravity Drainage in Fractured Reservoirs Through New Dual-Continuum Approach', SPE Reservoir Engineering, Aug 1989.
14. Kazemi, H., 'Numerical Simulation of Water Oil Flow in Naturally Fractured Reservoirs', SPEJ, Dec1976.
15. Gilman, J. R., and Kazemi, H., 'Improvements in Simulation of Naturally Fractured Reservoirs', SPEJ, Aug.1983.
16. Stone, H. L., 'Probability Model for Estimating Three Phase Relative Permeability', Trans. AIME, 1970.
17. Muskat, M., Wyckoff, R. D, Botset, H. G., and Meres, M. W., 'Flow of Gas Liquid Mixtures Through Sands', Trans. AIME, 1937.
18. Morgan T. J., and Gordon, D. T., 'Influence of Pore Geometry on Water-Oil Relative Permeability', Journal of Petroleum Technol., 1970.
19. Gorring, R. L., 'Multiphase Flow of Immiscible Fluids in Porous Media', Ph.D. Thesis, University of Michigan, Ann Arbour, 1966.
20. Crowell, D. C., Dean, G. W., and Coomis, A. G., 'Efficiency of Gas Displacement from a Water Drive Reservoir', U.S. Bureau of Mines, 6735, 1966.
21. Demekas, M. O., Mattax, C. C., and Davis, G. T., 'Effect of Crude Oil Components on Rock Wettability', Trans. AIME, 1959.
22. Honarpour, M., Koederitsz L., Harvey, H. A., 'Relative Permeability or Petroleum Reservoirs', 1986.
23. Osoba, J. S., Richardson J. G., Kerver, J. K., Hafford, J. A., and Blair, P. M., 'Laboratory Measurements of Relative Permeability', Trans. AIME, 1951.

24. Saraf, D. N., and Fatt, I., 'Three Phase Relative Permeability Measurements Using a N.M.R. Technique for Estimating Fluid Saturation', Soc. of Pet. Eng. J., 1967.
25. Land, C. S., 'Comparison of Calculated with Experimental Imbibition Relative Permeability', Trans. AIME., 1971.
26. Owens, W. W., Parrish, D. R., Archer, D. L., 'The Effect of Rock Wettability on Oil- Water Relative Permeability Relationships', Trans. AIME, 1971.
27. Geffen, T. M., Owens, W. W., Parrish, D. R., and Morse, R. A., 'Experimental Investigation of Factors Affecting Laboratory Relative Permeability Measurements', Trans. AIME, 1942.
28. Osoba, J. S. , Richardson, J. G., Kerver, J. K., Hafford, J. A. And Blair, P. M., 'Laboratory Measurements of Relative Permeability', Trans. AIME, 1951.
29. Naar, J., Wygal, R. J., and Henderson, J. H., 'Imbibition Relative Permeability in Unconsolidated Porous Media', Trans. AIME, 1962.
30. Levine, J. S., 'Displacement Experiments in a Consolidated Porous System', Trans. AIME, 1943.
31. Shelton, J. L., and Schneider, F. M., 'The effect of Water Injection on Miscible Flooding Methods Using Hydrocarbons and CO_2 ', Paper SPE 4580, SPE 48th Annual Meeting, Las Vegas, 1973.
32. Wilson, J. W., 'Determination of Relative Permeability under Simulated Reservoir Conditions', Alchej**,** 1968.
33. Merliss. F. E., Doane, J. D., and Rzasa, M. J., 'Influence of Rock and Fluid Properties and Immiscible Fluid Flow Behavior in Porous Media', Paper 510-G, Presented at the AIME Annual Meeting, New Orleans, 1955.
34. Edmondson, T. A., 'Effect of Temperature on Waterflooding', Can. J. Pet. Technol., 1965.

35. Weinbrandt, R. M., Ramey, H. J., Jr., and Mardsen, S. S. Jr., 'Effect of Temperature on Relative and Absolute Permeability of Sandstones', Soc. Pet. Eng. J., 1975.
36. Davidson, L. B., 'The Effect of Temperature on the Permeability Ratio of Different Fluid Pairs in Two-Phase Systems', J. Pet. Technol., 1969.
37. Sinnokrot, A. A., Ramey, H. J., Jr., and Mardsen, S. S., Jr., 'Effect of Temperature Level upon Capillary Pressure Curves', Soc.Pet. Eng. J., 1975.
38. Miller, M. A., and Ramey, H. J., Jr., 'Effect of Temperature on Oil/Water Relative Permeabilities of Unconsolidated and Consolidated Sands', SPE#12116, San Fransisco, Calif. 1983.
39. Moore, T. F., and Slobod, R. L., 'The Effect of Viscosity and Capillarity on the Displacement of Oil by Water', Prod. Mon., 1956.
40. Pirson., S. J., 'Oil Reservoir Engineering', Ed. McGraw-Hill, New York, 1958.
41. Henderson, J. H., and Yuster, S. T., 'Relative Permeability Study', World Oil, 1948.
42. Wyckoff, R. D., and Botset, H.G., 'Flow of Gas Mixtures through Sands', Trans.AIME, 1939.
43. Sandberg, J. R., Gourney L. S., Suppel R. F.,'Effect of Fluid Flow Rate and Viscosity on Laboratory Determination of Oil-Water Relative Permeabilities', Trans. AIME, 1959.
44. Donaldson, E. C., Lorenz. P. B., and Thomas, R. D., 'The Effect of Viscosity and Wettability on Oil/Water relative Permeability', Paper SPE 1562, Presented at the SPE 41st Annual Meeting, Dallas, 1966.
45. Geffen, T. M., Parrish. D. R., Haynes, G. W., and Morse, R. A., 'Efficiency of Gas Displacement from Porous Media by Liquid Flooding', Trans. AIME, 1952.
46. Muskat, M. Wyckoff. R. D., Botset. H. G., and Meres, M. W., 'Flow of Gas Liquid Mixtures through Sands', Trans. AIME, 1937.

47. Yuster, S. T., 'Theoretical Consideration of Multiphase Flow in Idealised Capillary System', Proceedings of the Third World Petroleum Congress, Hague, Netherlands, 1951.

48. Morse, R. A. Terwilliger, P. K., and Yuster, S. T., 'Relative Permeability Measurements on Small Core Samples', Oil Gas J., 1947.

49. Odeh, A. S., 'Effect of Viscosity Ratio on Relative Permeability', Trans. AIME, 1959.

50. Baker, P. E., 'Discussion of Effects of Viscosity Ratio on Relative Permeability', J. Pet. Technol, 1960.

51. Downie, J. and Crane, F. E., 'Effect of Viscosity on Relative Permeability', Soc. Pet. Eng. J., 1961.

52. Ehrlich., R, and Crane, F. E., 'A Model for Two-Phase Flow in Consolidated Materials', Trans. AIME, 1969

53. Perkins, F. M., Jr., 'An Investigation of the Role of Capillary Forces in Laboratory Waterfloods', J. Pet. Technol., 1957.

54. Pickell, J. J., Swanson, B. F., Hickman, W. B., 'Application of Air-Mercury and Oil-Air Capillary Pressure Data in the Study of Pore Structure and Fluid Distribution', Soc. Pet. Eng., J., 1966.

55. Levebwre du Prey, E. J., 'Factors Affecting Liquid- Liquid Relative Permeabilities of a Consolidated Porous Medium', Soc. Pet. Eng. J., 1973.

56. Odeh, A. S., 'Relative Permeability Studies', Masters Thesis, University of California, Los Angeles, 1953.

57. Caudle, B. H., Slobod. R. L., and Brownscombe, E. R., 'Further Developments in the Laboratory Determination of Relative Permeability', Trans. AIME, 1951.

58. McCaffery, F. G., and Bennion, D. W., 'The Effect of Wettability on Two-Phase Relative Permeabilities', J. Can. Pet. Technol., 1974.

59. Sarem, A.M., 'Significance of Oil Water Relative Permeability Data Calculated from Displacement Tests', Proc., Theory of Fluid Flow in Porous Media Conference, University of Oklahoma, Norman. 1959. 89.

60. Owens, W. W., Parrish, D. R., and Lamoreaux, W. E., 'An Evaluation of a Gas Drive Method For Determining Relative Permeability Relationships', Trans. AIEM, 1956.

61. Kyte, J. R. and Rappoport, L. A., 'Linear Waterflood Behavior of End-Effects in Water Porous Media', Trans. AIME, 1958.

62. Richardson, J. G., Kerver, J. K., Hafford, J. A., and Osoba, J. S., ' Laboratorty Determination of Relative Permeability', Trans. AIME, 1952.

63. Moore, T. F., and Slobod, R. L., 'The Effect of Viscosity and Capillarity on the Displacement of Oil by Water', Prod. Mon., 1956.

64. Huppler, J. D., 'Numerical Investigation of the Effects of the Core Heterogeneties on Waterflood Relative Permeability', Soc. Pet.Eng. J., 1970.

65. Rezaie, M., 'Relative Permeability Measurements in Homogeneous and Fractured Cores', Masters Thesis, Middle East Technical University, Sep 1992.

66. Giordano, R.M., Salter, S. J. and Mohanty, K.K., 'The Effect of Permeability Variations on Flow in Porous Media', Paper SPE 14365 Presented at the 1985 SPE Annual Technical Conference and Exhibition, Las Vegas, (Sept.22-25)

67. Littman, W, 'Polymer Flooding', Elsevier, Amsterdam, Oxford, New York, Tokyo, 1988.

68. Amyx, J. W., Bass, JR.D.M, Whiting, R.L., 'Petroleum Reservoir Engineering', Mc Graw Hill Book Company, New York, Toronto, London, 1960.
69. Warren, J.E., Root, P.J., 'The Behavior of Naturally Fractured Reservoirs', SPEJ, 1963.

70. Pruess, K., Narasimhan T.N., 'A Practical Method for Modelling Fluid and Heat Flow in Fractured Porous Media', Soc. Pet.Eng., 1985.

71. Fung, Colllins, 'Evaluation of the Improved Dual Porosity Model for the Simulation of Gravity Effects in Naturally Fractured Reservoirs', CIM paper no 88-39-05. 39th Annual Meeting of the Petroleum Society of Canadian Institute of Mining, 1988.

72. Akin, S., 'Estimation of Fracture Relative Permeabilities from Unsteady State Core Floods', Feb. 2001

73. Akin, S., Demiral, B., 'Genetic Algorithm for EstimatingRelative Permeabilities from Displacement Experiments', Comput. Geosci, 1998.
74. Jones, F. G., 'A Laboratory Study of the Effects of Confining Pressure on Fracture Flow and Storage Capacity in Carbonate Rocks', JPT, Jan.1985.
75. Van Golf Racht, T. D. and Manking, E., 'A New Forecast Method Applied to Rostam Fractured Reservoir', Preprint No 3720, European SPE Meeting, Amsterdam, 1972.

76. Abgrall, E., 'Porous Media Behavior vs. Temperature and Comparison Variations', French Institute of Petroleum Revue (IFP), Jul-Aug 1975.
77. Bradner, C. F., and Slatboom, R.A., 'Vertical Immiscible Displacement Experiments in a Non-Homogeneous Flow-Cell', Canadian Journal of Petroleum Tech., Jan.-March 1975.
78. Erlich, E., 'Relative Permeability Characteristics of Vugular Cores', Paper SPE 3553, Fall Meeting, SPE, New Orleans, 1971.

79. Racht, T. D., Fundamentals of Fractured Reservoir Engineering, Elsevier Scientific Pub. Company, Amsterdam, Oxford, New York, 1982.
80. Lefebvre du Prey, E. And Verre, R., 'Study of Multiphase Flow in Fractures', in French, IFP No 20950, Jan 1973.
81. Reiss, L. M., 'The Reservoir Engineering Aspects of Fractured Formations', Gulf Pub. Company, Houston, Paris, London, Tokyo.
82. Standing, M. B., 'Relative Permeability Relationships', Lectures given at Trondheim University.
83. Firoozobadi, A. And Hauge, J., 'Capillary Pressure in Fractured Porous Media', JPT, June 1990.
84. Thomas, L. K., 'Ekofisk Waterflood Pilot', JPT, Feb.1987.
85. Gilmen, G. R. and Kazemi H., 'Author's Reply to Discussion of Improved Calculations for Viscous and Gravity Displacement in Matrix Blocks in Dual Porosity Simulators', JPT, June 1988.
86. Horie, T., Firoozabadi, A., Ishimito K., 'Laboratory Studies of Capillary Interaction in Fracture-Matrix Systems', SPEJ, Aug.1990.
87. Hassler, G.L., Rice, R.R., and Leeman, E.H., 'Investigations of Recovery on the Oil from Sandstones by Gas Drive', Trans. AIME, 1936.
88. Rapoport, L.A. and Leas, W.J., 'Relative Permeability to Liquid in Liquid Gas Systems', Trans. AIME, 1951.
89. Hassler, G.L., US Patent 2345935, 1944.
90. Welge, H.J., 'A Simplified Method for Computing Recovery by Gas or Water Drive', Trans. AIME, 146, 107, 1952.
91. Johnson, E.F., Bossler D.P., and Neumann, v.o., 'Calculation of Relative Permeability from Displacement Experiments', Trans. AIME, 216, 370, 1959.
92. Heaviside, J., Black, C.J.J., 'Fundamentals of Relative Permeability Experimental and Theoretical Considerations', Paper SPE 12173.
93. Purcell, W.R., 'Capillary Pressures – Their Measurement Using Mercury and Calculation of Permeability Therefrom', Trans. AIME, 186, 39, 1949.

94. Fatt, I. and Dykstra H., 'Relative Permeability Studies', Trans AIME, 192, 41, 1951.
95. Slobod R. L., Chambers, A., and Prehn, W. L., 'Use of Centrifuge for Determining Connate Water, Residual Oil and Capillary Pressure Curves of Small Core Samples', Trans. AIME, 1952.
96. Van Sprencen, E., 'Three Phase Relative Permeability Measurements Using the Centrifuge Method', Paper SPE/DOE 10688.
97. O'Mera D. J .Jr, and Lease, W. O., 'Multiphase Relative Permeability Measurements Using an Automated Centrifuge', Paper SPE 12128.
98. Donaldson, E. C., and Dean, G. W., 'Two and Three-Phase Relative Permeability Studies', Report No: 6826, U.S. Department of Interior, Bureau of Mines, Bartlesville Okla, 1966.
99. Zaitoun, A., Bertin, H., and Lasseux, D., 'Two Phase Flow Property Modifications by Polymer Adsorption', Paper SPE/DOE 39631, presented at the SPE/DOE Improved Oil Recovery Symposium, 1998.
100. Liang, J., Seright, R., 'Further Investigations of Why Gels Reduce k_w More Than ko', Paper SPE 37249 presented at the SPE International Symposium on Oilfield Chemistry, Houston, 1977.
101. Eoff, L., Dairymple, E. D., Reddy, B. R., and Everett, D., 'Structure and Process Optimisation for the Use of a Polymeric Relative Permeability Modifier in Conformance Control', Paper SPE 64985, 2001.
102. Lake, L.W., 'Enhanced Oil Recovery', Prentice-Hall, New Jersey, 1989
103. Sorbie, K. S., 'Polymer Improved Oil Recovery', Blackie, Glasgow and London.
104. Akin, S., Demircioğlu, C., Yılmaz, S., 'Application of Artificial Neural Networks to Optimum Bit Selection', 2000, M.E.TU

105. Rumelhart, D. E., Hinton, G. E., and Williams, R. J., 1986. 'Learning Representations by Back-Propagating Errors', Nature, 323, 533-536.

106. Haykin, S. S., 1994. 'Neural Networks- A Comprehensive Foundation', Prentice-Hall International, London 842 pp.

107. Ali, J.K., 1994. 'Neural Networks: A New Tool for the Petroleum Industry Soc. Pet. Eng. Production Facilities', 9, Mar., 217.

108. Romeo, G., Mele F., Morelli A. 1995. 'Neural Networks and Discrimination of Seismic Signals', Computers & Geosciences 21 (2), 279-288.

109. Miller, D.M., Kaminsky, E.J., Rana S., 1995. 'Neural Network Classification of Remote-Sensing Data', Computers & Geosciences Vol. 21 (3), 377-386

110. Fletcher, P., Coveney, P.V., Hughes, T.L., Methven, C.M., 1995. 'Brief Predicting Quality and Performance of Oilfield Cements with Artificial Neural Networks and FTIR Spectroscopy', Journal of Petroleum Technology, 47 (2), 129-130

111. Vukelic, M.A., Miranda, E.N., 1996. 'Neural Networks in Petroleum Engineering', International Journal of Neural Systems, 7, 187.

112. Mohaghegh S., Arefi, R., Ameri, S., Hefner, M., 1994. 'A Methodological Approach for Reservoir Heterogeneity Characterization Using Artificial Neural Networks', In: SPE Annual Technical Conference and Exhibition, New Orleans, Sept. 25-28, SPE 28394.

113. Wang, L., Wong, P.M. Shibli S.A.R., 1999. 'Modeling Porosity Distribution in the A'nan Oilfield: Use of Geological Quantification, Neural Networks, and Geostatistics', Soc. Pet. Eng. Reservoir Eval. & Eng. 2 (6), 527-532.

114. AlKaabi, A., Lee, W. J., 1993. 'Using Artificial Neural Nets to Identify the Well Test Interpretation Model. Soc. Pet. Eng. Formation Evaluation', 8, Sept., 233-240.

115. Rogers, I.D. Guffey, C.G., Oldham, W.J.B., 'Artificial Neural Networks for Identification of Beam Pump Dynamometer Load Cards In Proceedings of the 65th Annual Technical Conference and Exhibition held in New Orleans', LA, Sept 23-236, SPE 20651, 349-359, 1990.

116. Odeh, A.S., 'Reservoir Simulation…What Is It?', SPE AIME, Mobil Research and Development Corp.

117. Staggs, H.M., Herbeck, E.F., 'Reservoir Simulation Models- An Engineering Overview', SPE AIME, Atlantic Richfield Co.

118. Computer Modelling Group Ltd., 'Stars Advanced Process and Thermal Reservoir Simulator', User's Guide, Version 2001., Calgary, Canada.

119. http://ai-dept.com/Articles/47/EANN-weights.html, accessed on 03/05/2005.

APPENDIX-A

TABLE A.1

Table A.1.List of experiments

Exp. #	Q(ml/min)	Core #	Frac.	K(md)	Porosity (%)	Sor (%)	FLUID TYPE			P_{conf}(psi)
							Water	Hexane	Polymer	
1	1	1A	NO	253	12,19	24,94	YES	YES	NO	600
2	1	1B	NO	---	12,19	25,96	NO	YES	NO	300
3	1,5	1C	NO	134	12,19	19,37	YES	YES	NO	1000
4	0,5	1D	NO	324,5	12,19	---	YES	YES	NO	300
5	0,5	1E	NO	316,2	12,19	11,76	YES	YES	NO	300
6	---	2A	NO	126,7	15,12	---	YES	NO	NO	600
7	1	2B	NO	256	15,12	53,39	YES	YES	NO	300
8	1	2C	NO	292	15,12	---	YES	YES	NO	300
9	1,5	2D	NO	72,2	15,12	47,67	YES	YES	NO	1000
10	0,5	2E	NO	132	15,12	28,86	YES	YES	NO	600
11	3	2F	YES	2452	20,43	59,11	YES	YES	NO	1000
12	1	2G	NO	---	14,85	27,22	YES	YES	YES	1000
13	1	3A	NO	200,2	14,85	52,98	YES	YES	NO	300
14	1	3B	NO	166	14,85	50,89	YES	YES	NO	1000
15	1	3C	NO	109	14,85	---	YES	YES	NO	1000
16	1	3D	NO	305,1	14,85	---	YES	YES	NO	300
17	1	3E	NO	258,3	14,85	31,74	YES	YES	NO	300
18	0,5	3F	NO	137	14,85	18,84	YES	YES	NO	300
19	1	2H	NO	----	14,85	54,22	YES	YES	YES	1000
20	1	3G	NO	----	14,85	46,31	YES	YES	YES	1000
21	2	3H	YES	---	19,54	9,27	YES	YES	YES	1000

APPENDIX B

ANN COMPUTATION DETAILS

Momentum Factor

Momentum factor is used to have a higher learning rate but it prevents the oscillatory behvaior that can sometimes result from a high learning rate.

Mean Square Error

Mean square error is a model fitness value needs to be assigned. Calculating mean square error used to evaluate the fitness involves summing over the square of the differences between the actual and the expected output at each node, and then taking the average over all output nodes. Error formula is as follows:

$$Error = \frac{\sum (output_{actual} - output_{expected})^2}{n} \quad \text{(B1)}$$

where n is the number of output nodes. **[119]**

The parameters used at the ANN model are tabulated below in **Table B1.**

Table B1. Parameters in ANN training

Momentum Factor	0,4
Learning Parameter	0,4
Number of Inputs	5
Number of Outputs	1
Number of Hidden Layers	1
Number of Training Cycles	500
Training Mode	Sequential

The input data is at **Table B2**.

Table B2. Input data for ANN computation.

Rate (ml/min)	P_{conf}(psi)	μ(cp)	DP(psi)	k_{abs} (d)	k_r
1.21	600.00	1.00	28.19	0.26	0.10
1.64	1000.00	1.00	28.94	0.15	0.24
0.78	300.00	1.00	24.88	0.32	0.06
0.78	300.00	1.00	25.19	0.43	0.04
1.21	300.00	1.00	29.25	0.26	0.10
1.21	300.00	1.00	28.94	0.29	0.09
1.64	1000.00	1.00	32.13	0.07	0.44
0.78	600.00	1.00	25.44	0.13	0.15
1.21	300.00	1.00	29.38	0.24	0.11
1.21	1000.00	1.00	30.50	0.17	0.15
1.21	1000.00	1.00	29.00	0.11	0.24
1.21	300.00	1.00	29.88	0.31	0.08
1.21	300.00	1.00	25.06	0.26	0.12
0.78	300.00	1.00	25.06	0.19	0.10
2.92	1000.00	1.00	28.38	0.61	0.11
1.21	1000.00	1.54	29.81	0.18	0.22
1.21	1000.00	1.54	31.25	0.19	0.19
1.21	1000.00	1.54	32.56	0.19	0.18
2.07	1000.00	1.54	24.56	0.19	0.42

Below is given a sample data set for k_r profile creation. The predictor values are given in **Table B3** The minimum,maximum and fixed values of the predictors fed into the ANN are given in **Table B3** and the related k_r profile is at **Figure B1. Table B4** is for the data tabulation of **Figure B1**.

Table B3. The predictor's values

	Rate (ml/min)	P_{conf}(psi)	μ(cp)	DP(psi)	k_{abs} (d)
min	0.78	300.00	1.00	24.56	0.07
max	2.92	1000.00	1.54	32.56	0.61
fix	1.30	600.00	1.00	28.34	0.24

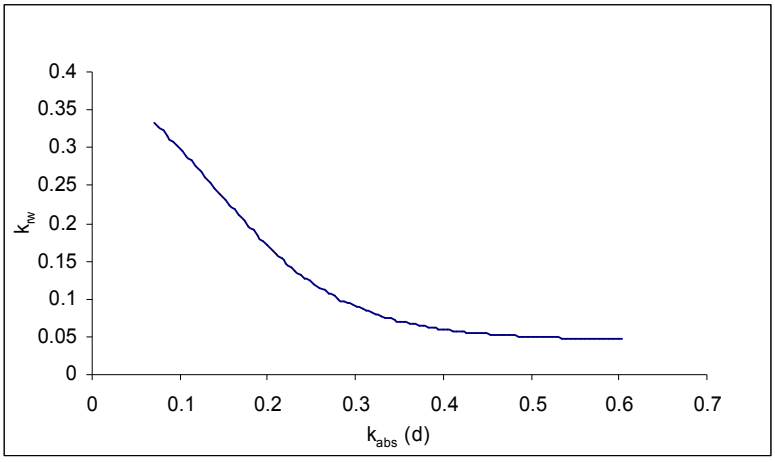

Figure B1. k_r profile created with ANN

TableB4. Data used for k_r profile creation

k_{abs} (d)	k_r	k_{abs} (d)	k_r	k_{abs} (d)	k_r
0.07	0.333683884	0.2644	0.11094	0.4588	0.052613
0.0754	0.3278253	0.2698	0.107224	0.4642	0.052182
0.0808	0.321779089	0.2752	0.103692	0.4696	0.051776
0.0862	0.315553831	0.2806	0.100339	0.475	0.051395
0.0916	0.309159681	0.286	0.097159	0.4804	0.051036
0.097	0.302608321	0.2914	0.094146	0.4858	0.050698
0.1024	0.295912907	0.2968	0.091295	0.4912	0.05038
0.1078	0.289088011	0.3022	0.088598	0.4966	0.050081
0.1132	0.282149468	0.3076	0.086049	0.502	0.049799
0.1186	0.275114304	0.313	0.083643	0.5074	0.049534
0.124	0.268000547	0.3184	0.081372	0.5128	0.049283
0.1294	0.260827017	0.3238	0.07923	0.5182	0.049048
0.1348	0.253613187	0.3292	0.077211	0.5236	0.048825
0.1402	0.246378929	0.3346	0.075309	0.529	0.048616
0.1456	0.2391443	0.34	0.073518	0.5344	0.048418
0.151	0.231929318	0.3454	0.071832	0.5398	0.048232
0.1564	0.224753754	0.3508	0.070245	0.5452	0.048056
0.1618	0.217636838	0.3562	0.068753	0.5506	0.04789
0.1672	0.210597169	0.3616	0.067349	0.556	0.047733
0.1726	0.203652445	0.367	0.06603	0.5614	0.047585
0.178	0.196819318	0.3724	0.064789	0.5668	0.047445
0.1834	0.190113246	0.3778	0.063624	0.5722	0.047312
0.1888	0.183548372	0.3832	0.062528	0.5776	0.047187
0.1942	0.177137434	0.3886	0.061499	0.583	0.047069
0.1996	0.1708917	0.394	0.060532	0.5884	0.046957
0.205	0.164820942	0.3994	0.059623	0.5938	0.046852
0.2104	0.158933367	0.4048	0.05877	0.5992	0.046751
0.2158	0.153235721	0.4102	0.057968	0.6046	0.046657
0.2212	0.147733261	0.4156	0.057214		
0.2266	0.142429821	0.421	0.056507		
0.232	0.137327889	0.4264	0.055842		
0.2374	0.132428682	0.4318	0.055217		
0.2428	0.127732255	0.4372	0.05463		
0.2482	0.123237549	0.4426	0.054078		
0.2536	0.118942575	0.448	0.053559		
0.259	0.114844463	0.4534	0.053071		

APPENDIX C

SAMPLE SIMULATION DATA

A sample pressure data for experiment 9 and the corresponding simulation data is given in **Table C 1**. In **Table C 2**, the production data is tabulated. In **Table C3**, the related end point relative permeabilities of the simulator results can be found.

Table C1. Simulator and experimental pressure data for experiment 9

Experiment		Simulator	
PV	DP (psi)	PV	DP (psi)
0	12.6165	0	13.95573502
0.166359026	13.9915	0.489359084	14.77589111
0.332718053	14.554	0.571848831	15.84040718
0.499077079	14.929	0.68318332	17.28606682
0.665436105	15.429	0.831495078	18.42353516
0.831795132	15.6165	1.024512772	16.34458237
0.998154158	15.8665	1.277007294	14.68945007
1.164513185	16.054	1.644640589	13.45266418
1.330872211	16.179	2.308625413	12.99050407
1.497231237	16.2415	3.67623215	12.88722496
1.663590264	16.304	6.619809975	12.87585335
1.82994929	16.429	7.693634342	12.87536316
1.996308316	16.4915	10.19864798	12.87530212
2.162667343	16.554	13.14222698	12.87530022
2.661744422	16.679	15.05258774	12.87530022
4.158975659	16.8665	17.99616674	12.87530022

Table C2. Experimental production data for experiment 9

PV	Q_{hexane} (ml)	Q_{water} (ml)
0	0	0
0.166359	1.35	0
0.332718	2.2	0
0.499077	3.2	0
0.665436	4.3	0.35
0.831795	5.45	0.35
0.998154	5.45	1.8
1.164513	6.3	3.1
1.330872	6.4	4.5
1.497231	6.4	5.6
1.66359	6.4	6.2
1.829949	6.4	7.2

Table C3. Simulation production data for experiment 9

Simulator			Simulator		
PV	Q_{hexane} (ml)	Q_{water} (ml)	PV	Q_{hexane} (ml)	Q_{water} (ml)
0	0	0	73.92421	7.499512	891.3318
0.489359	0.722168	0	76.8678	7.499512	927.3318
0.571849	1.723755	0	79.81138	7.499512	963.3318
0.683183	3.071655	0	82.75496	7.499512	999.3318
0.831495	4.740601	0.128417	85.69854	7.499512	1035.332
1.024513	6.121948	1.120057	88.64212	7.499512	1071.332
1.277007	6.956665	3.385132	91.5857	7.499512	1107.332
1.644641	7.32019	7.527496	94.52928	7.499512	1143.332
2.308625	7.462402	15.50962	97.47287	7.499512	1179.332
3.676232	7.495605	32.2031	100.4164	7.499512	1215.332
6.61981	7.499268	68.19911	103.36	7.499512	1251.332
7.693634	7.499512	81.33179	106.3036	7.499512	1287.332
10.19865	7.499512	111.9681	109.2472	7.499512	1323.332
13.14223	7.499512	147.968	112.1908	7.499512	1359.332
15.05259	7.499512	171.3318	115.1344	7.499512	1395.332
17.99617	7.499512	207.3318	118.0779	7.499512	1431.332
20.93975	7.499512	243.3318	121.0215	7.499512	1467.332
22.41154	7.499512	261.3318	123.9651	7.499512	1503.332
25.35512	7.499512	297.3318	126.9087	7.499512	1539.332
28.29871	7.499512	333.3318	129.8523	7.499512	1575.332
29.77049	7.499512	351.3318	132.7958	7.499512	1611.332
32.71407	7.499512	387.3318	135.7394	7.499512	1647.332
35.65766	7.499512	423.3318	138.683	7.499512	1683.332
38.60124	7.499512	459.3318	141.6266	7.499512	1719.332
41.54482	7.499512	495.3318	144.5702	7.499512	1755.332
44.4884	7.499512	531.3317	147.5137	7.499512	1791.332
47.43198	7.499512	567.3318	150.4573	7.499512	1827.332
50.37557	7.499512	603.3318	153.4009	7.499512	1863.332
53.31914	7.499512	639.3318	156.3445	7.499512	1899.332
56.26273	7.499512	675.3317	159.2881	7.499512	1935.332
59.20631	7.499512	711.3318	162.2317	7.499512	1971.332
62.14989	7.499512	747.3318	165.1752	7.499512	2007.332
65.09347	7.499512	783.3317	168.1188	7.499512	2043.332
68.03705	7.499512	819.3318			
70.98063	7.499512	855.3318			

Table C4. Simulator end point relative permeabilities.

S	k_{rh}	k_{rw}
1	0.35	0
0.8	0.4	0.0008
0.5	0.5	0.003225
0.2	0.6	0.005
0.1	0.7	0.03
0.05	0.75	0.0415
0	0.85	0.05
0	0.9	0.1
0	1	1